ARTICLES
https://doi.org/10.1038/s42255-022-00561-5
nature metabolism

Check for updates

Dysregulation of macrophage PEPD in obesity determines adipose tissue fibro-inflammation and insulin resistance

V. Pellegrinelli[1]✉, S. Rodriguez-Cuenca[1,2], C. Rouault[3], E. Figueroa-Juarez[1], H. Schilbert[4], S. Virtue[1], J. M. Moreno-Navarrete[5,6,7], G. Bidault[1], M. C. Vázquez-Borrego[1,8], A. R. Dias[1], B. Pucker[4,9], M. Dale[1], M. Campbell[1,2], S. Carobbio[1,10], Y. H. Lin[1,11], M. Vacca[1,12], J. Aron-Wisnewsky[3,13], S. Mora[14,15], M. M. Masiero[16], A. Emmanouilidou[16], S. Mukhopadhyay[17], G. Dougan[18,19], M. den Hoed[16], R. J. F. Loos[20,21,22], J. M. Fernández-Real[5,6,7], D. Chiarugi[1], K. Clément[3,13] and A. Vidal-Puig[1,2,10]✉

Resulting from impaired collagen turnover, fibrosis is a hallmark of adipose tissue (AT) dysfunction and obesity-associated insulin resistance (IR). Prolidase, also known as peptidase D (PEPD), plays a vital role in collagen turnover by degrading proline-containing dipeptides but its specific functional relevance in AT is unknown. Here we show that in human and mouse obesity, PEPD expression and activity decrease in AT, and PEPD is released into the systemic circulation, which promotes fibrosis and AT IR. Loss of the enzymatic function of PEPD by genetic ablation or pharmacological inhibition causes AT fibrosis in mice. In addition to its intracellular enzymatic role, secreted extracellular PEPD protein enhances macrophage and adipocyte fibro-inflammatory responses via EGFR signalling, thereby promoting AT fibrosis and IR. We further show that decreased prolidase activity is coupled with increased systemic levels of PEPD that act as a pathogenic trigger of AT fibrosis and IR. Thus, PEPD produced by macrophages might serve as a biomarker of AT fibro-inflammation and could represent a therapeutic target for AT fibrosis and obesity-associated IR and type 2 diabetes.

As obesity progresses, sterile inflammation and constitutive activation of pro-fibrotic cells (for example, macrophages and AT progenitors) occurs in the AT depots, leading to AT fibrosis[1,2]. Fibrosis of the AT impairs adipocyte hypertrophy and hyperplasia adaptations and associates with IR, and increased risk of type 2 diabetes (T2D)[3,4]. Following bariatric surgery, fibrosis in AT impedes weight loss due to the rigid fibrotic wall constraining the adipocytes and preventing efficient and timely AT lipid mobilization[5,6]. The degree of AT fibrosis and inflammation (fibro-inflammation) might be a more important risk factor for metabolic complications than the degree of obesity. Supporting this view, the spectrum of obesity includes patients with severe obesity who appear to be inappropriately metabolically healthy, in contrast with other mildly overweight patients who exhibit surprisingly severe metabolic complications[7]. Genome-wide association studies (GWAS) have identified DNA variants dissociating obesity from its metabolic complications helpful to investigate these clinical paradoxes. We and others identified the rs731839 variant in the locus corresponding to prolidase or PEPD, influencing lipid and glycaemic profiles[8,9]. The G allele was associated with metabolically unhealthy lipid (higher triglyceride and lower HDL cholesterol levels) and glycaemic (higher fasting insulin and lower adiponectin levels) profiles. Impaired lipid and carbohydrate metabolism were paradoxically associated with lower adiposity[10,11].

[1]Wellcome-MRC Institute of Metabolic Science and MRC Metabolic Diseases Unit, University of Cambridge, Cambridge, UK. [2]Cambridge University Nanjing Centre of Technology and Innovation, Nanjing, P. R. China. [3]Sorbonne University, INSERM, NutriOmique Research Unit, Paris, France. [4]Genetics and Genomics of Plants, Centre for Biotechnology (CeBiTec) & Faculty of Biology, Bielefeld University, Bielefeld, Germany. [5]Department of Diabetes, Endocrinology and Nutrition, Girona Biomedical Research Institute (IDIBGI), University Hospital of Girona Dr Josep Trueta, Girona, Spain. [6]Department of Medicine, University of Girona, Girona, Spain. [7]CIBERobn Pathophysiology of Obesity and Nutrition, Institut of Salud Carlos III, Madrid, Spain. [8]Maimonides Institute for Biomedical Research of Cordoba (IMIBIC), Cordoba, Spain. [9]Evolution and Diversity, Department of Plant Sciences, University of Cambridge, Cambridge, UK. [10]Centro de Investigacion Principe Felipe, Valencia, Spain. [11]Department of Surgery, Kaohsiung Chang Gung Memorial Hospital and Chang Gung University College of Medicine, Kaohsiung, Taiwan. [12]Insterdisciplinary Department of Medicine, Università degli Studi di Bari 'Aldo Moro', Bari, Italy. [13]Assistance-Publique Hôpitaux de Paris, Nutrition department, Pitié-Salpêtrière hospital, Paris, France. [14]Dept Biochemistry and Molecular Biomedicine, Faculty of Biology, University of Barcelona, Barcelona, Spain. [15]Institute of Biomedicine, University of Barcelona (IBUB), Barcelona, Spain. [16]The Beijer Laboratory and Department of Immunology, Genetics and Pathology, Uppsala University and SciLifeLab, Uppsala, Sweden. [17]MRC Centre for Transplantation Peter Gorer Department of Immunobiology School of Immunology & Microbial Sciences King's College, London, UK. [18]Cambridge Institute of Therapeutic Immunology and Infectious Disease, Jeffrey Cheah Biomedical Centre, University of Cambridge, Cambridge, UK. [19]Division of Infectious Diseases, Department of Medicine, University of Cambridge, Cambridge, UK. [20]Charles Bronfman Institute for Personalized Medicine, Icahn School of Medicine at Mount Sinai, New York, NY, USA. [21]The Mindich Child Health and Development Institute, Icahn School of Medicine at Mount Sinai, New York, NY, USA. [22]Novo Nordisk Foundation Center for Basic Metabolic Research, Faculty of Health and Medical Science, University of Copenhagen, Copenhagen, Denmark. ✉e-mail: vp332@medschl.cam.ac.uk; ajv22@medschl.cam.ac.uk

PEPD is a homodimer cytosolic protein responsible for degrading proline-containing dipeptides (Xaa-Pro or Xaa-hyp), playing a pivotal role in the final step of collagen degradation and turnover. Complete *PEPD* deficiency in humans is a rare genetic disorder characterized by a complex phenotype of angiopathies and defective wound healing, consistent with impairment of collagen turnover[12]. Impaired collagen turnover in PEPD-deficient patients leads to pulmonary fibrosis[13].

Evidence from cancer and liver fibro-inflammation stages indicates that PEPD protein is actively secreted, acting as a non-canonical ligand of the EGFR and ErBB2 receptors[14–17]. Therefore, we hypothesized that functional defects in PEPD may be pathogenically relevant in AT through impairing collagen degradation and defects in intracellular signalling mediated by its extracellular and non-enzymatic roles.

We observed decreased PEPD peptidase activity and increased PEPD protein secretion in inflammatory macrophages and AT from obese individuals and mouse models fed on a high-fat diet (HFD). Lower PEPD activity in AT and higher PEPD protein levels in serum are directly proportional to AT fibrosis, inflammation and metabolic dysfunction. Using pharmacological and genetic mouse models to target PEPD peptidase activity and/or its secretion, we show that dysfunctional PEPD intracellular dipeptidase activity induces AT fibrosis, whereas the PEPD secreted by AT is the main contributor to inflammation, IR and metabolic dysfunction. PEPD originated in inflammatory macrophages and plays an essential role in promoting fibro-inflammatory responses via activation of EGFR in macrophages and pre-adipocytes. Moreover, genetic ablation of *Pepd* in haematopoietic cells (HCs) prevented obesity-induced PEPD release and averted AT fibro-inflammation and obesity-associated metabolic dysfunction. Altogether, these data reveal that obesity-associated severity of AT fibro-inflammation and metabolic disturbances for a given fat mass depend on PEPD activity and PEPD extracellular levels.

Results

Low prolidase activity in obese adipose tissue associates with high PEPD release, insulin resistance and fibrosis. We measured *PEPD* mRNA expression, prolidase activity (PA) and secretion from AT of seven human cohorts spanning a broad spectrum of body mass index (BMI) values, ages and degrees of IR (Extended Data Fig. 1a). *PEPD* expression was lower in visceral white AT (VsW) of obese than lean individuals and lower in obese individuals with T2D than in obese normo-glycaemic participants (Fig. 1a,b). *PEPD* mRNA expression was lower in VsW than in subcutaneous white AT (ScW) in a paired sample cohort study (Fig. 1c), and lower *PEPD* expression in VsW was associated with higher BMI and collagen content in AT from obese individuals (measured as hydroxyproline (HPro) levels; Fig. 1d). Moreover, low *PEPD* expression in VsW was associated with lower expression of AT metabolic genes such as *PLIN1*, *PPARG* and *GLUT4* (Table 1) and reduced VsW *PEPD* expression in obese individuals was associated with reduced PA in VsW (cohort 2e,f; Fig. 1e). Lower PA matched the higher release of PEPD from the VsW of these participants (cohort 2e,f; Fig. 1f), suggesting a causal relationship between the reduction of the intracellular enzymatic activity and the enzyme's release. Among obese participants, those with higher VsW PEPD release were more prone to IR and T2D (Extended Data Fig. 1b). The receiver operating characteristic (ROC) curve analysis highlighted that both the PEPD released and low PA in VsW (but not ScW) predicted T2D (cohort 2e,f; Fig. 1h and Extended Data Fig. 1c,d). Higher PEPD release from VsW was coupled with higher PEPD serum levels in obese participants than lean individuals and was associated with elevated cholesterol and aspartate transaminase (ASAT) levels (cohort 2e, Fig. 1h and Extended Data Fig. 1e). Reanalysis of serum proteomic data from an independent set of insulin-resistant and insulin-sensitive obese participants[18] further confirmed the predictive value of PEPD for IR (Fig. 1i). Moreover, serum PEPD levels were positively correlated with lipid metabolism (for example, APOA proteins), inflammation (for example, S100A12 and DPP4) and extracellular matrix (ECM)-related proteins (for example, TNC and COL4A2; Fig. 1j,k). Altogether, these human data provide evidence for the potential relevance of PEPD as a marker of fibro-inflammation and IR in obese individuals.

A similar pattern of low AT PEPD activity coupled with high circulating levels of PEPD was recapitulated in two independent mouse models of obesity (that is, mice fed 45% HFD and 58% HFD; Extended Data Fig. 1f–m). We found that HFD only affected PEPD peptidase activity in AT but not in the liver or muscle (Extended Data Fig. 1f,g). In mice fed a HFD for 28 weeks, the tissue PA in AT was reduced in the first 8 weeks, followed by the release of PEPD (Extended Data Fig. 1i–k). Despite the increased PEPD serum level, the enzymatic activity of PEPD in serum remained stable during the HFD time course, suggesting that the activity of the enzyme in serum is reduced and might not affect the development of AT fibrosis (Extended Data Fig. 1l). While the liver contributed to the overall levels of serum PEPD in mice, only the gonadal white adipose tissue (GnW) depot showed a significantly increased PEPD release in response to a HFD (Fig. 1l). Dysregulation in PEPD activity and release were associated with AT fibrosis and metabolic disturbances (for example, hyperglycaemia and liver steatosis; Fig. 1m and Extended Data Fig. 1m). Accordingly, serum levels of PEPD predicted the degree of fibrosis (peri-adipocyte collagen) and inflammation (*Tnf* expression) in GnW (Fig. 1n).

Fig. 1 | Obesity reduces adipose tissue PEPD activity and promotes PEPD release associated with fibrosis and insulin resistance. a–c, *PEPD* gene expression in VsW from non-obese ($n=26$) and obese ($n=58$) participants from cohort 1 (**a**), in ScW and VsW (visceral, omental depot) obese non-diabetic (Ob ND, 14) and diabetic (Ob D, $n=8$) participants from cohort 2a,b (**b** and **c**). **d**, Pearson correlation matrix between ScW and VsW ECM remodelling markers and metabolic parameters in obese participants from cohort 2b ($n=14$). **e**, PA in ScW and VsW of obese diabetic (D, $n=10$) and non-diabetic (ND, $n=12$) participants from cohort 2e,f. **f**, ELISA analysis of PEPD levels from VsW explants medium of obese diabetic (D, $n=9$) and non-diabetic (ND, $n=12$) participants from cohort 2e,f. **g**, Area under the receiver operating curve (AUC) values (95% confidence interval (CI)) for PEPD VsW and ScW levels from cohort 2e,f to discriminate participants with type 2 diabetes. **h**, ELISA analysis of PEPD levels in serum from lean ($n=9$) and obese non-diabetic (ND) or diabetic (D; red dots; $n=9$) participants from cohort 2d,e. **i**, AUC values (95% CI) for PEPD serum levels from the Choi et al. cohort[18] to discriminate participants with IR. **j**,**k**, PEPD–protein correlations for the Choi et al. cohort[18], shown as volcano plots (**j**) and Gene Ontology enrichment analysis of the corresponding proteins (**k**). **l**, ELISA analysis of PEPD levels from tissue explants medium (that is, brown adipose tissue, ScW, GnW and liver) of C57BL/6 mice fed chow or 20 weeks on a HFD 58% ($n=4$ biologically independent animals per group). **m**, Pearson correlations between PEPD serum levels and metabolic parameters in chow and HFD conditions ($n=22$ biologically independent animals). **n**, AUC values (95% CI) for PEPD serum levels to predict a high degree of fibro-inflammation in GnW (that is, GnW peri-adipocyte (AD) collagen and GnW *Tnf* expression) from mice fed chow and a HFD 58% ($n=34$ biologically independent animals). Data are presented as mean values ± s.e.m. Data were analysed using a two-tailed Student's *t*-test (**a**–**c**, **f**, **h** and **l**). Two-way ANOVA with Sidak's post hoc multiple-comparisons test was performed; Diab, diabetic status; X, interaction (**e**). NS, not significant; TG, triglyceride.

Prolidase activity inhibition induces PEPD secretion, adipose tissue fibrosis and metabolic complications in lean mice. To uncouple the effects of PEPD from obesity, we treated chow-fed lean mice with *N*-benzyloxycarbonyl-L-proline (CBZ-Pro), a pharmacological inhibitor of PEPD activity[19]. CBZ-Pro-treated mice showed higher levels of the dipeptide glycine–proline in serum, confirming PEPD activity inhibition, and exhibited higher PEPD serum levels than control mice (Fig. 2a,b). CBZ-Pro-treated mice had similar body weight (BW), fat mass and tissue weight than control mice (Extended Data Fig. 2b–d). However, despite similar fat mass, they had more severe AT fibro-inflammation in GnW and were more hyperglycaemic, glucose intolerant and insulin resistant than controls (Fig. 2c–h). Of note, CBZ-Pro-treated mice showed comparable fasting insulin and free fatty acid (FFA) blood levels (Extended Data Fig. 2e,f) and no impairment to the expected insulin level increase in response to glucose compared to controls (Extended

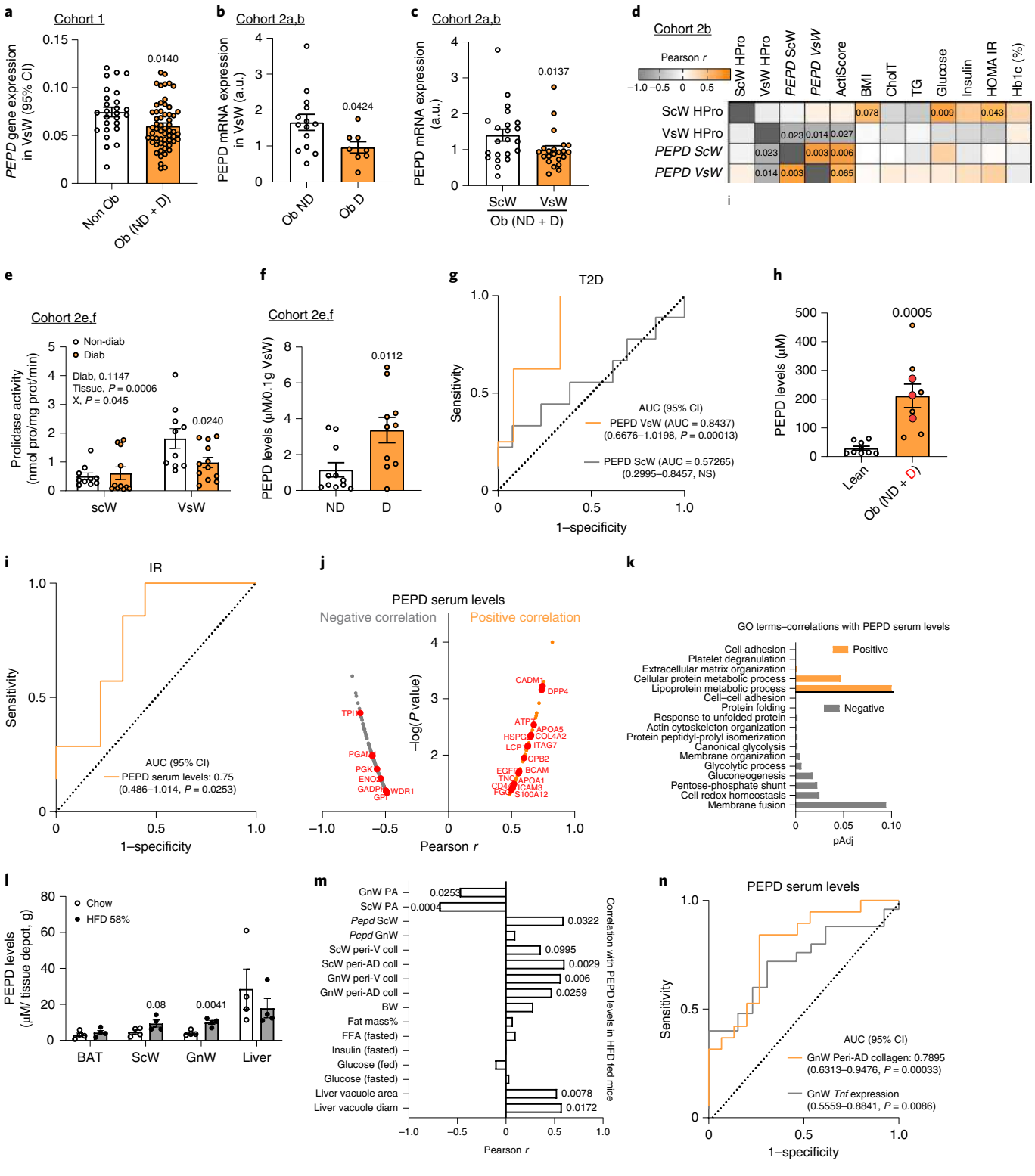

Table 1 | Clinical parameters and bivariate correlations between *PEPD* gene expression and metabolic parameters in cohorts 1 and 3

	Cohort 1				Cohort 3			
	VsW ($n=84$)		ScW ($n=70$)		VsW ($n=46$)		ScW ($n=36$)	
	r	*P*	*r*	*P*	*r*	*P*	*r*	*P*
Age (years)	0.36	0.001	0.05	0.6	0.21	0.1	−0.07	0.6
BMI (kg/m^2)	−0.34	0.002	0.25	0.04	−0.35	0.01	0.13	0.4
Fasting glucose (mg dl^{-1})	0.31	0.005	0.21	0.08	0.13	0.4	−0.14	0.4
Fasting triglycerides (mg dl^{-1})	0.16	0.1	0.07	0.5				
PLIN1 (RU)	0.37	0.01	0.36	0.02	0.61	<0.0001	0.22	0.2
CIDEC (RU)	0.32	0.03	0.24	0.1	0.63	<0.0001	0.17	0.3
PLIN2 (RU)	0.37	0.01	0.08	0.6	0.13	0.4	−0.23	0.1
PLIN3 (RU)	0.4	0.006	0.21	0.1	0.69	<0.0001	0.22	0.1
PPARG (RU)	0.51	<0.0001	0.09	0.5	0.28	0.07	0.07	0.7
FASN (RU)	0.16	0.1	−0.09	0.5	0.05	0.7	0.24	0.1
TNF (RU)	0.1	0.4	−0.04	0.7	0.21	0.2	0.27	0.1
COL6A3 (RU)	0.1	0.4	0.03	0.8				
COL6A6 (RU)	−0.19	0.1	0.1	0.6				
CD68 (RU)	0.23	0.05	0.1	0.4				
EGFR (RU)	0.22	0.05	−0.18	0.2	0.37	0.02	−0.02	0.9
COL4A1 (RU)					0.36	0.02	0.02	0.9
SLC2A4 (RU)					0.55	<0.0001	0.16	0.3
IRS1 (RU)					−0.08	0.6	−0.07	0.7
ADIPOQ (RU)					0.33	0.03	−0.02	0.8

RU, relative units of gene expression.

Data Fig. 2g). However, the phosphorylated-AKT/total-AKT ratio in non-stimulated conditions was lower in CBZ-Pro-treated mice than controls in both GnW (associated with a slight increase in AKT total) and skeletal muscle, suggesting higher AT and muscle IR (Extended Data Fig. 2h,i). The amount of PEPD into the serum of CBZ-Pro-treated mice was positively correlated with the degree of ScW fibrosis and glycaemia in the fed state (Fig. 2i). Altogether, these results show that downregulation of the intracellular PEPD activity in AT and concomitant increase in the serum levels of PEPD-induced AT fibro-inflammation and IR. Furthermore, in line with the human GWAS data, dysregulation of PEPD uncouples fibro-inflammation and metabolic dysfunctions from obesity[8,9,11].

Given this dual role of PEPD, it remained unclear which event—that is, decreased PEPD intracellular dipeptidase activity or increased PEPD released from the cells—was primarily responsible for AT fibrosis and/or metabolic alterations. We performed an exploratory factor analysis (EFA) to investigate how serum PEPD level/PEPD activity covaried with the metabolic parameters measured in the CBZ-Pro-treated mice and controls (Fig. 2j). EFA showed that factor 1, representing a cluster of AT fibrosis-related variables, covaried with PEPD serum levels and fed glucose levels. Moreover, factor 2, the cluster of 'obesity'-related variables (adiposity, glycaemia and steatosis), also covaried with PEPD serum levels, whereas factor 3 showed that the activity of GnW PEPD covaried with fasting glucose. Therefore, EFA indicated that the serum level of PEPD might explain the 'fibrotic' profile and hyperglycaemic status observed in CBZ-Pro mice.

The link between serum PEPD, fibrosis and glycaemia was further strengthened when we included the CBZ-Pro mice fed HFD 58% data in the EFA (factor 1; Extended Data Fig. 2i). However, the covariation between PEPD serum level and 'obesity'-related variables was not sustained (Extended Data Fig. 2j). We rationalized that because HFD per se downregulates PEPD activity/increases its secretion, it was likely that HFD-fed control mice might have developed fibro-inflammation as in CBZ-Pro-treated mice, matching the pro-fibrotic effects of this PEPD pharmacological inhibitor observed in chow-fed conditions. Confirming this interpretation, untreated control and CBZ-Pro-treated mice fed HFD 58% exhibited similar severe AT collagen deposition, fasting insulin, FFA and glucose levels and insulin intolerance (Extended Data Fig. 2e,f,k–m).

Global *Pepd* ablation worsens obesity-associated adipose tissue fibrosis and metabolic comorbidities. To dissect the role of inhibition of PEPD activity from the extracellular action of the released PEPD, we performed phenotyping of the global *Pepd* heterozygote (HET, +/−) and knock-out (KO, −/−) mice against wild-type (WT, +/+) littermates. PEPD activity and serum levels were not detected in the total KO group. Interestingly, *Pepd* HET mice showed 50% decreased PEPD activity but no differences in PEPD serum levels compared to WT mice (Fig. 3a,b and Extended data Fig. 3a,b) and were anatomically similar (that is, length, BW, fat mass and tissue weight; Extended Data Fig. 3c–f). In contrast, *Pepd* KO mice exhibited a runty phenotype characterized by short length, low BW and decreased fat mass (Extended Data Fig. 3c–f), making subsequent phenotyping difficult and of limited value to assess metabolism. Therefore, *Pepd* HET mice were subsequently metabolically phenotyped.

Higher collagen accumulation was observed in ScW (HET/KO) and GnW (KO) compared to WT littermates fed a chow diet, supporting the role of reduced PEPD activity in promoting fibrosis (Fig. 3c), an association strengthened by correlation matrix analysis (Extended Data Fig. 3g). Moreover, EFA analysis of chow-fed *Pepd* mice showed that factor 1, clustering GnW or ScW fibrosis-related variables, had strong loading of glucose blood levels and

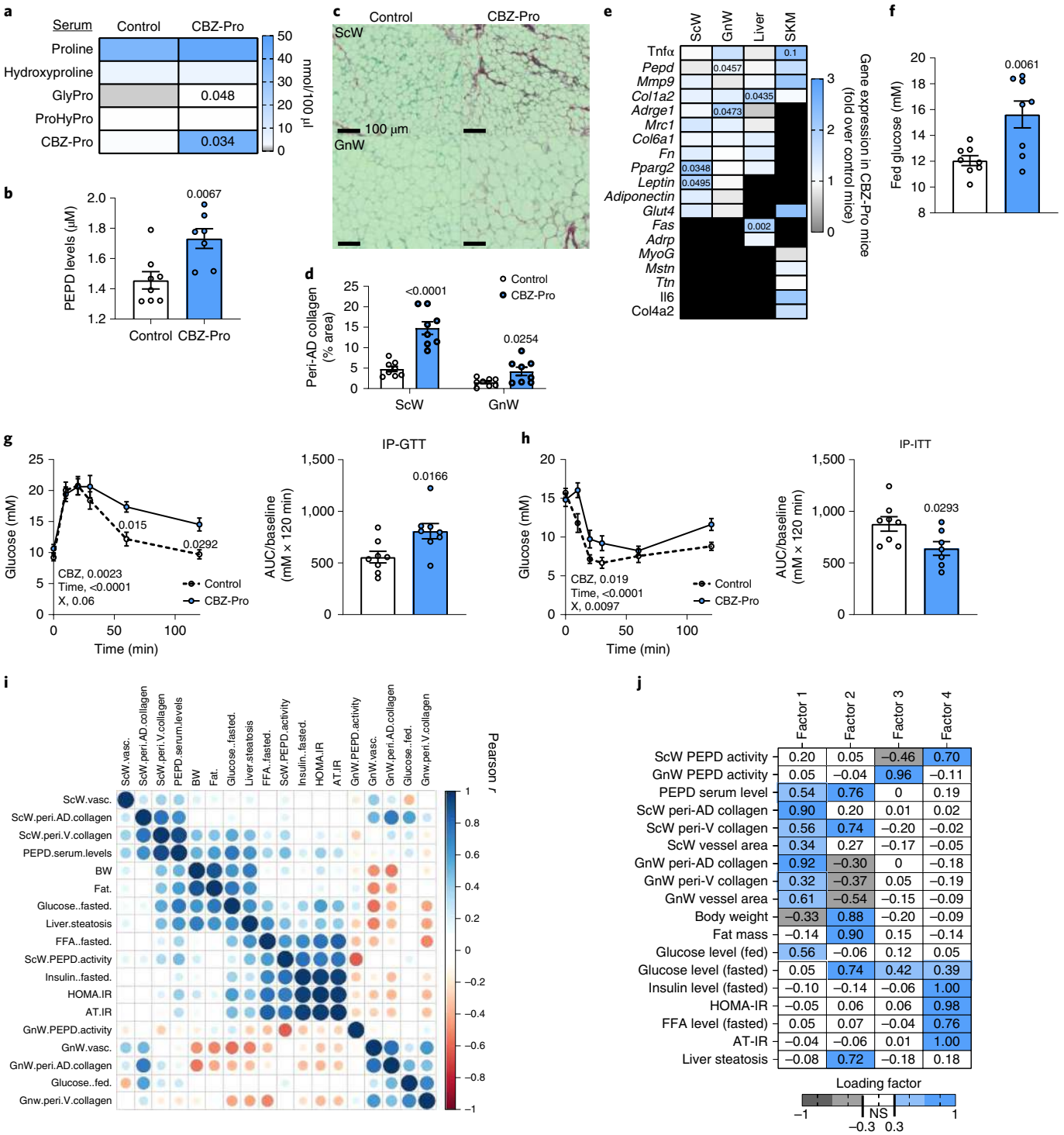

Fig. 2 | Pharmacological inhibition of PEPD promotes adipose tissue fibro-inflammation and insulin resistance in lean mice. a,**b**,**f**, Proline metabolism-related amino acids serum level (**a**), PEPD serum levels (**b**) and fed glucose levels (**f**) in CBZ-Pro-treated mice and littermate controls ($n = 8$ biologically independent animals per group). **c**,**d**, Representative images of red Sirius staining in ScW and GnW of control and CBZ-Pro-treated mice ($n = 8$ biologically independent animals per group) (**c**) and corresponding quantification (**d**) of peri-AD collagen deposition represented in the percentage area (peri-AD collagen). **g**,**h**. Blood glucose levels up to 120 min after an intraperitoneal injection of glucose (2 g per kg BW) in a GTT (**g**) or insulin (0.75 IU per kg BW) in an ITT (**h**) with the representative AUC (**g**) or area over the curve (AOC; **h**) values in control and CBZ-Pro-treated mice ($n = 8$ biologically independent animals per group). **i**, Pearson correlations between ScW and GnW ECM remodelling markers, PEPD serum levels and metabolic parameters in control and CBZ-Pro-treated mice ($n = 16$ biologically independent animals). **j**, Heat map representing the four factors extracted through EFA. The columns report the factor loadings of the observed variables. Data are presented as mean values ± s.e.m. Data were analysed using a two-tailed Student's *t*-test (**a**, **b** and **d**–**h**). Two-way ANOVA with Sidak's post hoc multiple-comparisons tests (**g** and **h**) was used.

negative loading of PEPD activity in AT depots (Fig. 3d). Additionally, correlation matrix analysis showed a positive association between AT fibrosis and IR (Extended Data Fig. 3g). *Pepd* HET showed similar glucose, FFA levels, and glucose and insulin tolerance than WT mice despite lower fasting insulin levels (Extended Data Fig. 3h–k). However, we found that insulin-induced AKT phosphorylation was lower in both GnW and liver from *Pepd* HET chow-fed mice than WTs, with no observed differences in skeletal muscle (Extended Data Fig. 3l–n).

The development of metabolic complications in *Pepd* HET mice (that is, IR, increased fasting FFA and liver steatosis) was exacerbated on a HFD compared to a chow diet. There were no differences in BW among genotypes following HFD feeding (Extended Data Fig. 4a). *Pepd* HET mice fed HFD 45% resulted in higher fed glucose levels and insulin intolerance than WT mice, despite maintaining similar fasted glucose, insulin and FFA levels (Extended Data Fig. 4b–d). When challenged with HFD 58%[20], *Pepd* HET mice exhibited greater fibro-inflammation in GnW than when challenged with HFD 45% (Extended Data Fig. 4e,f) and demonstrated a trend to glucose and insulin intolerance despite showing lower fasting glucose than WT mice (Fig. 3e–g). *Pepd* HET mice also showed higher FFA levels than controls (Fig. 3g). In addition, the basal AKT phosphorylation in GnW was decreased in *Pepd* HET mice, and the index of adipose tissue and insulin resistance (AT-IR)[21] was higher than in WT mice (Fig. 3h,i). Similarly, the liver of *Pepd* HET mice exhibited more steatosis than that in WT (Fig. 3j). Of note, the basal AKT phosphorylation in the gastrocnemius muscle was not significantly different in *Pepd* HET mice fed either chow or HFD (Extended Data Fig. 4g). Collectively, these results indicate that reduced PEPD activity in *Pepd* HET mice was sufficient to develop AT fibrosis in the absence of obesity and that HFD further exacerbated metabolic complications. Moreover, EFA revealed that IR and liver steatosis could be linked to BW and GnW fibrosis in *Pepd* HET mice fed either chow or HFD (45% and 58%), as these variables clustered and covaried together (factor 2; Fig. 3k).

To unmask the molecular mechanisms underlying the fibrogenic and pathogenic effectors driven by the downregulation of *Pepd*, we performed RNA-sequencing (RNA-seq) analysis for GnW and liver of *Pepd* HET and KO mice fed chow and HFD 45%. Of relevance, gene expression profiling of the gastrocnemius muscle did not differ in *Pepd* mice among genotypes and dietary interventions (Extended Data Fig. 4h). The 45% HFD nutritional challenge was selected to prevent the confounding fibro-inflammatory effect resulting from HFD 58% downregulating *Pepd* in WT mice (Extended Data Fig. 4i). Analysis of differentially expressed gene (DEGs) and the top differentially regulated pathways in GnW *Pepd* HET and KO mice (fed 45% HFD) versus WT mice revealed that *Pepd* HET and KO mice had higher expression of genes involved in actin cytoskeleton and cell cycle regulation, immune system, inflammatory-related pathways and ECM/ECM organization-related proteins (Fig. 4a, Extended Data Fig. 4j and Supplementary Tables 2a–5a). Also, *Pepd* HET mice fed HFD 45% showed lower expression of genes involved in metabolic pathways, including fatty acids, leptin and insulin signalling. The *Pepd* KO mice showed higher expression of genes in the pro-diabetes-related cluster. Validation of these data using additional in vitro and ex vivo experiments confirmed that partial or total *Pepd* ablation results in AT dysfunction characterized by impaired adipogenesis from GnW progenitors, lipolysis in mature adipocytes and leptin secretion from GnW tissue explants (Fig. 4b–f).

Next, we focused on analysing the DEGs related to AT function and fibro-inflammation regulated by HFD 45% on each genotype (Fig. 4g and Supplementary Tables 6a–8a). In response to HFD 45% and compared with chow diet, GnW of the *Pepd* HET mice exhibited higher expression of pro-fibrotic, ECM components, ECM remodelling genes, inflammatory and immune cells and lower expression of metabolic genes.

Extending the transcriptomic analysis to the liver, we observed an enrichment of the DEGs related to 'immune system'-related pathways—mainly T cell-related pathways—were upregulated in *Pepd* KO and HET compared to WT in mice fed a HFD 45%. The 'diabetes' pathway was also enriched in the DEGs upregulated in *Pepd* KO versus WT mice. However, 'matrisome' and 'collagen-formation' pathways were downregulated in both *Pepd* KO and HET livers compared to WT (Fig. 4h, Extended Data Fig. 4k and Supplementary Tables 2b–5b). Further analysis of the DEGs related to fibro-inflammation and steatosis did not reveal significant differences between *Pepd* HET and WT mice in response to HFD (Fig. 4i and Supplementary Tables 6b–8b). These results align with the absence of liver fibrosis in *Pepd*-ablated mice fed HFD 45% (Fig. 4j). However, *Pepd* HET mice showed a more significant upregulation of pro-steatosis markers in response to HFD (that is, beta-oxidation and cholesterol metabolism) than WT mice (Fig. 4i and Supplementary Tables 6b–8b).

Collectively, transcriptomic analyses in GnW and liver confirmed exacerbated GnW fibro-inflammation and dysfunction in both the KO and HET mice when challenged with HFD 45%. The GnW fibro-inflammatory response to HFD was stronger in *Pepd* HET mice than in WT mice. Notably, fibro-inflammation was not exacerbated in the liver of *Pepd*-ablated mice. This supports the relevance of PEPD in ECM remodelling of the AT when challenged with HFD and suggests that hepatosteatosis observed in *Pepd* HET mice might not directly result from ablation of *Pepd* in the liver but as a consequence of AT dysfunction and fibro-inflammation.

The strong pro-inflammatory fingerprint observed in the RNA-seq data suggested that GnW macrophages and immune

Fig. 3 | *Pepd* silencing exacerbates adipose tissue fibro-inflammation and metabolic dysfunctions in diet-induced obese mice. a, PA in ScW, GnW and liver from *Pepd* WT ($n=6$), HET ($n=8$) and KO ($n=5$) mice. **b**, ELISA analysis of PEPD levels in the serum of *Pepd* WT (6) and HET (10) fed chow. **c**, Representative images of red Sirius staining in ScW and GnW from *Pepd* WT ($n=6$), HET ($n=8$) and KO ($n=6$) mice fed chow and quantification of the percentage area of peri-AD collagen. **d**,**k**, Heat map representing the four factors extracted through EFA in *Pepd* mice fed chow (**d**) and HFD 58% (**k**). The columns report the factor loadings of the observed variables. **e**,**f**, Blood glucose levels up to 120 min after an intraperitoneal injection of glucose in a GTT (**e**) or insulin (0.75 IU per kg) in an ITT (**f**) with the representative AUC (**e**) or AOC (**f**) in *Pepd* WT ($n=8$), HET ($n=11$) and KO ($n=9$) mice fed HFD 58%. **g**, Fasting glucose, insulin and FFA levels in *Pepd* WT ($n=8$), HET ($n=11$) and KO ($n=9$) mice fed HFD 58%. **h**, Representative images of blots of total and phosphorylated (S473) AKT protein and beta-actin in GnW from *Pepd* WT ($n=8$), HET ($n=11$) and KO ($n=9$) mice fed HFD 58%. **i**, AT-IR index in *Pepd* WT, HET and KO mice in chow ($n=6$, 8 and 6 biologically independent animals per group, respectively), HFD 45% ($n=9$, 11 and 9 biologically independent animals per group, respectively) and HFD 58% ($n=8$, 11 and 9 biologically independent animals per group, respectively) conditions. **j**, Representative images of H&E staining in liver from *Pepd* WT, HET and KO mice fed chow ($n=4$, 6 and 4, respectively), HFD 45% ($n=7$, 10 and 6 biologically independent animals per group, respectively) and HFD 58% ($n=9$, 11 and 6 biologically independent animals per group, respectively) conditions and quantification of liver steatosis. **k**, Heat map representing the four factors extracted through EFA. The columns report the factor loadings of the observed variables. Data are presented as mean values ± s.e.m. Data were analysed using two-way ANOVA with Turkey's post hoc multiple-comparisons test; G, genotype; X, interaction (**a**, **b**, **e**, **f**, **i** and **j**). One-way ANOVA with Sidak's (**e** and **f**) or Dunnett's (**c**, **g** and **h**) post hoc multiple-comparisons test were used. ND, not detected.

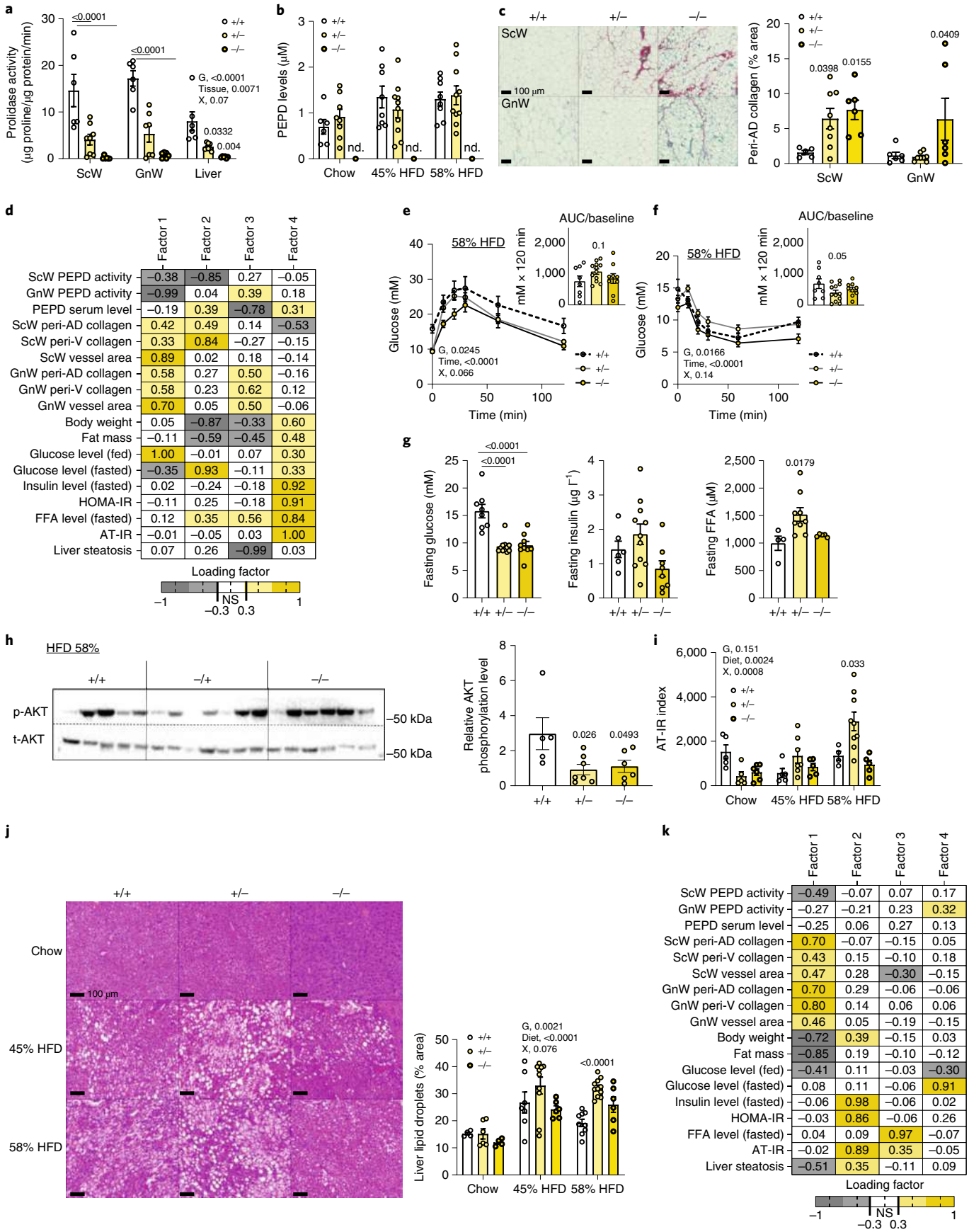
a
Prolidase activity (μg proline/μg protein/min)
<0.0001
<0.0001
G, <0.0001
Tissue, 0.0071
X, 0.07
0.0332
0.004
+/+
+/–
–/–
ScW
GnW
Liver
b
PEPD levels (μM)
nd.
nd.
nd.
Chow
45% HFD
58% HFD
c
+/+
+/–
–/–
ScW
GnW
100 μm
Peri-AD collagen (% area)
0.0398
0.0155
0.0409
d
Factor 1
Factor 2
Factor 3
Factor 4
ScW PEPD activity –0.38 –0.85 0.27 –0.05
GnW PEPD activity –0.99 0.04 0.39 0.18
PEPD serum level –0.19 0.39 –0.78 0.31
ScW peri-AD collagen 0.42 0.49 0.14 –0.53
ScW peri-V collagen 0.33 0.84 –0.27 –0.15
ScW vessel area 0.89 0.02 0.18 –0.14
GnW peri-AD collagen 0.58 0.27 0.50 –0.16
GnW peri-V collagen 0.58 0.23 0.62 0.12
GnW vessel area 0.70 0.05 0.50 –0.06
Body weight 0.05 –0.87 –0.33 0.60
Fat mass –0.11 –0.59 –0.45 0.48
Glucose level (fed) 1.00 –0.01 0.07 0.30
Glucose level (fasted) –0.35 0.93 –0.11 0.33
Insulin level (fasted) 0.02 –0.24 –0.18 0.92
HOMA-IR –0.11 0.25 –0.18 0.91
FFA level (fasted) 0.12 0.35 0.56 0.84
AT-IR –0.01 –0.05 0.03 1.00
Liver steatosis 0.07 0.26 –0.99 0.03
Loading factor
–1
NS
–0.3 0.3
1
e
58% HFD
AUC/baseline
Glucose (mM)
mM × 120 min
G, 0.0245
Time, <0.0001
X, 0.066
0.1
Time (min)
f
58% HFD
AUC/baseline
Glucose (mM)
mM × 120 min
G, 0.0166
Time, <0.0001
X, 0.14
0.05
Time (min)
g
<0.0001
<0.0001
Fasting glucose (mM)
Fasting insulin (μg l⁻¹)
0.0179
Fasting FFA (μM)
+/+ +/– –/–
h
HFD 58%
+/+
–/+
–/–
p-AKT
t-AKT
–50 kDa
–50 kDa
Relative AKT phosphorylation level
0.026
0.0493
i
G, 0.151
Diet, 0.0024
X, 0.0008
0.033
AT-IR index
Chow
45% HFD
58% HFD
j
+/+
+/–
–/–
Chow
45% HFD
58% HFD
100 μm
G, 0.0021
Diet, <0.0001
X, 0.076
<0.0001
Liver lipid droplets (% area)
k
Factor 1
Factor 2
Factor 3
Factor 4
ScW PEPD activity –0.49 –0.07 0.07 0.17
GnW PEPD activity –0.27 –0.21 0.23 0.32
PEPD serum level –0.25 0.06 0.27 0.13
ScW peri-AD collagen 0.70 –0.07 –0.15 0.05
ScW peri-V collagen 0.43 0.15 –0.10 0.18
ScW vessel area 0.47 0.28 –0.30 –0.15
GnW peri-AD collagen 0.70 0.29 –0.06 –0.06
GnW peri-V collagen 0.80 0.14 0.06 0.06
GnW vessel area 0.46 0.05 –0.19 –0.15
Body weight –0.72 0.39 –0.15 0.03
Fat mass –0.85 0.19 –0.10 –0.12
Glucose level (fed) –0.41 0.11 –0.03 –0.30
Glucose level (fasted) 0.08 0.11 –0.06 0.91
Insulin level (fasted) –0.06 0.98 –0.06 0.02
HOMA-IR –0.03 0.86 –0.06 0.26
FFA level (fasted) 0.04 0.09 0.97 –0.07
AT-IR –0.02 0.89 0.35 –0.05
Liver steatosis –0.51 0.35 –0.11 0.09
Loading factor
–1
NS
–0.3 0.3
1

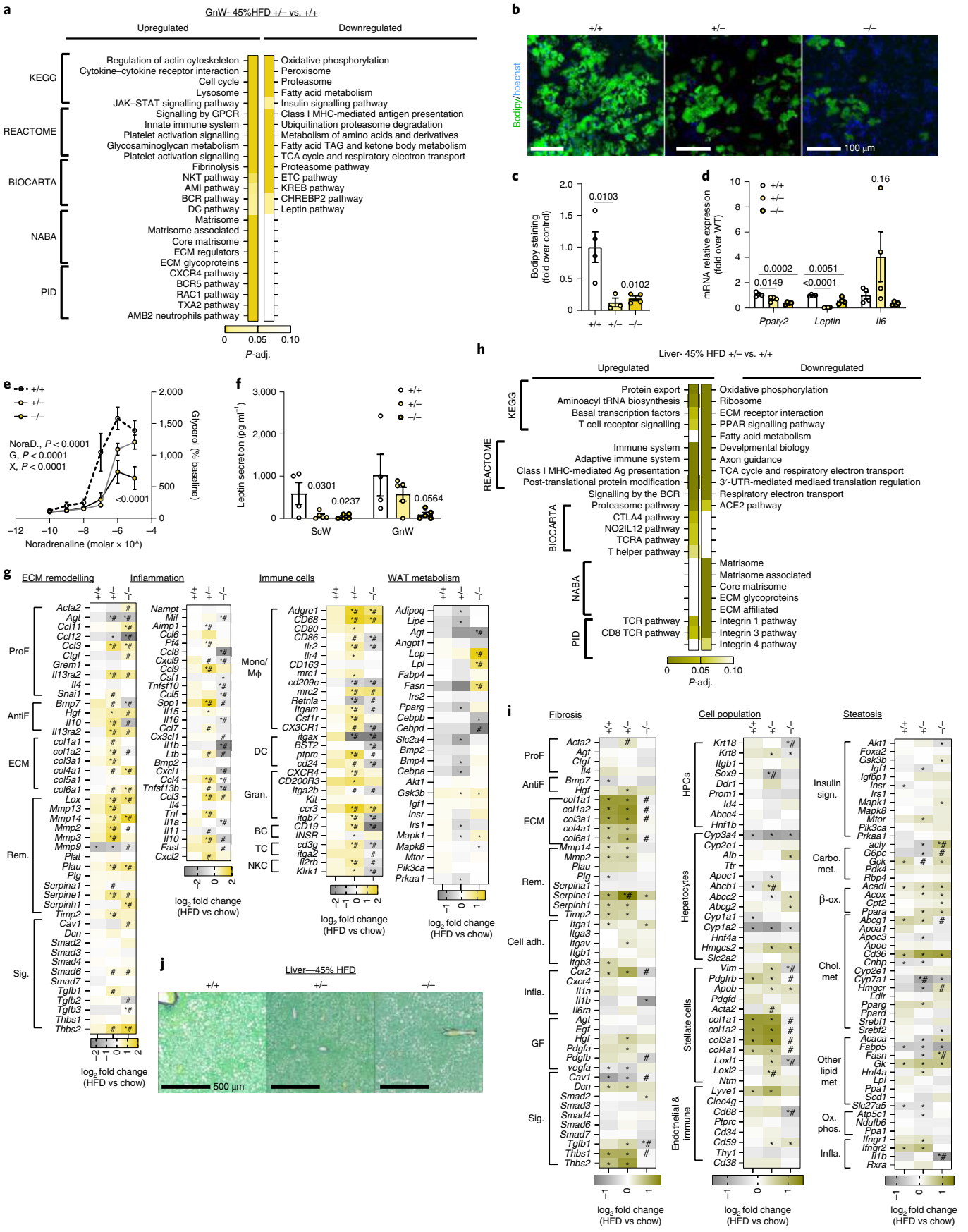
a
GnW- 45%HFD +/– vs. +/+
Upregulated
Downregulated
KEGG
REACTOME
BIOCARTA
NABA
PID
Regulation of actin cytoskeleton
Cytokine–cytokine receptor interaction
Cell cycle
Lysosome
JAK–STAT signalling pathway
Signalling by GPCR
Innate immune system
Platelet activation signalling
Glycosaminoglycan metabolism
Platelet activation signalling
Fibrinolysis
NKT pathway
AMI pathway
BCR pathway
DC pathway
Matrisome
Matrisome associated
Core matrisome
ECM regulators
ECM glycoproteins
CXCR4 pathway
BCR5 pathway
RAC1 pathway
TXA2 pathway
AMB2 neutrophils pathway
Oxidative phosphorylation
Peroxisome
Proteasome
Fatty acid metabolism
Insulin signalling pathway
Class I MHC-mediated antigen presentation
Ubiquitination proteasome degradation
Metabolism of amino acids and derivatives
Fatty acid TAG and ketone body metabolism
TCA cycle and respiratory electron transport
Proteasome pathway
ETC pathway
KREB pathway
CHREBP2 pathway
Leptin pathway
0
0.05
0.10
P-adj.
b
+/+
+/–
–/–
Bodipy/hoechst
100 µm
c
Bodipy staining (fold over control)
0.0103
0.0102
+/+ +/– –/–
d
mRNA relative expression (fold over WT)
+/+
+/–
–/–
0.0002
0.0051
0.0149
<0.0001
0.16
Pparγ2
Leptin
Il6
e
+/+
+/–
–/–
NoraD., P < 0.0001
G, P < 0.0001
X, P < 0.0001
<0.0001
Glycerol (% baseline)
Noradrenaline (molar × 10^)
f
+/+
+/–
–/–
Leptin secretion (pg ml−1)
0.0301
0.0237
0.0564
ScW
GnW
g
ECM remodelling
Inflammation
Immune cells
WAT metabolism
ProF
AntiF
ECM
Rem.
Sig.
Mono/Mϕ
DC
Gran.
BC
TC
NKC
log2 fold change (HFD vs chow)
h
Liver- 45% HFD +/– vs. +/+
Upregulated
Downregulated
KEGG
REACTOME
BIOCARTA
NABA
PID
Protein export
Aminoacyl tRNA biosynthesis
Basal transcription factors
T cell receptor signalling
Immune system
Adaptive immune system
Class I MHC-mediated Ag presentation
Post-translational protein modification
Signalling by the BCR
Proteasome pathway
CTLA4 pathway
NO2IL12 pathway
TCRA pathway
T helper pathway
TCR pathway
CD8 TCR pathway
Oxidative phosphorylation
Ribosome
ECM receptor interaction
PPAR signalling pathway
Fatty acid metabolism
Develpmental biology
Axon guidance
TCA cycle and respiratory electron transport
3′-UTR-mediated mediaed translation regulation
Respiratory electron transport
ACE2 pathway
Matrisome
Matrisome associated
Core matrisome
ECM glycoproteins
ECM affiliated
Integrin 1 pathway
Integrin 3 pathway
Integrin 4 pathway
0
0.05
0.10
P-adj.
i
Fibrosis
Cell population
Steatosis
ProF
AntiF
ECM
Rem.
Cell adh.
Infla.
GF
Sig.
HPCs
Hepatocytes
Stellate cells
Endothelial & immune
Insulin sign.
Carbo. met.
β-ox.
Chol. met
Other lipid met
Ox. phos.
Infla.
log2 fold change (HFD vs chow)
j
Liver—45% HFD
+/+
+/–
–/–
500 µm

Fig. 4 | 'Fibro-inflammatory' and 'adipose tissue dysfunction'-related pathways are enriched in the gonadal white adipose tissue from *Pepd* HET mice. **a**,**h**, Pathway enrichment analysis of the DEGs in GnW (**a**) and liver (**h**) from *Pepd* HET (C; $n=10$) and KO (D, $n=9$) mice compared to WT mice ($n=8$) fed HFD 45%, using different databases (KEGG, Reactome, Biocarta, NABA and PID). The heat maps indicate the level of significant changes (false discovery rate-adjusted *P* value). **b**,**c**, Representative image of confocal analysis (Bodipy staining in green, **b**) and quantification of lipid accumulation (**c**) in primary differentiated adipocytes isolated from GnW of *Pepd* WT, HET and KO mice ($n=4$ biologically independent animals per group). **d**, Gene expression in primary differentiated adipocytes isolated from GnW of *Pepd* WT, HET and KO mice ($n=4$ biologically independent animals per group). **e**, Lipolytic dose-response curves for mature adipocytes isolated from GnW of from *Pepd* WT ($n=5$), HET ($n=7$) and KO mice ($n=6$) in chow condition in response to 2 h of treatment with noradrenaline. **f**, ELISA analysis of leptin secretion from ScW and GnW explants from *Pepd* WT ($n=4$), HET ($n=5$) and KO ($n=5$) mice in chow condition. **g**,**i**, Heat maps of fibro-inflammatory-related (**g** and **i**), metabolism-related (**g**) and steatosis-related (**i**) DEGs in GnW (**g**) and liver (**i**) of *Pepd* WT, HET and KO mice in HFD 45% ($n=8$, 1 and 9 biologically independent animals per group, respectively) expressed as $\log_2$ fold-change ($\log_2$FC) variation over chow diet ($n=4$, 8 and 5 biologically independent animals per group, respectively). ProF, pro-fibrotic; AntiF, anti-fibrotic; Rem, ECM remodelling; Sig, ECM-related signalling; mono/Mφ, monocyte/macrophage; DC, dendritic cell; Gran, granulocyte; BC, B cell; TC, T cell; NKC, natural killer cell. **j**, Representative images of red Sirius staining in the liver from *Pepd* WT ($n=6$), HET ($n=8$) and KO ($n=6$) mice fed HFD 45%. Data are presented as mean values ± s.e.m. One-way ANOVA with Dunnett's post hoc multiple-comparisons test (**c**, **d** and **f**) or two-way ANOVA with Tukey's post hoc multiple-comparisons test (**e**) were used. *Adjusted *P* value < 0.1, significant DEG compared to chow diet. $^{\#}q < 0.05$ compared to *Pepd* WT (+/+). Statistical analysis of the RNA-seq data is detailed in the Methods.

cell-derived factors might contribute to the metabolic phenotypes associated with the genetic ablation of *Pepd* in AT, pointing to a pathogenic link between PEPD dysregulation and immune regulation. Cellular fractionation of GnW from lean mice revealed that macrophages (CD11b$^+$) reported the highest levels of *Pepd* expression compared to mature adipocytes (AD), other immune cells (CD45$^+$), endothelial cells (CD31$^+$) or stromal vascular fractions (SVFs; Fig. 5a). Moreover, PEPD activity increased during macrophage differentiation using bone marrow-derived macrophages (BMDMs; Extended Data Fig. 5a). Consistent with the results from total AT, the expression of *Pepd* was lower in AT macrophages from 16-week-old *ob/ob* mice and mice fed 20 weeks with HFD 45% compared with their controls (genetically lean and chow-fed mice; Fig. 5b and Extended Data Fig. 5b). These findings were validated in humans by showing enrichment of PEPD in human AT immune cells (CD45$^+$; Fig. 5c). Reanalysis of proteomic data from human-induced pluripotent stem cell-derived macrophages (iPSDMs; PXD001953)[22], confirmed the high abundance of PEPD in macrophages compared to undifferentiated induced pluripotent stem cells (iPSCs; Extended Data Fig. 5c). Given that obesity is associated with an imbalance between classically activated macrophages (inflammatory) and alternatively activated macrophages (non-inflammatory), we assessed the modulation of *Pepd* expression by specific macrophage polarizing agents[23]. In keeping with the reduction of *Pepd* expression in inflamed AT of obese mice, *Pepd* expression was also lower in pro-inflammatory M(lipopolysaccharide (LPS)) cells, whereas it was higher in M(GC) and not modulated in M(interleukin (IL)-4)-treated cells compared to unstimulated macrophages (Extended Data Fig. 5d). Additional evidence of the relevance of human macrophages was provided by RNA-seq data comparing undifferentiated human iPSCs and differentiated and analysis of the effect of LPS on human macrophages derived from monocytes (MDMs) and iPSDMs (EGAS00001000563)[24]. In line with mouse models, stem cell transcriptomic analysis confirmed that (1) *PEPD* expression increases during human macrophages differentiation; (2) iPSDMs and MDMs display similar *PEPD* expression levels; and (3) PEPD expression decreases in response to LPS in both iPSDMs and MDMs (Fig. 5d). We then validated at the cellular level that BMDMs treated with CBZ-Pro or LPS decreased PEPD activity (Fig. 5e) and increased PEPD released to the medium compared to non-activated or activated macrophages (Fig. 5f and Extended Data Fig. 5e–g). These results strengthen the functional coupling between the lower enzymatic activity of PEPD in AT and the higher release of PEPD to the extracellular compartment. Interestingly, higher PEPD release from LPS-activated BMDMs was not associated with higher PA in the culture medium, suggesting that released PEPD might exhibit reduced PA following post-translational modifications (Extended Data Fig. 5h).

Fig. 5 | Haematopoietic-specific *Pepd* silencing reduced adipose tissue fibro-inflammation and improved insulin sensitivity in obese mice. **a**, Pie chart illustration of *Pepd* mRNA relative expression distribution in GnW from C57BL/6 mice fed a chow diet ($n=4$ biologically independent animals). AD, adipocytes; CD11b$^+$, macrophages; CD45$^+$, immune cells; CD31$^+$ endothelial cells; SVF$^-$, negative SVF. **b**, *Pepd* mRNA relative expression in CD11b-positive fraction (MΦ) of the GnW from C57BL/6 mice fed chow ($n=4$) and HFD 45% ($n=5$; 20 weeks). **c**, *Pepd* mRNA relative expression in CD45$^+$ and CD45$^-$ cells isolated from VsW of obese participants from cohort 2c ($n=14$ biologically independent samples). **d**, Global transcriptome of iPS cells ($n=6$), iPSDMs ($n=4$) and MDMs ($n=5$) were compared by RNA-seq; and transcripts per million (TPM) values of PEPD mRNA for each condition are plotted on the bar diagram. iPSDMs and MDMs were treated with either 2.5 ng LPS for 6 h or left untreated. **e**,**f**, PA (**e**) and PEPD released level from BMDMs treated or not (control) 24 h with LPS or CBZ-Pro ($n=6$ biologically independent samples per group). **g**, Schematic of the BMT strategy. **h**, Representative image of western blot analysis of PEPD and actin protein expression in BMDMs from *Pepd* WT ($n=5$) and KO mice ($n=4$). **i**,**j**, PA in peritoneal macrophages (**i**), BAT, SCW, GnW, liver and SKM (gastrocnemius) (**j**) from BMT WT ($n=8$) mice compared to BMT KO mice ($n=6$). **k**, ELISA analysis of PEPD levels in the serum of BMT WT ($n=8$) and KO ($n=6$) mice fed chow and HFD 58%. **l**, Representative images of red Sirius staining ScW and GnW from BMT WT ($n=8$) mice compared to BMT KO mice ($n=6$) fed chow and quantification of peri-AD collagen represented as percentages. **m**,**n**, Blood glucose levels up to 120 min after an intraperitoneal injection of glucose (2 g per kilogram BW) in a GTT (**m**) or insulin (0.75 IU per kg BW) in an ITT (**n**) in BMT WT mice ($n=8$) and KO mice ($n=6$) fed HFD 58% for 20 weeks. Respective AUC (**m**) or AOC (**n**) are represented**.** **o**, Representative images of red Sirius staining in liver and quantification of liver steatosis expressed as the percentage lipid droplet area in BMT WT mice ($n=8$) and KO mice ($n=6$) fed a HFD 58% for 20 weeks. *Compared to BMT +/+ chow. $^{\#}P < 0.05$ compared to BMT +/+ HFD 58%. **p**, Heat map of gene expression in GnW, liver and SKM (gastrocnemius) from BMT KO mice ($n=6$) fed chow and HFD 58% (20 weeks) expressed as fold-change variation over BMT WT mice ($n=8$). *q*, Heat map representing the four factors extracted through EFA. The columns report the factor loadings of the observed variables. Data are presented as mean values ± s.e.m. One-way ANOVA with Dunnett's (**a**, **e** and **f**) or Tukey's (**d**) post hoc multiple-comparisons test was used. Data were analysed using a two-tailed Student's *t*-test (**b**, **c**, **m**, **n** and **p**). Two-way ANOVA with Turkey's (**l** and **o**), Sidak's (**j** and **l**–**n**) or Dunnett's (**k**) multiple-comparisons test were used; G, genotype; X, interaction.

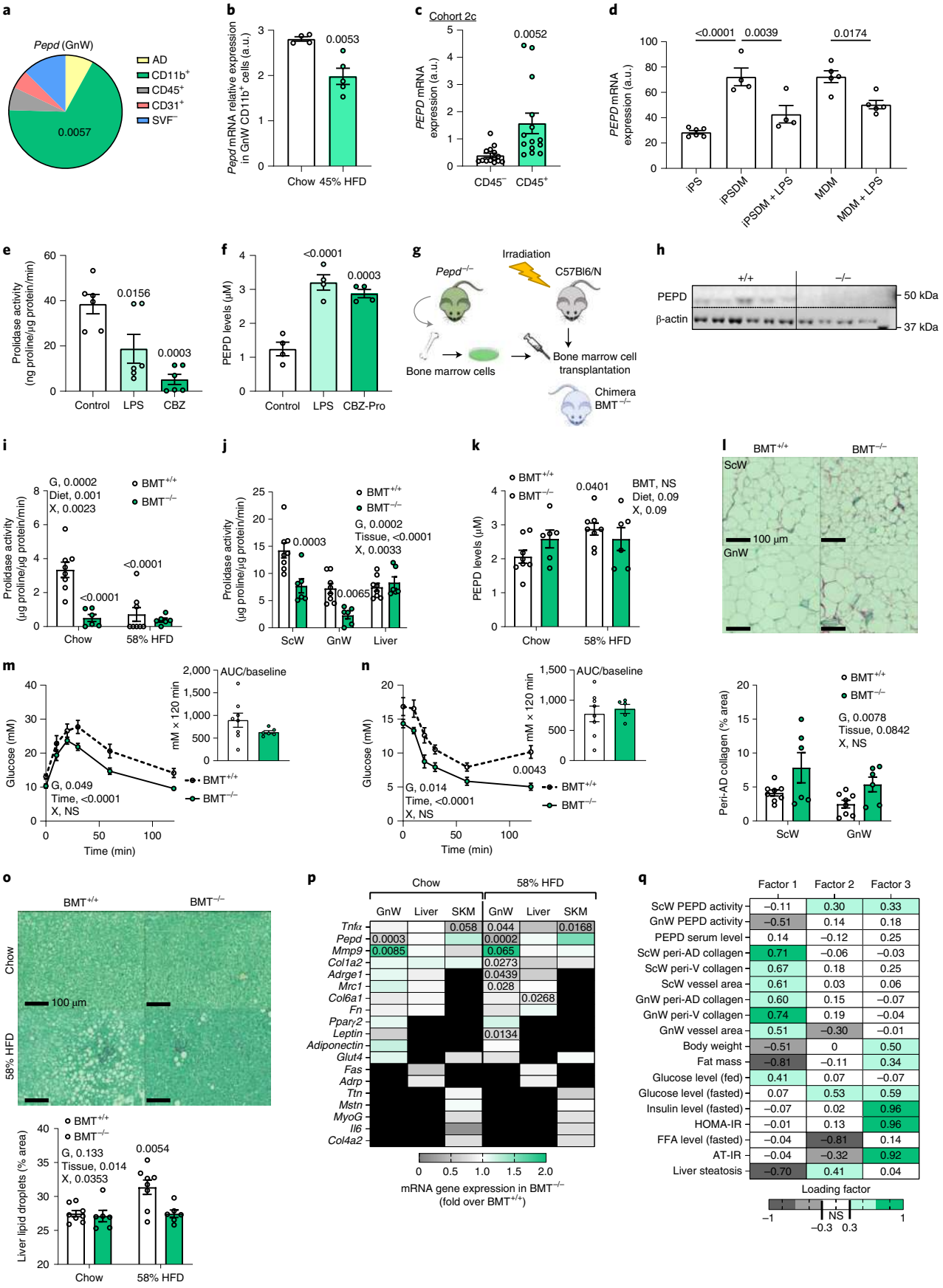
a
Pepd (GnW)
AD
CD11b+
CD45+
CD31+
SVF−
0.0057
b
Pepd mRNA relative expression in GnW CD11b+ cells (a.u.)
0.0053
Chow 45% HFD
c
Cohort 2c
PEPD mRNA expression (a.u.)
0.0052
CD45− CD45+
d
PEPD mRNA expression (a.u.)
<0.0001 0.0039 0.0174
iPS iPSDM iPSDM + LPS MDM MDM + LPS
e
Prolidase activity (ng proline/µg protein/min)
0.0156 0.0003
Control LPS CBZ
f
PEPD levels (µM)
<0.0001 0.0003
Control LPS CBZ-Pro
g
Pepd−/−
Irradiation
C57Bl6/N
Bone marrow cells
Bone marrow cell transplantation
Chimera BMT−/−
h
+/+ −/−
PEPD
β-actin
50 kDa
37 kDa
i
Prolidase activity (µg proline/µg protein/min)
G, 0.0002
Diet, 0.001
X, 0.0023
BMT+/+
BMT−/−
<0.0001 <0.0001
Chow 58% HFD
j
Prolidase activity (µg proline/µg protein/min)
BMT+/+
BMT−/−
G, 0.0002
Tissue, <0.0001
X, 0.0033
0.0003 0.0065
ScW GnW Liver
k
PEPD levels (µM)
BMT+/+
BMT−/−
0.0401
BMT, NS
Diet, 0.09
X, 0.09
Chow 58% HFD
l
BMT+/+ BMT−/−
ScW
100 µm
GnW
m
Glucose (mM)
G, 0.049
Time, <0.0001
X, NS
Time (min)
AUC/baseline
mM × 120 min
BMT+/+
BMT−/−
n
Glucose (mM)
G, 0.014
Time, <0.0001
X, NS
Time (min)
AUC/baseline
mM × 120 min
0.0043
BMT+/+
BMT−/−
Peri-AD collagen (% area)
BMT+/+
BMT−/−
G, 0.0078
Tissue, 0.0842
X, NS
ScW GnW
o
BMT+/+ BMT−/−
Chow
58% HFD
100 µm
Liver lipid droplets (% area)
BMT+/+
BMT−/−
G, 0.133
Tissue, 0.014
X, 0.0353
0.0054
Chow 58% HFD
p
Chow 58% HFD
GnW Liver SKM GnW Liver SKM
Tnfα 0.058 0.044 0.0168
Pepd 0.0003 0.0002
Mmp9 0.0085 0.065
Col1a2 0.0273
Adrge1 0.0439
Mrc1 0.028
Col6a1 0.0268
Fn
Pparγ2
Leptin 0.0134
Adiponectin
Glut4
Fas
Adrp
Ttn
Mstn
MyoG
Il6
Col4a2
0 0.5 1.0 1.5 2.0
mRNA gene expression in BMT−/−
(fold over BMT+/+)
q
Factor 1 Factor 2 Factor 3
ScW PEPD activity −0.11 0.30 0.33
GnW PEPD activity −0.51 0.14 0.18
PEPD serum level 0.14 −0.12 0.25
ScW peri-AD collagen 0.71 −0.06 −0.03
ScW peri-V collagen 0.67 0.18 0.25
ScW vessel area 0.61 0.03 0.06
GnW peri-AD collagen 0.60 0.15 −0.07
GnW peri-V collagen 0.74 0.19 −0.04
GnW vessel area 0.51 −0.30 −0.01
Body weight −0.51 0 0.50
Fat mass −0.81 −0.11 0.34
Glucose level (fed) 0.41 0.07 −0.07
Glucose level (fasted) 0.07 0.53 0.59
Insulin level (fasted) −0.07 0.02 0.96
HOMA-IR −0.01 0.13 0.96
FFA level (fasted) −0.04 −0.81 0.14
AT-IR −0.04 −0.32 0.92
Liver steatosis −0.70 0.41 0.04
Loading factor
−1 NS 1
−0.3 0.3

***Pepd* ablation in haematopoietic cells uncouples adipose tissue fibrosis from metabolic alterations.** To dissect the pivotal role of PEPD secreted from macrophages driving fibro-inflammation and metabolic disturbances, we performed a bone marrow transplant (BMT) from *Pepd* KO into WT recipient mice to ablate *Pepd* exclusively in HCs (Fig. 5g,h). BMT is commonly used in the literature to target adipose tissue macrophages (ATMs)[25–27] as approximately 85% of the ATMs originate from the bone marrow[28]. Thus, BMT KO mice showed similar adiposity to BMT WT mice (when fed a chow diet). BMT KO mice showed reduced PA of 85% in peritoneal macrophages and 50% in the whole AT (Fig. 5i,j). As anticipated, the reduction in PEPD activity by genetic manipulation was not associated with increased PEPD levels in serum. This contrasted with the increase observed in secreted PEPD levels in CBZ-Pro-treated mice or dietary models of obesity (Fig. 5k). As previously seen in models with global decreased PEPD activity, the BMT KO also had increased collagen accumulation in AT compared to BMT WT (Fig. 5l). However, the BMT KO mice maintained carbohydrate metabolic homeostasis in contrast to the chow-fed CBZ-Pro-treated mice, in which the decreased PEPD activity was inversely associated with PEPD secretion (Extended Data Fig. 5i–n). Of note, BMT KO mice adiposity was marginally lower than that of WT mice when fed a chow diet but it was significantly lower when fed 58% HFD (Extended Data Fig. 5o–q). Furthermore, when fed 58% HFD, the BMT KO mice exhibited more fibrosis than WT mice but were resistant to obesity and associated metabolic disturbances (that is, glucose and insulin tolerance, AT IR and liver steatosis; Fig. 5l–o and Extended Data Fig. 5r,s). In addition, while GnW showed reduced fibro-inflammatory markers expression, liver and skeletal muscle did not show significant changes at the gene expression level, reinforcing the importance of macrophage PEPD of the GnW in regulating metabolic functions (Fig. 5p). Thus, the BMT KO model exhibited increased AT fibrosis uncoupled from metabolic complications such as IR and liver steatosis, and pointed to the relevance of the extracellular PEPD produced by macrophages as a critical trigger of fibro-inflammation and metabolic complications. Moreover, EFA run for BMT chow-fed mice confirmed the negative association between AT fibrosis and PEPD enzymatic activity (factor 1; Fig. 5q), and factor 3 showed that AT IR-related parameters (that is, AT-IR and FFA levels) covaried with PEPD serum levels (Fig. 5q). Thus, these results support that extracellular PEPD might be an essential trigger of AT fibro-inflammation and related metabolic dysfunctions.

We investigated whether the released PEPD per se was a determinant of macrophages polarization and could trigger inflammation. Treatment of macrophages with purified PEPD protein-induced phosphorylation of nuclear factor-kappa B (NF-κB; ser536) and the expression of inflammatory markers, such as *cox2* and *il-1β*, while non-inflammatory markers *mgl1* and *mrc2* were downregulated (Fig. 6a and Extended Data Fig. 6d). Phospho-kinase proteome analysis using a profiler array on PEPD-treated BMDMs confirmed that PEPD phosphorylated EGFR (Extended Data Fig. 6e,f)[15]. Pretreatment of macrophages with erlotinib, an EGFR-specific tyrosine kinase inhibitor, attenuated PEPD-induced NF-κB phosphorylation, as well as *cox2* and *il1β* expression (Fig. 6b,c and Extended Data Fig. 6g). We further confirmed this association by showing that PEPD-induced *Cox2* and *Il1β* expression was reduced in response to *Egfr* silencing (~75%) (Extended Data Fig. 6h–j).

Purified PEPD promotes adipose tissue fibro-inflammation and insulin resistance. Using the Tabula Muris database[29], we observed that AT, liver and muscle were the organs with the highest *Egfr* expression (Extended Data Fig. 6k). We rationalized that secreted PEPD from macrophages could also signal to other cells in AT or other organs through EGFR-dependent pathways. To test the effect of PEPD at the whole-organism level, C57BL/6N chow-fed mice were injected intraperitoneally with purified PEPD protein three times a week for 6 weeks. We investigated the gene expression of *Cox2*, known to be induced by PEPD through EGFR-dependent pathways[15] and found that GnW showed the most significant increase in *Cox2* expression (Fig. 6l). Following injection of PEPD, the tissular PA remained unchanged compared to control mice (Extended Data Fig. 6m), indicating that the effects observed in mice injected were independent of its enzymatic activity. While BW, body composition, insulin tolerance test (ITT) and glucose tolerance test (GTT) were unaltered after PEPD injection (Fig. 6d and Extended Data Fig. 6n–r), we observed active tissue remodelling, notably in the GnW, with increased peri-adipocyte fibrosis in PEPD-injected mice compared to control (Fig. 6e). Of relevance, the collagen and ECM remodelling enzymes' mRNA expression levels were strongly downregulated, suggesting the existence of compensatory mechanisms (Fig. 6f,g). We observed higher presence of crown-like structures around adipocytes close to high expression of macrophage markers of 'M2 tissue remodelling' in PEPD-injected mice compared to controls (Fig. 6e,g). Expression of adipocyte markers was reduced in AT from PEPD-injected mice (Fig. 6h), and both basal AKT phosphorylation levels and GLUT4 protein expression were reduced in GnW, indicative of reduced AT insulin sensitivity (Fig. 6i).

In support of these in vivo results, we characterized in vitro the effect of added extracellular PEPD on differentiated and non-differentiated preadipocytes, considered critical pro-fibrotic cellular effectors in the AT[30,31], and on mature primary adipocytes. Supporting a direct pro-inflammatory role, purified PEPD increased *Il6* expression in differentiated preadipocytes, promoted the production of collagen I, and prevented lipid accumulation in preadipocytes in part through a mechanism involving EGFR signalling (Extended Data Fig. 7a). Purified PEPD protein also induced IL-6 release from mature adipocytes (Extended Data Fig. 7b). However, while purified PEPD increased mRNA expression of inflammatory markers and deposition of collagen from hepatic stellate cells

Fig. 6 | Purified PEPD protein induces fibro-inflammation and adipose tissue insulin resistance. a, Heat map of gene expression in BMDMs after 4 h of treatment with purified PEPD protein ($n = 4$ biologically independent samples). **b**, Representative images of blots and quantification of total and phosphorylated (S536) NF-kB protein and beta-actin in BMDMs ($n = 4$ biologically independent samples) pretreated or not with erlotinib (5 μM) and prior treatment with purified PEPD protein (0, 10 and 60 min; 250 nM), and quantification. **c**, *IL1B* mRNA relative expression in BMDMs ($n = 4$ biologically independent samples) pretreated or not (PBS) with erlotinib 5 μM and prior treatment with (PEPD) or without (control) purified PEPD protein (250 nM) for 24 h. *compared to control PBS, #compared to PEPD PBS. **d**, BW curve in PEPD-treated mice compared to control (saline) mice ($n = 11$ biologically independent animals per group) fed a chow diet between 0 and 6 weeks of treatment. **e**, Representative images of red Sirius staining in GnW PEPD-treated mice compared to control (saline) mice ($n = 11$ biologically independent animals per group) fed chow diet and quantification of peri-AD collagen (represented as a percentage) and crown-like structures (CLS). **f**–**h**, mRNA expression of ECM remodelling (**f**), macrophage polarization markers (**g**) and adipocyte markers (**h**) in GnW (from PEPD-injected mice compared to controls; $n = 11$ biologically independent animals per group). **i**, Representative images of blots of total and phosphorylated (S473) AKT protein, GLUT4, GADPH and beta-actin in GnW from PEPD-injected mice compared to controls ($n = 11$ biologically independent animals per group). **j**, Heat map representing the four factors extracted through EFA. The columns report the factor loadings of the observed variables. Data are presented as mean values ± s.e.m. Data were analysed using a two-tailed Student's *t*-test (**a**, **e**–**i**). Two-way ANOVA with Tukey's (**b** and **c**) or Sidak's (**e**) multiple-comparisons test was used; erlo, erlotinib; X, interaction.

(HSCs) in vitro, we did not observe any effect on liver fibrosis or lipid accumulation, nor changes in gene expression profile (of functional, inflammatory and fibrotic genes) in the liver in vivo (Extended Data Fig. 7c–g). Similarly, we did not observe any effect on skeletal muscle fibro-inflammation, despite higher mRNA expression of *Tnf* compared to control mice (Extended Data Fig. 7h,i). In vitro, PEPD

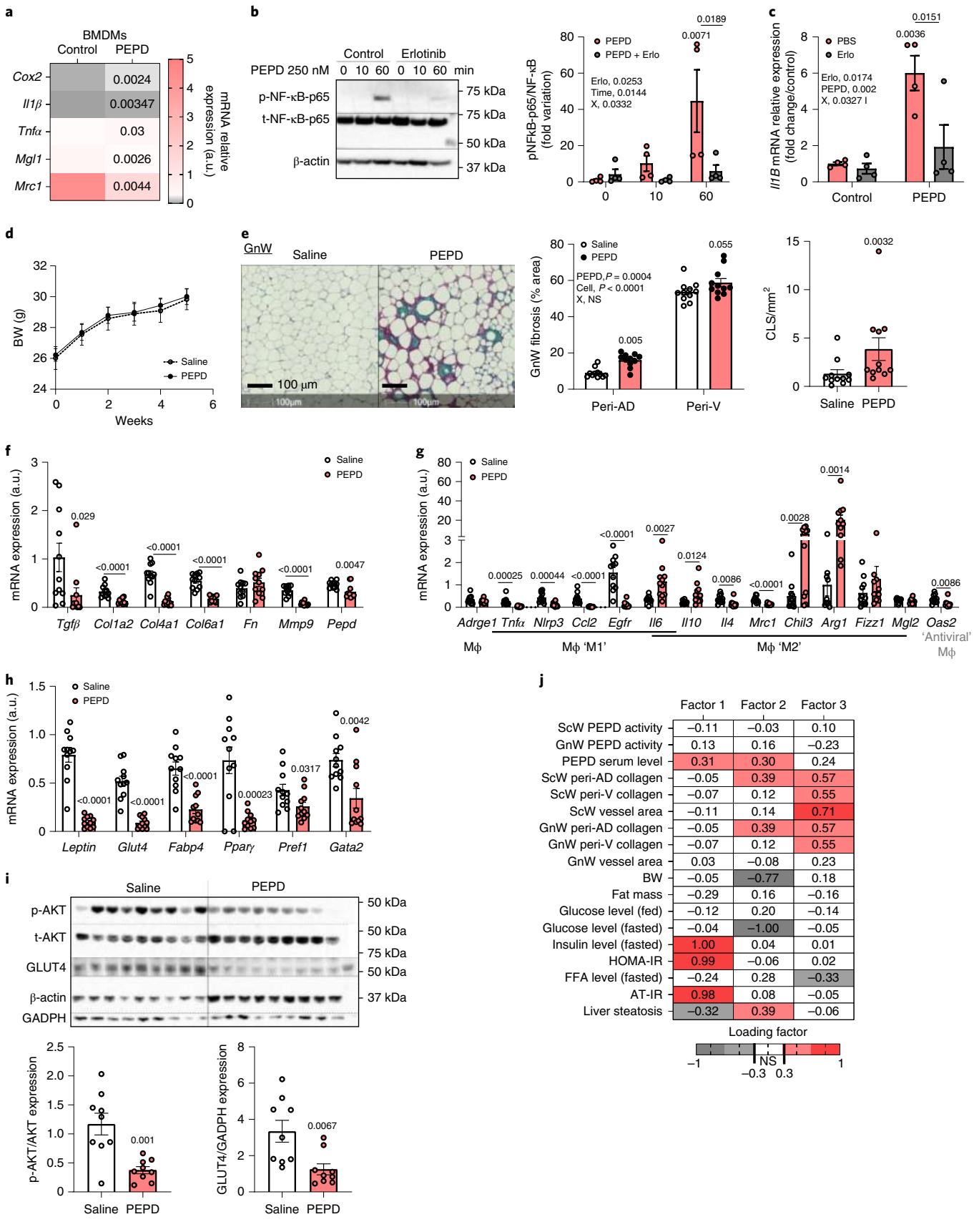

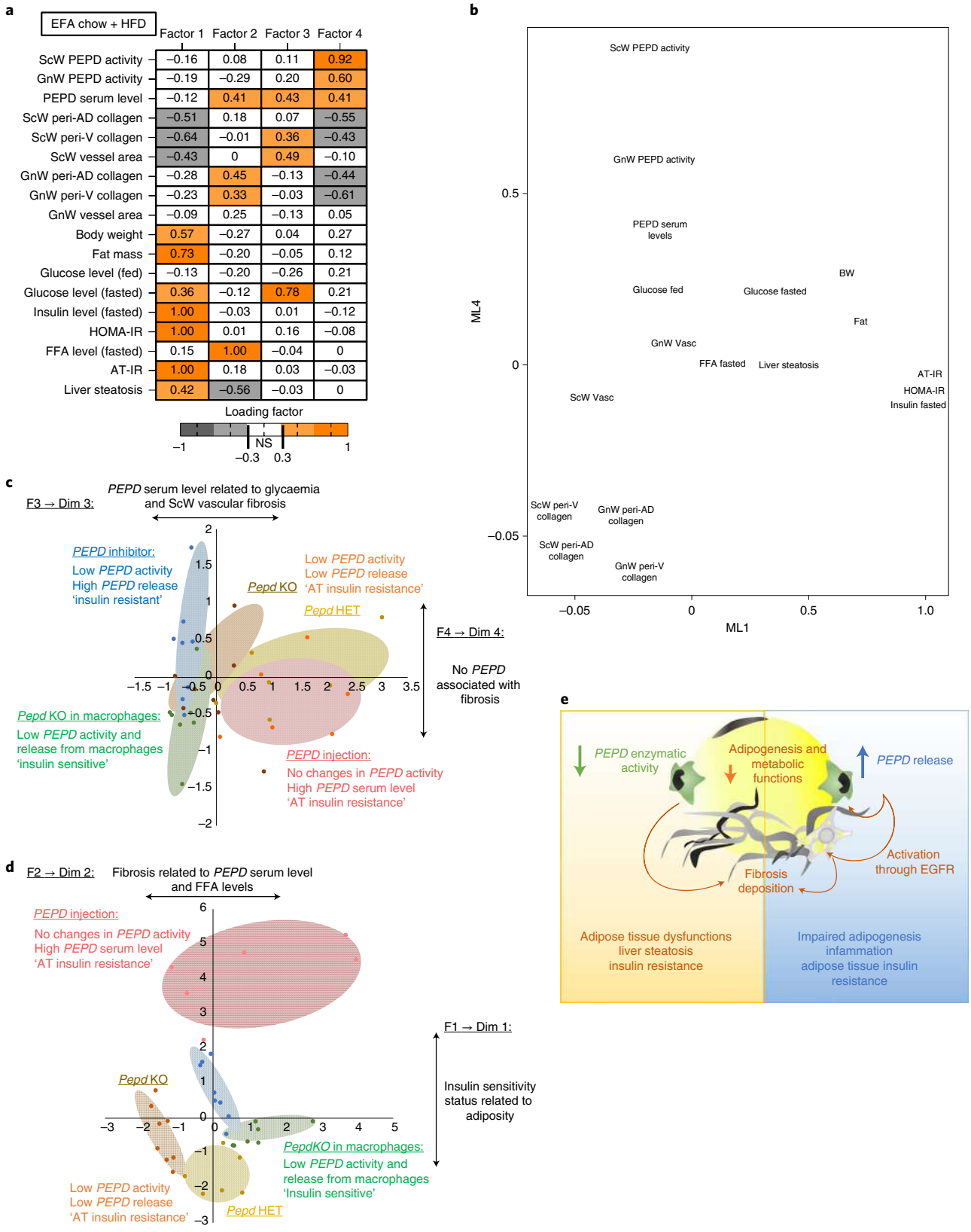

Fig. 7 | High PEPD serum levels are associated with adipose tissue insulin resistance and drives the differences between the pharmacological and genetic animal models of PEPD downregulation. a, Heat map representing the four factors extracted through EFA performed among the mice from the four animal models (that is, PEPD, CBZ-Pro, BMT and PEPD injection) that were fed a chow or a HFD. The columns report the factor loadings of the observed variables. **b**–**d**, Metabolic/fibro-inflammatory parameters (**b**) and mice from the four animal models (that is, CBZ-Pro, PEPD, BMT and PEPD injection; **c**) were plotted according to factors 1 and 4 (**b**), to factors 1 and 2 (**c**) or factors 3 and 4 (**d**). **e**, Summary of proposed roles of PEPD in obesity-associated AT dysfunctions and metabolic complications.

had a mild effect on muscle fibroblasts, inducing *Cox2* and *Ccnd1* expression (Extended Data Fig. 7j). These effects were reversed in response to erlotinib, supporting the role of EGFR as a mediator of PEPD effects. While PEPD did not modify collagen production in muscle, we found that it did increase αSMA protein expression suggesting activation of fibroblasts in response to exogenous PEPD. Nevertheless, this effect on αSMA staining was not reversed in the presence of erlotinib (Extended Data Fig. 7k). Altogether, these results suggest that purified PEPD treatment targeted GnW inducing severe tissue remodelling and IR. Moreover, EFA supported a causal relationship between serum PEPD levels, insulin sensitivity (factor 1) and GnW fibrosis (factor 2; Fig. 6j).

Secreted PEPD is the primary pathogenic factor in fibro-inflammation. To dissect the main pathogenic factors linking specific PEPD dysregulation and metabolic and fibro-inflammatory differences, we performed a global integrative correlation matrix analysis and EFA, integrating the four PEPD in vivo experimental models (pharmacological, genetic, macrophage-specific genetic ablation and exogenous PEPD treatment). Correlation analysis, including either chow-fed mice alone or with HFD-fed animals, revealed a negative correlation between the level of AT fibrosis and PEPD activity accounting for the reduced AT PEPD activity and fibrosis in these models (except the PEPD injection experiment; Extended Data Fig. 8b,c). In agreement with this, EFA performed in chow-fed mice showed that factor 3, clustering AT fibrosis-related variables, had negative loading of AT PEPD activity and BW (Extended Data Fig. 8a). This inverse relationship was observed between AT fibrosis and PEPD activity when EFA included chow-fed and HFD-fed animals (factor 4; Fig. 7a). We then transformed the data to plot and visualize in two dimensions the relationship between the variables (Fig. 7b and Extended Data Fig. 8d) and the animal models. We observed that CBZ-Pro and BMT mice diverged in dimension 4 (corresponding to factor 4), in which fibrosis covaried negatively with both PEPD activity and serum level, that is, fibrosis could be explained by the absence of PEPD (Fig. 7c). This association is consistent with evidence that, in contrast to BMT KO mice with no PEPD released from macrophages, the CBZ-Pro-treated mice displayed a higher release of PEPD. Notably, they also differed in terms of insulin sensitivity status. Therefore, these data strengthen the role of PEPD released from macrophages in promoting IR. Factor 3, clustering ScW vascular fibrosis and glucose levels, had high loading of PEPD serum levels (Fig. 7a). Interestingly, *Pepd* HET mice fed a HFD 58% and PEPD-injected mice overlapped in this dimension (dim 3), suggesting similarities between these two models regarding the role of serum PEPD in promoting AT fibrosis (Fig. 7c). Of note, these two models also shared AT IR. However, *Pepd* HET mice fed HFD 58% and PEPD-injected mice diverged in dimension 1 (corresponding to factor 1), in which the insulin sensitivity status could be explained by adiposity (Fig. 7a,d). Indeed, while both models displayed AT IR, *Pepd* HET mice fed a HFD were obese, while PEPD-injected mice remained lean. Finally, *Pepd* KO mice and both CBZ-Pro/PEPD-injected mice diverged on dimension 2 (corresponding to factor 2) in which GnW fibrosis and FFA levels covaried with PEPD serum levels, that is, AT fibrosis and higher FFA levels could be explained by higher PEPD serum level (Fig. 7a,d). Therefore, *Pepd* KO mice differed from CBZ-Pro mice and PEPD-injected mice because displaying higher PEPD serum levels exacerbated metabolic complications and fibrosis deposition in GnW.

Discussion

Departing from human GWAS identifying PEPD as a potential causal gene of IR and dyslipidaemia[8,9,11], we focused on its role in metabolic organs in the context of obesity. In obesity, PEPD was downregulated exclusively in AT, notably in the gonadal depot, where we posited that it would play a central role, but not in skeletal muscle or liver. A critical observation was that the lower the PA in GnW (or the visceral depot in humans), the higher the PEPD levels detected in the serum of obese mice and humans. The liver appeared to be an essential organ contributing to serum levels of PEPD. However, gonadal fat was the only tissue where PEPD release is altered by HFD. We, therefore, hypothesized that the higher PEPD serum level observed in obese participants might reflect the release of PEPD from the GnW. Our in vivo and in vitro time-course HFD and LPS treatments, respectively, suggest that the release of PEPD might occur secondary to the decreased PA. In line with this hypothesis, our animal/cellular models in which PEPD was pharmacologically/nutritionally manipulated (HFD, CBZ-Pro or LPs-treated macrophages) showed that when the PA was inhibited, the PEPD release (in serum or the extracellular compartment) was increased. Conversely, in genetically manipulated mice—that is, in both PEPD total KO and macrophage-specific KO (BMT model), the *Pepd* gene had been ablated. Therefore, both PEPD activity and release are suppressed, either globally (totally in the KO and partially in the HET mice) or in the HCs (BMT model). These designs justify why the decreased PA in PEPD genetic models is not associated with an increased release of PEPD at the systemic level. Of note, the serum level of PEPD changed in the BMT KO mice that were fed a HFD. Collectively these data suggest that, under physiological conditions, the amount of PEPD released from/by the macrophage population might be quantitatively marginal compared to the contribution of other organs/cell types. However, under pathogenic conditions, such as a HFD, the expected increase in PEPD serum level was blunted suggesting that macrophages might play a more relevant role in contributing to the elevated serum PEPD observed in obesity. We cannot completely exclude that other cells in the haematopoietic fraction might also contribute to the phenotype of the BMT KO mice, a question that will require further investigation.

The specific routes and mechanisms regulating the release of PEPD from cells still need to be defined. PEPD has been reported in several large-scale profiling studies to be secreted in exosomes[32–35]. Inflammation (for example, obesity in vivo and LPS in vitro) could also be a possible trigger. There is some evidence supporting a role for reactive oxygen species and reactive nitrogen species regulating the secretion of PEPD and its intracellular peptidase activity[36–38].

Our results indicate that the extracellular PEPD exacerbated fibro-inflammation and IR in obesity. However, whereas PEPD serum levels were higher in obese mice, their serum PA was not modified, suggesting that the extracellular effect was independent of the peptidase activity of PEPD. While *Pepd* HET, BMT KO and CBZ-Pro-treated mice shared decreased intracellular PEPD enzymatic activity and increased fibrosis in AT, they diverged in other metabolic aspects. The CBZ-Pro-treated mice had a low residual enzymatic activity level and the highest increase in secreted PEPD, exhibiting the most severe metabolic phenotype in terms of AT fibro-inflammation and metabolic disorders. In contrast, when fed a chow diet, *Pepd* HET and BMT KO mice did not exhibit increased PEPD in the serum and showed a milder metabolic phenotype. *Pepd* HET mice only showed mild metabolic dysfunction when fed a 58% HFD, known to promote PEPD release from the AT further. Using purified PEPD exogenously, we showed that in vivo and in vitro PEPD treatment promotes AT fibrosis and IR. Thus, we propose that 'decreased PA' and 'increased PEPD serum level' independently induce metabolic complications.

Our results conclude that dysregulation of PEPD elicits a dual role in mediating AT fibrosis and metabolic risk through complementary mechanisms. This conclusion was obtained by integrating the phenotypical data from mouse in vivo models of dysregulated PEPD activity and/or secretion. This study provides a strong rationale for measuring serum PEPD in obese individuals to identify and stratify those at a higher metabolic risk by recognizing their susceptibility to AT fibrosis and inflammation.

Methods

Human studies. Age, BMI and glycaemic status of the different cohorts can be found in Supplementary Fig. 1a.

Cohorts 1 and 3. In cohort 1, we analysed 84 VsW and 70 ScW samples from participants from Dr Josep Trueta University Hospital (Girona) with a wide range of adiposity (BMI between 20 and 68 kg/m^2). In cohort 3, 46 VsW and 36 ScW samples from morbidly obese participants (BMI > 35 kg/m^2) were analysed. Participants were of European ancestry with stable BW for 3 months. Participants were studied in the post-absorptive state, had no systemic disease other than obesity, and were free of any infections in the month before the study. Specific biochemical tests excluded liver diseases (tumoral disease and hepatitis C virus infection) and thyroid dysfunction. All participants gave written informed consent, which was validated and approved by the ethical committee. Samples were partially provided by the FATBANK (CIBEROBN) coordinated by the IDIBGI Biobank (Biobanc IDIBGI, B.0000872), Spanish National Biobanks Network, processed following standard operating procedures with approval of the Ethics, External Scientific and FATBANK Internal Scientific Committees. Subcutaneous and visceral AT samples were obtained from cholecystectomy, abdominal hernia and gastric bypass surgical procedures.

Cohort 2. ScW and VsW (omental) biopsy samples were obtained from severely obese (BMI > 35 kg/m^2) and lean participants (BMI ≤ 25 kg/m^2) undergoing elective surgery. Obese individuals who were candidates for bariatric surgery were studied in Paris following the Helsinki Declaration and Ethics Committee of Clinical Research (CPP Ile-de-France 1, Fibrota study, clinical trial no. NCT01655017). Patient phenotyping is described in ref. [39]. Blood sampling was performed fasted 1 month before the surgery. The same surgeon obtained paired ScW and VscW samples. Among glucose-intolerant and diabetic participants (n = 15), 7 were treated with metformin, 3 with insulin and 2 with a GLP1 agonist. Exclusion criteria included anaemia, abnormal thyroid-stimulating hormone, human immunodeficiency virus and/or hepatitis C virus infection, severe hepatic and/or renal failure and inflammatory disorders. Signed informed consents were obtained in all lean and obese individuals who agreed with ethics regulations.

Animals. Male C57BL/6J mice aged 8–10 weeks old were purchased from Charles River. *Pepd* KO mice were generated by the Wellcome Trust Sanger Institute Mouse Genetics Project on a C57BL/6J background by mating heterozygous mice. *Pepd* homozygous (null and WT) and heterozygous pups were observed in normal Mendelian ratios. In respect to the 3R, only a subpopulation of the pups born was selected for each study. Male *Pepd* WT, HET and KO mice aged 8–10 weeks old were used for each experiment. Male WT and leptin-deficient mice aged 8–10 weeks, *Lep*$^{Ob/Ob}$, were on a C57BL/6 background. Details of the mouse models are provided in Supplementary Table 9. This research has been regulated under the Animals (Scientific Procedures) Act 1986 Amendment Regulations 2012 following ethical review by the University of Cambridge Animal Welfare and Ethical Review Body under pathogen-free conditions and housed according to UK Home Office guidelines and carried out in the Disease Model Core unit. Animals were housed in groups of 3–4 mice per cage in a temperature-controlled room (22 °C) with a 12-h light–dark cycle, with 55% relative humidity and ad libitum access to food and water. A standard chow diet (DS-105, Safe Diets) was administered to all animals from weaning, consisting of 64.3% carbohydrate, 22.4% protein and 13.3% lipid of total calories. Only male mice were used for in vivo experiments, isolation of primary cells (that is, adipose cells, HSCs and muscle fibroblasts) and preparation of BMDMs.

Generation of bone marrow chimeras. C57BL6/J mice at 10 weeks of age received a sublethal dose of whole-body irradiation (9 Gy). The day after irradiation, donor *Pepd* KO mice were culled, and their femurs and tibias were removed aseptically. Marrow cavities were flushed in RPMI medium, and single-cell suspensions were prepared. The irradiated recipients received 1×10^7 bone marrow cells in 0.1 ml of PBS by tail-vein injection. During 4 weeks after BMT, Bactrim (Roche) was added to drinking water. After two additional weeks, mice were switched to a 58% HFD. Mice were culled 16 weeks later to collect blood and tissues.

Diets and pharmacological challenges. *Diets.* Diets for animal studies included standard chow (10% calories from lipid), HFD 45% (D12451, Research Diets, 45% calories from lipid) and HFD 58% (D12331, Research Diets, 58% calories from lipid). Standard chow or HFD was provided ad libitum to animals from 8 weeks old until indicated.

Insulin injection. Male 8- to 10-week-old WT, *pepd* HET and *Pepd* KO mice were injected intraperitoneally with saline solution or insulin (2 U per kilogram BW) for 15 min.

Pharmacological inhibition of PEPD. Male 8-week-old C57BL/6J male mice were first fed with chow or HFD 58% for 10 weeks. CBZ-Pro-supplemented pellets (both chow and HFD 58%) were prepared daily by spraying and mixing a solution of CBZ-Pro (2 mM) dissolved in 70% ethanol. Mice consumed an approximatively daily dose of 60 mg per kg BW of CBZ-Pro, a dose previously used in other murine studies[19], with treatment lasting for 6 weeks, and control mice were offered regular pellets. CBZ-Pro does not alter viability or promote toxic effects in mice[19]. CBZ-Pro-treated mice did not show evidence of hepatotoxicity/liver damage (alanine aminotransferase or ASAT levels; Extended Data Fig. 2a).

PEPD treatment. Male 8- to 10-week-old C57BL/6N mice were injected intraperitoneally with the purified PEPD protein (0.2 mg per kg BW) or saline three times a week for 6 weeks[40]. ITTs and DTTs were performed at weeks 4 and 5. PEPD treatment did not modify the ASAT levels (Extended Data Fig. 7e).

Body composition. Fat and lean masses were calculated by time-domain nuclear magnetic resonance using a minispec Live Mice Analyzer LF50 (Bruker).

Glucose and insulin tolerance tests. For the GTT, mice were fasted overnight (16 h) with free access to drinking water. Glucose was administered intraperitoneally (2 g per kg BW), and blood glucose levels were monitored from the tip of the tail with a glucometer. For ITTs, insulin was administered intraperitoneally (0.75 mU per gram BW), and blood glucose was measured at various timepoints after injection.

Serum biochemistry. Triglycerides and transaminases were measured on the Dimension RXL analyser (Siemens Healthcare) or Perkin Elmer DELFIA using reagents and calibrators (Siemens). FFAs were measured using the Roche Free Fatty Acid Kit (half-micro test, 11383175001). Insulin was measured using electrochemical luminescence immunoassay on the MesoScale Discovery immunoassay platform.

Explants for conditioned medium. Approximately 100 mg of freshly dissected BAT, ScW, GnW and liver pieces from 30-week-old mice in chow-fed and HFD-fed conditions, or VsW from human participants cut into fine pieces were incubated for 6 h at 37 °C in 5% CO_2 in DMEM with 5% heat-inactivated FBS, 20 mM HEPES, 100 units per ml penicillin, 100 µg ml^{-1} streptomycin and 20 mM L-glutamine (1 ml of medium per 100 mg of tissue).

Magnetic-activated cell sorting. GnW from 10- to 12-week-old C57BL/6 mice were dissociated by collagenase treatment isolating unilocular adipocytes from the SVF. SVF was resuspended in MACS buffer (PBS, 2 mM EDTA (sterile) and 0.5% BSA) and incubated with Microbeads conjugated to monoclonal antihuman/mouse CD11b (Mac-1α) antibodies (isotype: rat IgG2b, dilution 1:10, Miltenyi Biotech, 130-049-601). Cd11$^+$ fractions were isolated using MACS LS columns according to manufacturer instructions (Miltenyi Biotech).

Bone marrow-derived macrophage preparation and treatments. Femur and tibia bones from 10- to 16-week-old C57BL/6 mice or *Pepd* WT, HET and KO mice were isolated and cleaned, and 10 ml of RPMI 1640 was flushed through each bone. Total bone marrow cells were passed into a 100-µm cell strainer and counted using Countess II automated cell counter (Thermo Fisher). Cells were spun (400*g*, 5 min), resuspended in BMDM culture medium (RPMI 1640 supplemented with 20% of L929-conditioned cell medium, 10% heat-inactivated FBS and 1% penicillin–streptomycin). To make L929-conditioned cell medium, L929 cells (CCL-1, American Type Culture Collection (ATCC)) were seeded in DMEM supplemented with 10% heat-inactivated FBS, 100 U ml^{-1} penicillin–streptomycin and 2 mM L-glutamine (Sigma) at a density of 250,000 cells per 50 ml of medium per T175 tissue culture flask. The medium was collected after 1 week of culture, and then 50 ml of fresh DMEM supplemented with 10% heat-inactivated FBS, 100 U ml^{-1} penicillin–streptomycin and 2 mM L-glutamine were added onto cells and harvested 1 week later. Batches obtained after the first and second weeks of culture were mixed at a 1:1 ratio, aliquoted and stored at −20 °C.

Total bone marrow cells were seeded in 10-cm non-culture-treated plates (Falcon) at a density of 5×10^6 cells per plate per 10 ml of macrophage differentiation medium and cultured for 7 d at 37 °C in 5% CO_2. On day 5 of differentiation, the medium was removed and replaced with 10 ml of fresh BMDM culture medium. On day 7, BMDMs were detached using ice-cold PBS-EDTA 1 mM, spun (400*g*, 5 min) and resuspended in fresh BMDM culture medium. Differentiated BMDMs were counted using a Countess II automated cell counter, and cell concentration adjusted to 5×10^5 cells per ml. Immediately after, cells were plated for experiments at the following densities: 100 µl per well of a 96-well plate, 500 µl per well of a 24-well plate, 1 ml per well of a 12-well plate, 2 ml per well of a 6-well plate and 10 ml for each 10-cm plate. Cells were incubated for 16–24 h after plating before conducting experiments.

Macrophage purity was routinely tested by the expression of CD11b and F4/80 by flow cytometry, and 93–97% of the cells expressed high CD11b and F4/80 levels after 7 d of differentiation.

After differentiation, BMDMs were cultured in 12-well-culture plates (5×10^5 cells) for 24 h in BMDM medium before 6–24 h of stimulation with LPS (100 ng ml^{-1}), DEX (100 nM), IL-4 (10 ng ml^{-1}), purified PEPD (250 nM), Gly-Pro (10 mM) or CBZ-Pro (6 mM) and stored at −80 °C before RNA extraction or prolidase assay. Erlotinib (5 µM) was added to the culture medium 2 h before and during

the treatment with PEPD. We validated PEPD-specific effects by measuring *Cox2* expression in BMDMs, reported as a PEPD target gene[15]. In addition, we discarded the potential cytotoxic effects of purified PEPD on BMDMs and its potential endotoxin contamination by boiling the purified protein and tested it on BMDMs for *Cox2* induction (Extended Data Fig. 7a–c).

Cell culture. *RAW264.7 macrophage culture and transfection.* RAW264.7 cells (TIB-71, ATCC) were cultured in DMEM (4.5 g l^{-1} glucose) supplemented with 10% heat-inactivated FBS, 100 U ml^{-1} penicillin–streptomycin and 2 mM L-glutamine (Sigma). In total, 100,000 cells per well were seeded in a 24-well plate for knockdown experiments. The following day, cells were transfected using Lipofectamine LTX Reagent with PLUS (Invitrogen, Thermo Fisher) according to the manufacturer's instructions. ON-TARGET plus siRNA against EGFR or CTR were obtained from Dharmacon (Horizon). At 24 h after transfection, RAW264.7 cells were treated 24 h with purified PEPD 250 nM. Erlotinib (5 µM) was added to the culture medium 2 h before and during the treatment with PEPD.

3T3-L1 adipocytes. 3T3-L1 cells were differentiated into adipocytes (day 9) accordingly to the protocol described by Roberts et al.[41].

Primary adipose cells. GnW from 10-week-old *Pepd* WT, HET and KO mice was dissociated by collagenase treatment isolating unilocular adipocytes from the SVF. Floating adipocytes were collected and used for lipolysis assay (on the day of isolation) or culture in hydrogel (48 h)[6] to measure IL-6 secretion in response to purified PEPD. Preadipocytes were isolated from the SVF and differentiated into adipocytes (day 9) accordingly to the protocol described by Lacasa et al.[42].

Primary hepatic stellate cells. HSCs were isolated from livers of 10- to 12-week-old C57BL/6 mice. Liver tissue was digested with pronase and collagenase B (Roche), and the cell suspension was subsequently separated by an 11.5% Optiprep gradient (Sigma). HSCs were cultured into plastic (Corning) using DMEM supplemented with pyruvate (1%), glutamine (1%), penicillin–streptomycin (1%) and heat-inactivated FBS (during the activation process, 16%; in fully activated HSCs, 10%); all reagents were from Life Technologies. HSCs were grown at a confluence of 35,000 cells per cm^2 on Corning well 6 plates (RNA) or (for immunofluorescence (IF)) in the Nunc Lab-Tek Permanox plastic Chamber Slide System (Sigma, C7182-1PAK). HSCs were treated with purified PEPD (250 nM) for 24 h (RNA) or 5 d (IF).

Primary muscle fibroblasts. Both hind limbs from 10- to 12-week-old C57BL/6 mice were removed by dislocating hip joints and were dissected in 5 ml of digestion medium (30 mg collagenase II, 36 mg dispase II, 1 M HEPES 2.5%, DMEM high glucose and 15 ml 1% penicillin–streptomycin). Enzymatic digestion was carried out for 20 min in a 37 °C shaking bath and stopped with DMEM (20% FBS). Sequentially, the cell mixture was passed through 100-µm, 70-µm and 40-µm cell strainers and pelleted at 400*g* for 5 min at room temperature (RT). Cells were resuspended in 12 ml of seeding medium (Ham F12, 20% FBS, 10% horse serum, 1% L-glutamine, 1% penicillin–streptomycin and 10 ng ml^{-1} basic fibroblast growth factor and plated on an uncoated 10-cm petri dish for 1 h at 37 °C, 5% CO_2. The medium was changed for fresh seeding medium and renewed every 2 d until reaching 70% confluence. Fibroblasts were grown at a confluence of 50,000 cells per well in 12-well plates (for RNA) or 25,000 cells per well in 24-well plates (on coverslips, for IF). Fibroblasts were pretreated or not with erlotinib (5 µM) before treatment with purified PEPD protein (250 nM) for 24 h (RNA) or 5 d (IF).

Lipolysis assays. Primary mature adipocytes were isolated from GnW of C57BL/6 mice and incubated in Krebs–Ringer bicarbonate buffer with an increasing dose of noradrenaline (from 10^{-10} to 10^{-5} M) for 2 h at 37 °C. Glycerol was measured as an index of lipolysis by using free glycerol reagent (Sigma) against a glycerol standard curve.

Prolidase activity. PA was determined optimizing Myara's spectrophotometric procedure, modified from the Chinard technique[43,44] and miniaturized in acid-resistant 96-well plates. Briefly, tissue and macrophage cell extracts were mixed (vol/vol) with PBS 50 mM HEPES/1 mM $MnCl_2$ and 0.75 mM glutathione and incubated 20 min at 50 °C. The activated mixture was then added (vol/vol) to PBS with 94 mM glycyl-proline (Gly-Pro) for a final concentration of 47 mM and incubated or not (control corresponding to basal levels of proline in the cell/tissue extracts) for 60 min at 37 °C. The reaction was stopped by adding 6 V of 0.45 M trichloroacetic acid and centrifuged at 4,300 r.p.m. for 60 min. The supernatant (1 V) was then added to 4 V of a 1:1 mixture of glacial acetic acid and Chinard's reagent (25 g of ninhydrin dissolved at 70 °C in 600 ml of glacial acetic acid and 400 ml of 6 M orthophosphoric acid) and incubated for 15–45 min at 90 °C. Absorbance was read at 515 nm, and proline concentration was calculated using proline standards ranging from 0.5 µg to 32 µg. Enzyme activity was reported in micromoles of proline released per minute per milligram of protein.

Gas chromatography–mass spectrometry analysis of amino acids. Plasma and GnW explants samples were analysed for free amino acid concentrations using the EZ:faast GC–MS Kit (KGO-7166 Phenomenex).

Extraction. AT (~100 mg) was weighed and amino acids were extracted into 1 ml of 75% 0.01 M HCL and 25% acetonitrile using a FastPrep (MP Biomedical). All liquid was removed to a 1.5-ml microcentrifuge tube and centrifuged at 16,000*g* for 10 min. Following centrifugation, the upper lipid layer was discarded and the lower acetonitrile/aqueous layer was removed to a fresh microcentrifuge tube and the centrifugation step was repeated. Samples were transferred to another fresh microcentrifuge tube and dried overnight using a SpeedVac before being resuspended in 100 µl of 0.9% saline by repeatedly pipetting up and down and vortexing (3×) for 5 s. After resuspension, samples were centrifuged at maximum speed for a further 10 min and analysed following the EZ:faast protocol.

Modified EZ:FaaST protocol. Amino acids were analysed using the EZ:faast free (physiological) amino acid analysis kit (KGO-7166) for gas chromatography–mass spectrometry (GC–MS) according to the manufacturer's instructions up to the chromatography step. Briefly, 100 µl of serum or WAT extract was mixed with 100 µl of reagent 1, which contained 0.2 mM norvaline as an internal standard. Samples were drawn into the proprietary sorbent tip and then washed by drawing a further 200 µl of reagent 2 followed by air through the tip until dry. Samples were eluted by attaching a new syringe to the tip, drawing the eluting medium (200 µl total) into the tip until the sorbent granules were wet and then ejecting the granules. Samples were then derivatized by adding 50 µl of reagent 4 using a Drummond Dialamatic Microdispenser and vortexing for 5–8 s. Samples were allowed to stand for 1 min, then vortexed again and allowed to stand for a further min. In total, 100 µl of reagent 5 was added and samples were vortexed for 5 s and allowed to stand for 1 min. The upper layer was transferred to an autosampler vial and dried under nitrogen for 10 min. Samples were resuspended in 100 µl of reagent 6 and transferred into an insert in the same autosampler vial. The samples then proceeded to chromatography.

Chromatography. GC–MS analysis was performed using an Aglient 7890B GC and an Agilent 5977A MSD using a 0.25-mm ID, 0.25-µm film thickness 15 M DB-1701 (122-0712, Agilent) column. The GC conditions were as follows:

Inlet conditions: temperature, 250 °C; split 10:1 for serum, splitless for Gly-Pro determination and AT; inlet liner Liner, Phenomenex AG0-4680: 900 µl (FocusLiner)—part of kit; column flow, 2 ml min^{-1}; injection volume, 1 µl.

Temperature programme: 75 °C hold for 2 min; 16.3 °C per min until 280 °C; 280 °C hold for 5.5 min; MSD transfer line, 280 °C.

MSD conditions: scan, 45–450, 4 Hz; MS source temperature, 240 °C; MS Quad temperature, 180 °C.

Data were acquired using MassHunter Workstation Software.

Peak integration and quantification were performed using MassHunter Workstation Quantitative Analysis software (vB.07.00, Agilent) selecting ions for each amino acid specified in the EZ:faast protocol. Data were analysed by first normalizing all data points to the Norvaline internal standard. Amino acid concentrations were then determined using a three-point standard curve made using 25, 50 and 100 µl of the 0.2 mM standards provided in the EZ:faast kit. AT extracts and serum were expressed as nanomoles per 100 µl of sample.

Histological analysis. AT and liver samples were fixed in 4% paraformaldehyde for 24 h, embedded in paraffin, sectioned into 5-µm sections and processed for Sirius (fibrosis) or H&E (liver steatosis) staining. The slides were scanned (Microscopy Zeiss Axioscan Z1 Slidescanner) and processed for fibrosis (Sirius staining excluding vessels) and steatosis (vacuole percentage area) quantification using HALO image analysis software (Indica Labs).

Confocal analysis. Cells were fixed in 4% paraformaldehyde for 1 h at RT, then transferred to PBS, and stored at 4 °C until IF analysis. Samples were blocked in 1 M glycine and PBS with 3% BSA and 0.1% Triton X-100 and then incubated overnight (4 °C, in agitation) with primary antibody diluted in blocking buffer (PBS 3% Albumin, pH 7.4). Antibodies used were anti-αSMA 1A4 (1:200 dilution; Sigma, A2547) and anti-collagen I (1:200 dilution; Abcam, ab21286). After washing in PBS and blocking, cells were incubated with the secondary antibodies conjugated to Alexa Fluor dyes, either Alexa Fluor 555-conjugated anti-rabbit (1:250 dilution; Life technologies, A21428) or Alexa Fluor 488-conjugated anti-mouse (1:250 dilution; Life technologies, A21202), BODIPY 493/503 (1:2,000 dilution; Life science, D-3922), used as a stain for neutral lipids, and Phalloidin-iFluor 594 (1:200 dilution; Abcam, ab176757), used to stain the actin filaments, for 1 h at RT in blocking buffer, followed by Hoechst 33342 (1:2,000 dilution; Thermo Fisher, H3570) for 5 min, and multiple PBS washes. Samples were mounted and imaged blind using a Zeiss LSM 510 Meta Confocal microscope with LSM 3D software (Carl Zeiss). At least three images per sample for each stain were used for quantification and was performed blind. Staining quantification was performed using Fiji software (https://imagej.net/software/fiji/). A detailed list of the antibodies used for this study is presented in Supplementary Table 9.

Hydroxyproline assay. HPro measurement was done using a HPro colorimetric assay (BioVision) as previously described[45]. Briefly, frozen fat is weighted and heated in 6 N HCl at 110 °C overnight in sealed tubes, as 10 µl of HCl per mg of WAT. Ten microliters are evaporated before incubation with chloramine-T and

p-dimethylaminobenzaldehyde (DMAB) at 60 °C for 90 min. The absorbance was read at 560 nm, and the concentration was determined using the standard curve created with HPro.

ELISA assays. Mouse and human PEPD protein concentrations were measured using an ELISA kit for Mouse Xaa-Pro dipeptidase (PEPD) ELISA kit (CSB-EL017784MO, CUSABIO) and Human PEPD (Peptidase D) ELISA Kit (E-EL-H5575.96, Elabscience), respectively, in tissue explants (from which debris was removed by centrifugation) and serum according to the manufacturer's instructions. Leptin protein concentration in AT explant media was measured using an ELISA kit for murine leptin (R&D systems, DY498). IL-6 protein concentration in conditioned media from mature adipocytes isolated from GnW was measured using an ELISA kit for mouse IL-6 (R&D systems, DY406). A standard curve was prepared according to the manufacturer's instructions, and the value associated with an unconditioned medium blank was subtracted from that of conditioned medium.

RNA extraction and real-time PCR. RNA from cells was extracted using RNeasy Mini columns (Qiagen) according to the manufacturer's instructions. RNA was harvested from frozen tissue using RNA-STAT-60TM (AMS Bio) and purified by chloroform extraction and isopropanol precipitation. Reverse transcription was performed using the Reverse Transcriptase System (Promega) according to the manufacturer's instructions. Real-time PCR was carried out using TaqMan or Sybr Green reagents using an Abi 7900 real-time PCR machine with default thermal cycler conditions. Primer sequences are described in Supplementary Table 9. Reactions were run in duplicate, checked for reproducibility, and then averaged. A standard curve generated from a pool of all cDNA samples was used for quantification. The expression of genes of interest was normalized using the geometric average of four housekeeping genes (18 s, 36b4, βactin and B2m), and data are expressed as arbitrary units.

Regarding human samples (cohorts 1, 2 and 3), RNA purification, gene expression procedures and analyses were performed, as previously described[46,47]. Total RNA was briefly extracted and purified using the RNeasy Lipid Tissue Mini kit, and Agilent Bioanalyzer checked the integrity. Total RNA was quantified using a spectrophotometer. The same amount of total RNA was reverse transcribed to cDNA from all samples using a High-Capacity cDNA Archive kit following the manufacturers' instructions. Gene expression was assessed using a LightCycler 480 real-time PCR system, using TaqMan and SYBRgreen technology suitable for relative gene expression quantification. The commercially available and pre-validated TaqMan primer/probe sets used are described Supplementary Tables 9 and 10.

RNA sequencing. *Library preparation and sequencing.* Total RNA of GnW and liver was extracted using the miRNeasy mini kit (Qiagen) according to the manufacturer's instructions. For each experiment, 4–10 independent biological repeats were used.

Total RNA was quality checked (RIN score > 7) via the Agilent Bioanalyser 2100 system, using the Agilent RNA 6000 Nano Kit. A total of 1 µg of RNA was used to construct barcoded sequencing libraries with the TruSeq Stranded mRNA HT Sample Prep Kit (Illumina) following the supplier's instruction. All the libraries were validated using the Agilent Bioanalyser DNA 12000 and then multiplexed and sequenced on two lanes of an Illumina HiSeq 4000 at SE50 at CR-UK Cambridge Institute Genomics Core Facility.

Processing of RNA-seq data. RNA-seq reads (Supplementary Table 1) were mapped to the most recent ENSEMBLE version GRCm38.p5 of the mouse reference genome sequence (GRCm38.p5) using STAR (v2.5.1b)[48] including the annotations as hints for exon–intron borders. Reads were considered mapped if the similarity was at least 95% over at least 90% of the read length as previously described[49]. FeatureCounts (v1.5)[50] was applied for the generation of count tables based on the mapping files. Customized Python scripts[49] were deployed for downstream processing, including the raw counts' normalization to the total number of assigned reads per gene (TPMs) and the combined exon length (fragments per kilobase of exon per million mapped fragments), respectively.

Gene expression and pathway enrichment analyses. Raw counts were subjected to differential gene expression analysis via DESeq2 (ref. [51]) and different R packages (Supplementary Information). Genes that showed raw counts lower or equal to 2 in 50% of all samples were removed before the differentially expressed analysis. The Wald test was applied to extract DEGs (Supplementary Tables 2, 3 and 6–8). Obtained DEGs were annotated via customized Python scripts. Pathway enrichment analyses were performed with PIANO[52], using the gene-set collection C2 retrieved from the Molecular Signatures Database (MSigDB)[53,54] (Supplementary Tables 4 and 5). The Bonferroni and Holm method was applied to correct for multiple testing.

Western blotting. Proteins were extracted from tissue in lysis buffer (20 mM Tris-HCl, 150 mM NaCl, 1 mM EDTA, 1 mM EDTA, 1% Triton X-100, pH 7.5) with added protease inhibitor (Roche) and phosphatase inhibitor (Roche) cocktails. Debris and fat were cleared from lysates by centrifugation. Protein concentration was determined by Dc Protein assay (Bio-Rad). After dilution in Laemmli buffer with 0.5% 2-mercaptoethanol, 30 µg protein was loaded per well and subjected to SDS–PAGE in a 4–12% gradient gel using the Novex NuPage midi system (Life Technologies) and transferred using the iBlot transfer system and reagents (Life Technologies). Membranes were blocked for 1 h in 3% BSA in Tris-buffered saline at RT and incubated overnight at 4 °C with the following primary antibodies: anti-PEPD (1:1,000 dilution; Abcam, ab86507), anti-phospho-NF-κB p65 (S536; 1:1,000 dilution; clone 93H1, Cell Signaling, 3033), anti-NF-κB p65 (1:1,000 dilution; Cell Signaling, 3034), anti-β-Actin (1:2,000 dilution; Abcam, ab8227), anti-GADPH (1:1,000 dilution; Cell Signaling, 97166S), anti-β-Tubulin (1:1,000 dilution, Cell Signaling, 2146S), anti-phospho-AKT (S473) (D9E); 1:1,000 dilution; Cell Signaling, 4060) and anti-AKT (1:1,000 dilution; 9272). Bound primary antibodies were detected using peroxidase-coupled secondary anti-rabbit (1:10,000 dilution; 7074, Cell Signaling) or anti-mouse (1:10,000 dilution; Cell Signaling, 7076) and enhanced chemiluminescence (WBLUF0500, Millipore). Blots were exposed digitally using the ChemiDoc MP System (Bio-Rad), and bands were quantified using Fiji software (https://imagej.net/software/fiji/). The expression of proteins was normalized to protein levels of a housekeeping protein (β-actin, GADPH or β-tubulin), and the phosphorylation status was determined by normalizing to a respective total protein. All protein quantification data are expressed as arbitrary units. A detailed list of the antibodies used for this study is presented in Supplementary Table 9.

Array-based detection of phosphorylated receptor tyrosine kinase. The Proteome Profiler Mouse Phospho-RTK Array Kit (R&D Systems, ARY014) was used to screen for the phosphorylation level of receptor tyrosine kinase in BMDMs in response to purified PEPD, according to the manufacturer's instructions. Briefly, the array membranes were incubated for 1 h with an array blocking buffer before incubation overnight at 4 °C on an orbital shaker with 1.5 ml of cellular extract. The membrane was then washed and incubated for 30 min with a streptavidin–horseradish peroxidase solution. Membranes were exposed digitally using the ChemiDoc MP System (Bio-Rad), and spots were quantified using Fiji software (https://imagej.net/software/fiji/). One condition corresponds to a pool of cellular extracts from four independent experiments. All the arrays were measured three times; each spot was normalized to the positive controls. The results are presented in a heat map and considered relevant when the fold variation was >1.3 or <0.6.

Cytotoxicity assays. To determine the cytotoxic effect of compounds on macrophages, cells were seeded in RPMI 1640 medium without FBS supplemented at a density of 15,000 cells per well in wells of a 96-well plate. Cells were treated with the given compounds at the stated concentrations for 24 h, and cytotoxicity was measured using an LDH-Cytotoxicity Calorimetric Assay Kit (BioVision) according to the manufacturer's instructions.

Data analysis. The number of animals or independent experiments was determined based on pilot data and indicated in the figure legends. No statistical methods were used to predetermine the total number of animals needed for this study. Animal allocation to cages (four mice per cage) and diet were not randomized as we ensured each cage had mice from the three genotypes and each group (chow and HFD, control and CBZ-Pro) had the same average of initial BW. All data from experiments are summarized by their mean and standard error. The number of replicates is reported in the figure legends. When the pairwise comparison results are expressed as a fold-change value, it is declared in the figure legends to what value the data were normalized. Statistical analyses were performed using GraphPad Prism (v8.0.2). Comparisons between two groups were conducted using an unpaired *t*-test. Comparison between more than two groups was conducted using a one-way ANOVA followed by appropriate post hoc multiple-comparison tests. Comparisons between more than two groups and factors were conducted using a two-way ANOVA followed by appropriate post hoc testing. Pearson's coefficients were evaluated to estimate the correlation between data series.

Data were excluded when identified as outliers using Grubbs' test (https://www.graphpad.com/quickcalcs/Grubbs1.cfm). The animals were randomly assigned to the different experimental settings (GTT and ITT). Areas under the ROC curves were determined for each variable to identify the predictors of AT fibro-inflammation and IR/T2D. A ROC curve is a plot of sensitivity (true positive) versus 1–specificity (false positive) showing the ability of a biomarker (PEPD level) to discriminate between true positives (for example, insulin resistant) and true negatives (for example, insulin sensitive). The best marker has a ROC curve shifted to the left with the area under the curve close to unity[55]. The Youden index was calculated (sensitivity + specificity − 1) to determine the optimal cut-off values for fibro-inflammatory status or IR indices. The values for the maximum of the Youden index were considered the optimal cut-off points using the Web-tool easyROC[56].

Exploratory factor analysis. EFA is an unbiased statistical method that establishes the cluster of biological variables with high loadings (correlation equivalent) on each specific factor in a reduced number of underlying variables ('factors')

considered as 'superfamilies' of variables[57]. EFA was conducted to determine the possible latent structure of the variables (listed; for example, in Fig. 1p, rows of the depicted matrix) measured in each animal model, that is, *Pepd* CBZ-Pro-treated mice, BMT mice and PEPD-treated mice. Factor analysis identifies a minimum number of new variables (factors), which are linear combinations of the original (measured) ones, such that the new (fewer) variables contain most or all the information and can facilitate the interpretation of a complex multivariate scenario. First, a matrix of correlation coefficients is computed, and a set of principal components (factors) is extracted from it. The relationships between the original variables and the factors are expressed in terms of 'factor loadings', which estimate the degree of correlation between the original variables and the factors.

We determined whether our data were appropriate for EFA using the Kaiser–Meyer–Olkin (KMO) measure of sampling adequacy and Bartlett's test of sphericity. Data were considered appropriate if the KMO > 0.7 and Bartlett's test was significant at $P < 0.05$. To determine the number of factors to retain, we decided to rule out the components associated with eigenvalues less than 1. The parallel analysis confirmed that our choice was viable. Factors extraction was computed using the maximum-likelihood-estimate method, implemented in the function 'fa' of the psych R package[58]. Plots were produced using either in-house scripts or built-in functions of the FactoMineR package in R[59].

Principal-component analysis. Principal-component analyses of the Lukk and the own dataset were performed in R v3.1.2 using the prcomp function of the stats package[60].

Reporting Summary. Further information on research design is available in the Nature Research Reporting Summary linked to this article.

Data availability

DEGs and pathways from the RNA-seq analysis are available in Supplementary Tables 1–10. The RNA-seq dataset is deposited in the Gene Expression Omnibus under accession number GSE198358. Source data are provided with this paper. All other raw data are available upon request.

Code availability

Code is available at https://github.com/bpucker/RNA-Seq_analysis/. An archived version is available at https://zenodo.org/record/6192463/.

Received: 11 August 2020; Accepted: 18 March 2022;
Published online: 25 April 2022

References

1. Sun, K., Tordjman, J., Clément, K. & Scherer, P. E. Fibrosis and adipose tissue dysfunction. *Cell Metab.* **18**, 470–477 (2013).
2. Vidal-Puig, A. Adipose tissue expandability, lipotoxicity and the metabolic syndrome. *Endocrinol. Nutr.* **60**, 39–43 (2013).
3. Crewe, C., An, Y. A. & Scherer, P. E. The ominous triad of adipose tissue dysfunction: inflammation, fibrosis, and impaired angiogenesis. *J. Clin. Invest.* **127**, 74–82 (2017).
4. Sorisky, A., Molgat, A. S. D. & Gagnon, A. Macrophage-induced adipose tissue dysfunction and the preadipocyte: should I stay (and differentiate) or should I go? *Adv. Nutr.* **4**, 67–75 (2013).
5. Abdennour, M. et al. Association of adipose tissue and liver fibrosis with tissue stiffness in morbid obesity: links with diabetes and BMI loss after gastric bypass. *J. Clin. Endocrinol. Metab*. https://doi.org/10.1210/jc.2013-3253 (2014).
6. Pellegrinelli, V. et al. Human adipocyte function is impacted by mechanical cues. *J. Pathol.* **233**, 183–195 (2014).
7. Lavie, C. J., De Schutter, A. & Milani, R. V. Healthy obese versus unhealthy lean: the obesity paradox. *Nat. Rev. Endocrinol.* **11**, 55–62 (2015).
8. Manning, A. K. et al. A genome-wide approach accounting for body mass index identifies genetic variants influencing fasting glycemic traits and insulin resistance. *Nat. Genet.* **44**, 659–669 (2012).
9. Willer, C. J. et al. Discovery and refinement of loci associated with lipid levels. *Nat. Genet.* **45**, 1274–1283 (2013).
10. Kluth, O. et al. Differential transcriptome analysis of diabetes-resistant and -sensitive mouse islets reveals significant overlap with human diabetes susceptibility genes. *Diabetes* **63**, 4230–4238 (2014).
11. Yaghootkar, H. et al. Genetic evidence for a normal-weight 'metabolically obese' phenotype linking insulin resistance, hypertension, coronary artery disease, and type 2 diabetes. *Diabetes* **63**, 4369–4377 (2014).
12. Kitchener, R. L. & Grunden, A. M. Prolidase function in proline metabolism and its medical and biotechnological applications. *J. Appl. Microbiol.* **113**, 233–247 (2012).
13. Rayment, J. H., Jobling, R., Bowdin, S., Cutz, E. & Dell, S. D. Prolidase deficiency diagnosed by whole-exome sequencing in a child with pulmonary capillaritis. *ERJ Open Res.* **5**, 00205–02018 (2019).
14. Olivares, O. et al. Collagen-derived proline promotes pancreatic ductal adenocarcinoma cell survival under nutrient limited conditions. *Nat. Commun.* **8**, 16031 (2017).
15. Yang, L. et al. Prolidase directly binds and activates epidermal growth factor receptor and stimulates downstream signaling. *J. Biol. Chem.* **288**, 2365–2375 (2013).
16. Yang, L., Li, Y. & Zhang, Y. Identification of prolidase as a high affinity ligand of the ErbB2 receptor and its regulation of ErbB2 signaling and cell growth. *Cell Death Dis.* **5**, e1211 (2014).
17. Yang, L., Li, Y., Bhattacharya, A. & Zhang, Y. A recombinant human protein targeting HER2 overcomes drug resistance in HER2-positive breast cancer. *Sci. Transl. Med.* **11**, eaav1620 (2019).
18. Choi, H. et al. Plasma protein and microRNA miomarkers of insulin resistance: a network-based integrative -omics analysis. *Front. Physiol.* **10**, 379 (2019).
19. Lupi, A. et al. *N*-benzyloxycarbonyl-L-proline: an in vitro and in vivo inhibitor of prolidase. *Biochim. Biophys. Acta* **1744**, 157–163 (2005).
20. Small, L., Brandon, A. E., Turner, N. & Cooney, G. J. Modeling insulin resistance in rodents by alterations in diet: what have high-fat and high-calorie diets revealed. *Am. J. Physiol. Endocrinol. Metab.* **314**, E251–E265 (2018).
21. Søndergaard, E., Espinosa De Ycaza, A. E., Morgan-Bathke, M. & Jensen, M. D. How to measure adipose tissue insulin sensitivity. *J. Clin. Endocrinol. Metab.* **102**, 1193–1199 (2017).
22. Blohmke, C. J. et al. Interferon-driven alterations of the host's amino acid metabolism in the pathogenesis of typhoid fever. *J. Exp. Med.* **213**, 1061–1077 (2016).
23. Murray, P. J. et al. Macrophage activation and polarization: nomenclature and experimental guidelines. *Immunity* **41**, 14–20 (2014).
24. Alasoo, K. et al. Transcriptional profiling of macrophages derived from monocytes and iPS cells identifies a conserved response to LPS and novel alternative transcription. *Sci. Rep.* **5**, 12524 (2015).
25. Vila, I. K. et al. Immune cell Toll-like receptor 4 mediates the development of obesity- and endotoxemia-associated adipose tissue fibrosis. *Cell Rep.* **7**, 1116–1129 (2014).
26. Petkevicius, K. et al. Accelerated phosphatidylcholine turnover in macrophages promotes adipose tissue inflammation in obesity. *Elife* **8**, e47990 (2019).
27. Sharif, O. et al. Beneficial metabolic effects of TREM2 in obesity are uncoupled from its expression on macrophages. *Diabetes* **70**, 2042–2057 (2021).
28. Weisberg, S. P. et al. Obesity is associated with macrophage accumulation in adipose tissue. *J. Clin. Invest.* **112**, 1796–1808 (2003).
29. Tabula Muris Consortium. Single-cell transcriptomics of 20 mouse organs creates a Tabula Muris. *Nature* **562**, 367–372 (2018).
30. Iwayama, T. et al. PDGFRα signaling drives adipose tissue fibrosis by targeting progenitor cell plasticity. *Genes Dev.* **29**, 1106–1119 (2015).
31. Keophiphath, M. et al. Macrophage-secreted factors promote a profibrotic phenotype in human preadipocytes. *Mol. Endocrinol.* **23**, 11–24 (2009).
32. Liang, B. et al. Characterization and proteomic analysis of ovarian cancer-derived exosomes. *J. Proteom.* **80**, 171–182 (2013).
33. Gonzales, P. A. et al. Large-scale proteomics and phosphoproteomics of urinary exosomes. *J. Am. Soc. Nephrol.* **20**, 363–379 (2009).
34. Kharaziha, P. et al. Molecular profiling of prostate cancer derived exosomes may reveal a predictive signature for response to docetaxel. *Oncotarget* **6**, 21740–21754 (2015).
35. Lazar, I. et al. Proteome characterization of melanoma exosomes reveals a specific signature for metastatic cell lines. *Pigment Cell Melanoma Res.* **28**, 464–475 (2015).
36. Yang, L., Li, Y., Bhattacharya, A. & Zhang, Y. PEPD is a pivotal regulator of p53 tumor suppressor. *Nat. Commun.* **8**, 2052 (2017).
37. Surazynski, A., Liu, Y., Miltyk, W. & Phang, J. M. Nitric oxide regulates prolidase activity by serine/threonine phosphorylation. *J. Cell. Biochem.* **96**, 1086–1094 (2005).
38. Aslan, M., Duzenli, U., Esen, R. & Soyoral, Y. U. Serum prolidase enzyme activity in obese subjects and its relationship with oxidative stress markers. *Clin. Chim. Acta* **473**, 186–190 (2017).
39. Bel Lassen, P. et al. The FAT score, a fibrosis score of adipose tissue: predicting weight-loss outcome after gastric bypass. *J. Clin. Endocrinol. Metab.* **102**, 2443–2453 (2017).
40. Yang, L., Li, Y., Bhattacharya, A. & Zhang, Y. Inhibition of ERBB2-overexpressing tumors by recombinant human prolidase and its enzymatically inactive mutant. *EBioMedicine* **2**, 396–405 (2015).
41. Roberts, A. W. G-CSF: a key regulator of neutrophil production, but that's not all! *Growth Factors* **23**, 33–41 (2005).
42. Lacasa, D., Taleb, S., Keophiphath, M., Miranville, A. & Clement, K. Macrophage-secreted factors impair human adipogenesis: involvement of proinflammatory state in preadipocytes. *Endocrinology* **148**, 868–877 (2007).
43. Besio, R. et al. Improved prolidase activity assay allowed enzyme kinetic characterization and faster prolidase deficiency diagnosis. *Clin. Chim. Acta* **412**, 1814–1820 (2011).

44. Myara, I., Charpentier, C. & Lemonnier, A. Optimal conditions for prolidase assay by proline colorimetric determination: application to iminodipeptiduria. *Clin. Chim. Acta* **125**, 193–205 (1982).
45. Marcelin, G. et al. A PDGFRα-mediated switch toward CD9^{high} adipocyte progenitors controls obesity-induced adipose tissue fibrosis. *Cell Metab.* **25**, 673–685 (2017).
46. Moreno-Navarrete, J. M. et al. Insulin resistance modulates iron-related proteins in adipose tissue. *Dia Care* **37**, 1092–1100 (2014).
47. Reggio, S. et al. Increased basement membrane components in adipose tissue during obesity: links with TGFβ and metabolic phenotypes. *J. Clin. Endocrinol. Metab.* **101**, 2578–2587 (2016).
48. Dobin, A. et al. STAR: ultrafast universal RNA-seq aligner. *Bioinformatics* **29**, 15–21 (2013).
49. Haak, M. et al. High quality de novo transcriptome assembly of *Croton tiglium*. *Front Mol. Biosci.* **5**, 62 (2018).
50. Liao, Y., Smyth, G. K. & Shi, W. The Subread aligner: fast, accurate and scalable read mapping by seed-and-vote. *Nucleic Acids Res.* **41**, e108 (2013).
51. Love, M. I., Huber, W. & Anders, S. Moderated estimation of fold change and dispersion for RNA-seq data with DESeq2. *Genome Biol.* **15**, 550 (2014).
52. Väremo, L., Nielsen, J. & Nookaew, I. Enriching the gene-set analysis of genome-wide data by incorporating directionality of gene expression and combining statistical hypotheses and methods. *Nucleic Acids Res.* **41**, 4378–4391 (2013).
53. Liberzon, A. et al. Molecular signatures database (MSigDB) 3.0. *Bioinformatics* **27**, 1739–1740 (2011).
54. Subramanian, A. et al. Gene set enrichment analysis: a knowledge-based approach for interpreting genome-wide expression profiles. *Proc. Natl Acad. Sci. USA* **102**, 15545–15550 (2005).
55. Grund, B. & Sabin, C. Analysis of biomarker data: logs, odds ratios, and receiver operating characteristic curves. *Curr. Opin. HIV AIDS* **5**, 473–479 (2010).
56. Goksuluk, D., Korkmaz, S., Zararsiz, G. & Karaagaoglu, A. E. easyROC: an interactive web-tool for ROC curve analysis using R language environment. *R. J.* **8**, 213–226 (2016).
57. Yong, A. G. & Pearce, S. A beginner's guide to factor analysis: focusing on exploratory factor. *Quant. Methods Psychol.* **9**, 79–94 (2013).
58. Revelle, W. Procedures for psychological, psychometric and personality research (R package psych version 2.1.9). https://CRAN.R-project.org/package=psych (2021).
59. Lê, S., Josse, J. & Husson, F. FactoMineR: an R package for multivariate analysis. *J. Stat. Soft.* **25**, 10 (2008).
60. R Core Team (2020). R: a language and environment for statistical computing (R Foundation for Statistical Computing). https://www.R-project.org/ (2020).

Acknowledgements

This work was funded by a Wellcome Trust strategic award (100574/Z/12/Z), MRC MDU (MC_UU_12012/2), H2020 EPoS (Elucidating Pathways of Steatohepatitis grant agreement 634413) and the British Heart Foundation (RG/18/7/33636). The Disease Model Core, Biochemistry Assay Lab, the Histology Core and the Genomics and Transcriptomics Core are funded by MRC_MC_UU_12012/5 and a Wellcome Trust Strategic Award (208363/Z/17/Z). We thank the Wellcome Trust Sanger Institute Mouse Genetics Project (Sanger MGP) and its funders for providing the mutant mouse line (Pepd$^{tm1a(KOMP)Wtsi}$). We thank the Disease Model Core from the Wellcome-MRC Institute of Metabolic Science and A. Lukasik for their technical assistance in animal work. All animal work was carried out in the Disease Model Core (MRC Metabolic Diseases Unit (MRC_MC_UU_12012/5); Wellcome Trust Strategic Award (100574/Z/12/Z)). We also thank Genomics and Transcriptomics core, the Histology core and G. Strachan from the Imaging core for their technical assistance. All serum biochemistry was conducted by the Biochemistry Assay Laboratory (MRC Metabolic Diseases Unit (MRC_MC_UU_12012/5)). Clinical studies in France were supported by 'Contrat de Recherche Clinic' (CRC APHP, Fibrota to J.A.-W. and K.C.), by the National Agency of Research (ANR-Captor to C.R. and K.C.) and by EFSD (to K.C.). H2020 EPoS funded K.C. (Elucidating Pathways of Steatohepatitis grant agreement 634413). A.R.D., Y.H.L., M.D. and M.C. were funded by MRC MDU (MRC_MC_UU_00014/5). M.D. also receives funding from the National Institute for Health Research (Cambridge Biomedical Research Centre at the Cambridge University Hospitals NHS Foundation Trust). D.C. was supported by MRC MDU (MRC_MC_UU_12012/4). S.C. was supported by the ERC Senior Investigator award (669879). We also thank all the patients and their physicians, L. Genser for the surgical procedures, C. Poitou for patient recruitment and F. Marcheli for data management. R. J. F. Loos is supported by a grant from the National Institutes of Health (NIH R01DK107786). M.d.H. is a fellow of the Swedish Heart-Lung Foundation (20170872), is a Kjell and Märta Beijer Foundation researcher and is supported by project grants from the Swedish Heart-Lung Foundation (20140543, 20170678 and 20180706) and the Swedish Research Council (2015-03657 and 2019-01417). We also acknowledge the FATBANK platform promoted by the CIBEROBN and the IDIBGI Biobank (Biobanc IDIBGI, B.0000872), integrated into the Spanish National Biobanks Network, for their collaboration and coordination. The funders had no role in study design, data collection and interpretation, or submitting the work for publication. The authors' views are their own and not necessarily those of the NHS, the NIHR or the Department of Health and Social Care.

Author contributions

V.P. developed the hypothesis, designed the experiments, performed the experimental work, collected and analysed the data, coordinated and directed the project, created the images and wrote the manuscript. S.R.C. designed and conducted part of the experimental work and edited the manuscript. C.R. and J.-M.M.-N. performed and analysed human experiments. S.V. performed the BMT in mice and the GC–MS for the detection of imidopeptides. H.S., G.B., M.C.V.-B., A.R.D., M.D., M.C., S.C., S. Mora, M.M.M., A.E., S. Mukhopadhyay and M.d.H. conducted experiments. J.A.-W. and K.C. supervised enrolment and clinical phenotyping of obese participants. H.S., B.P. and D.C. performed bioinformatics analysis. D.C. also edited the manuscript. G.D., R.L., J.M.F. and K.C. provided access to human data and discussed the manuscript. A.V.P. developed the hypothesis, coordinated and directed the project, wrote the manuscript, is the guarantor of this work and, as such, had full access to all the data in the study and takes responsibility for the integrity of the data and the accuracy of the data analysis. All authors critically reviewed and edited the manuscript.

Competing interests

The authors declare no competing interests.

Additional information

Extended data is available for this paper at https://doi.org/10.1038/s42255-022-00561-5.

Supplementary information The online version contains supplementary material available at https://doi.org/10.1038/s42255-022-00561-5.

Correspondence and requests for materials should be addressed to V. Pellegrinelli or A. Vidal-Puig.

Peer review information *Nature Metabolism* thanks Kai Sun, Anthony Ferrante and the other, anonymous, reviewer(s) for their contribution to the peer review of this work. Primary Handling Editor: Christoph Schmitt, in collaboration with the *Nature Metabolism* team.

Reprints and permissions information is available at www.nature.com/reprints.

Publisher's note Springer Nature remains neutral with regard to jurisdictional claims in published maps and institutional affiliations.

a

Cohort	Status	N	age	BMI	Gly mmol/L	Ins µUI/L	HOMA IR	HbA1C %	CholTmmol/L	Trigly mmol/L
Cohort 1	Non obese	26	53.6±12.2	25.9±2.9	95.5 (86-104.2)					111 (81.7-152.7)
	Obese	58	**44.3±8.9****	**44.8±7.3*****	95.5 (86.2-115.7)					96.5 (78.7-136.2)
Cohort 2a	Lean	8	46.3±4	23.9±0.6						
	Obese non diabetic (ND)	8	40.5±2.5	**51.1±2.8*****						
Cohort 2b	Obese non diabetic (ND)	6	35.3±5.3	44.7±1.8	4.8±0.117	15.22±4.3	3.3±0.99	5.42±0.09	4.9±0.2	1.19±0.198
	Obese diabetic/glucose intolerant (D/GI)	2/6	36.5±5.89	46.78±2.07	5.413±0.47	22.29±5.03	5.19±1.07	**6.143±0.17****	4.61±0.28	1.214±0.135
Cohort2c	Obese	12								
Cohort 2d	Lean	10	43.9±4.3	27.4±1						
Cohort2e	Obese	9	44.4±2.3	**42.8±0.5*****	5.4±0.4	19.6±4.4	4.8±1.4	5.9±0.1	5.6±0.4	1.4±0.3
Cohort2f	Obese non diabetic (ND)	6	36.5±5	46±3.1	5.2±0.2	19.7±4.6	4.6±1.2	5.5±0.1	5.3±0.3	1.5±0.1
	Obese diabetic/glucose intolerant (D/GI)	1/6	46.9±5.5	43.7±2.6	**6.2±0.3***	14.8±1.9	3.6±0.6	**6.7±0.2*****	4.8±0.5	1.7±0.2

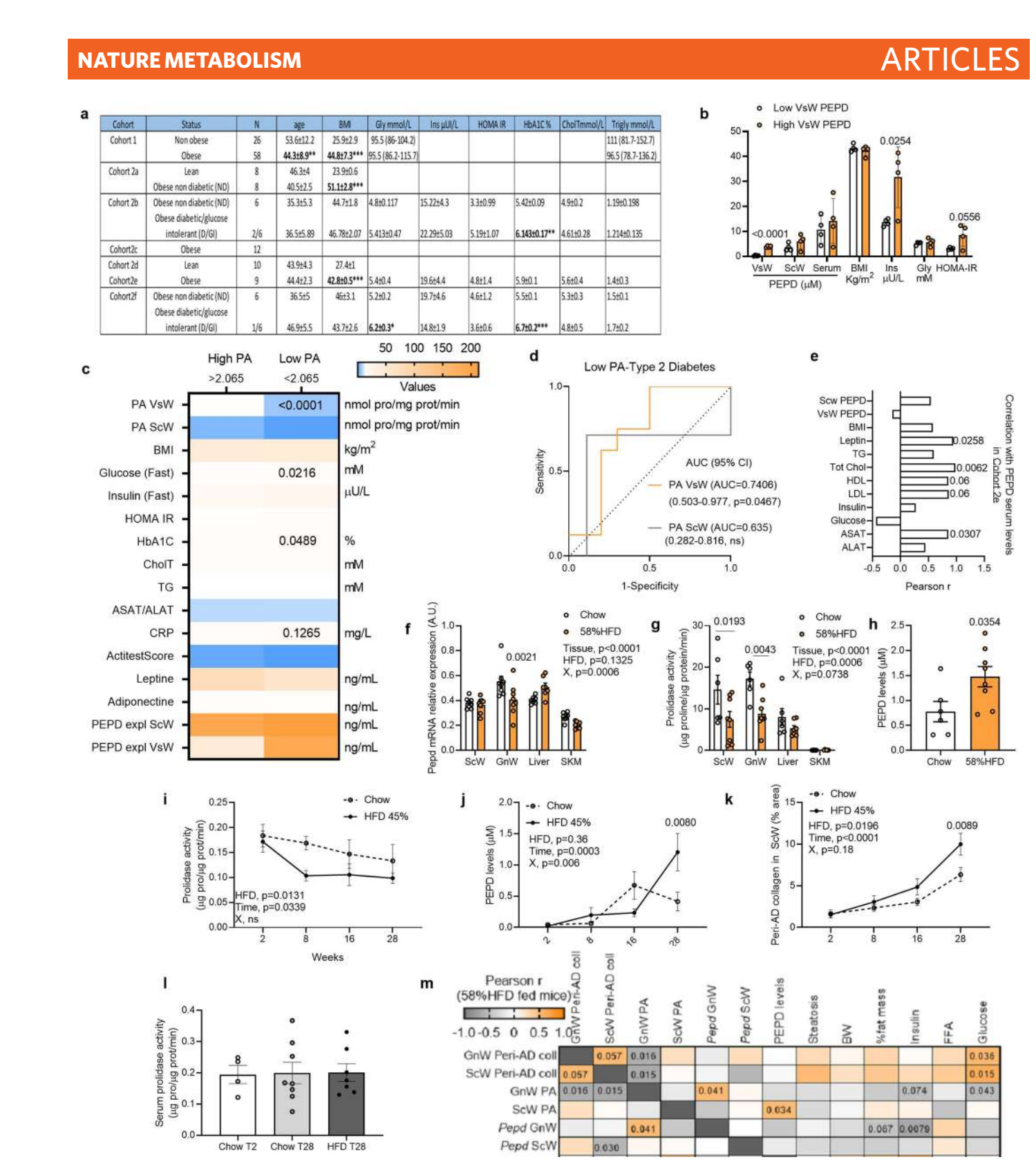

Extended Data Fig. 1 | See next page for caption.

Extended Data Fig. 1 | Obesity reduces AT PEPD activity and promotes PEPD release in association with AT fibrosis and insulin resistance. a, Age, BMI, glycaemic and lipidic status in the different human cohorts. **b**, PEPD serum/ScW levels, BMI and metabolic parameters in obese subjects from cohort cohort 2e (n = 9) with low vs. high VsW PEPD levels. **c**, PEPD activity/ecplants levels, BMI, blood chemistry parameters and liver Actitest score in obese subjects (cohort 2e,f) with high (>2.065 nmol pro/mg prot/min) *vs.* low (<2.065 nmol pro/mg prot/min) PEPD peptidase activity in VsW. **d**, Area under the receiver operating curve (AUC) values (95% CI) for VsW and ScW PEPD peptidase activity (PA) to discriminate subjects with type 2 diabetes (cohort 2e,f).**e**, Pearson correlation between PEPD serum levels and, ScW and VsW ECM remodelling markers and metabolic parameters in obese subjects from cohort 2b (n = 14 biologically independent samples). **f, g**, Pepd mRNA relative expression (f), and PEPD prolidase activity (g) in ScW, GnW and liver from C57Bl/6 mice in chow (n = 6) and 58% HFD (n = 8, 20 weeks) conditions.* compared to chow diet. **h**, ELISA analysis of PEPD protein in serum from C57/Bl6 mice fed chow (n = 6) or 20 weeks 58% HFD (n = 8). **I-k**. ScW prolidase activity (i), PEPD serum level (j) and ScW peri-ad collagen in C57Bl/6 mice fed 2, 8, 16 or 28 weeks (n = 8/group) with chow diet (ch) of HFD 45% (HF). **l**, Prolidase activity in the serum of C57Bl6 mice fed chow (2, 28 weeks) or HFD 58% (28 weeks). **m**, Pearson correlation matrix between ScW and GnW ECM remodelling markers and metabolic parameters in chow and HFD conditions (n = 22). Data presented as mean values +/− SEM. Data was analysed using a two-tailed Student's *t*-test (b, c, h) or a 2-way ANOVA followed by a Sidak post-hoc multiple comparisons test (f, g, i-k).

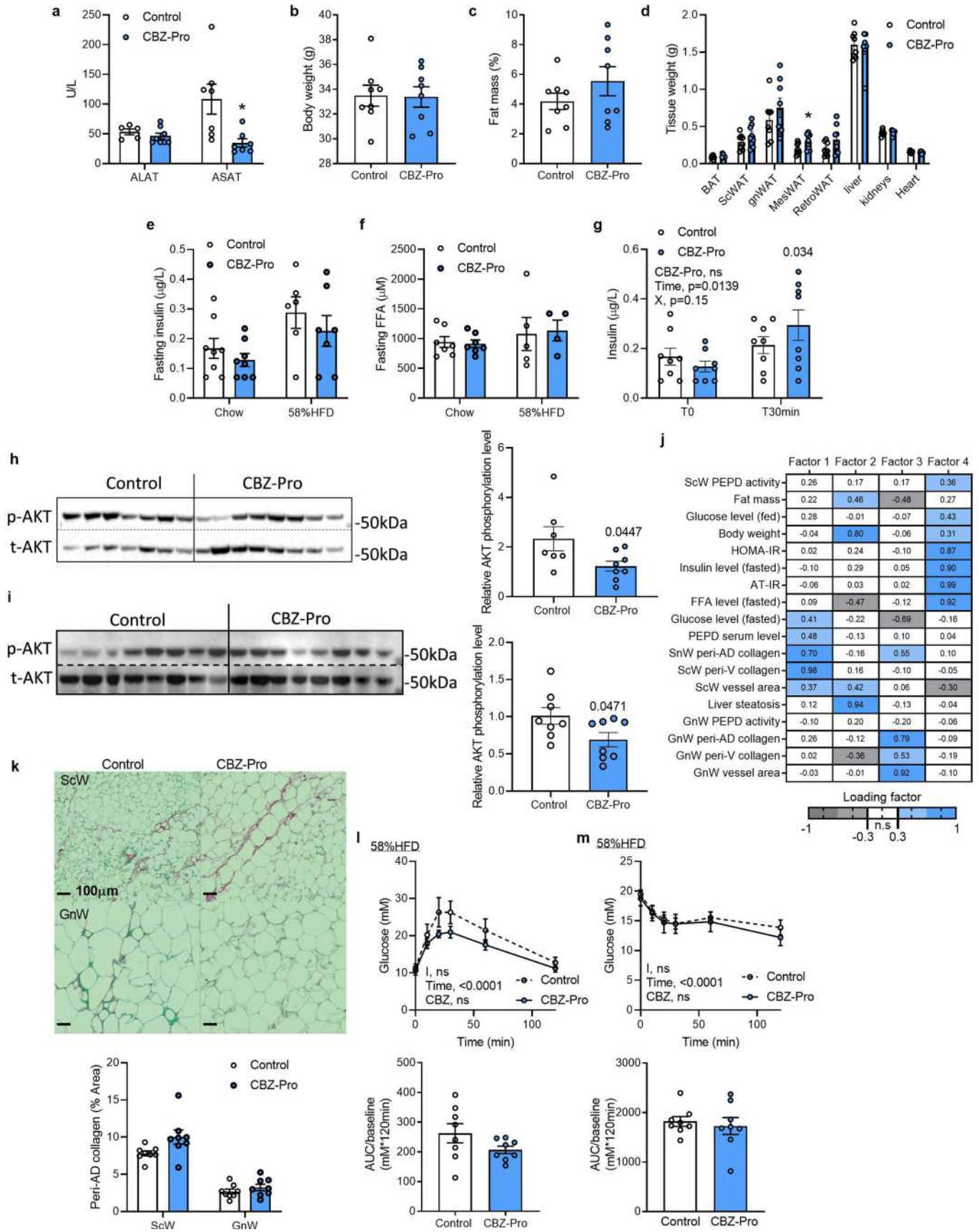

Extended Data Fig. 2 | See next page for caption.

Extended Data Fig. 2 | PEPD pharmacological inhibition promotes AT fibro-inflammation independently from obesity. a-d. ALAT and ASAT serum levels (a), body weight (b), and fat mass % (c), and tissue weight (d) in mice treated 10 weeks or not (control) with CBZ-Pro (n = 8 biologically independent animals per group). **e, f**. Fasting insulin and FFA blood levels from CBZ-Pro-treated mice compared to control mice (n = 8 biologically independent animals per group) fed chow and HFD 58% for 16 weeks. **g**. Fasting insulin blood level before and 30 min after glucose injection (2 g/kg) in CBZ-Pro-treated mice compared to controls (n = 8 biologically independent animals per group). **h,i**. Representative images of blots and quantification of total and basal phosphorylated (Ser473) AKT in GnW (h) and gastrocnemius muscle (i) of CBZ-Pro- treated mice compared to controls (n = 8 biologically independent animals per group). **j**. Heat map representing the four factors extracted through exploratory factor analysis. The columns report the factors loadings of the observed variables. **k**. Representative images of red Sirius staining in ScW and GnW of control and CBZ-Pro treated mice (n = 8 biologically independent animals per group) fed HFD 58%, and corresponding quantification of peri-adipocyte collagen content (peri-AD) represented in % Area (excluding perivascular staining). **l, m**. Blood glucose levels up to 120 min. after an intraperitoneal injection of glucose (2 g/kg) in a glucose tolerance test (l) or insulin (0.75 IU/kg) in an insulin tolerance test (m) in control and CBZ-Pro treated mice (n = 8 biologically independent animals per group) fed HFD 58%. Respective AUC are represented. Data is presented as mean values +/− SEM. Data was analysed using a two-tailed Student's *t*-test (a-d, h, i l, m) or a 2-way ANOVA followed by a Turkey (e-g) or Sidak (k-m) post-hoc multiple comparisons test.

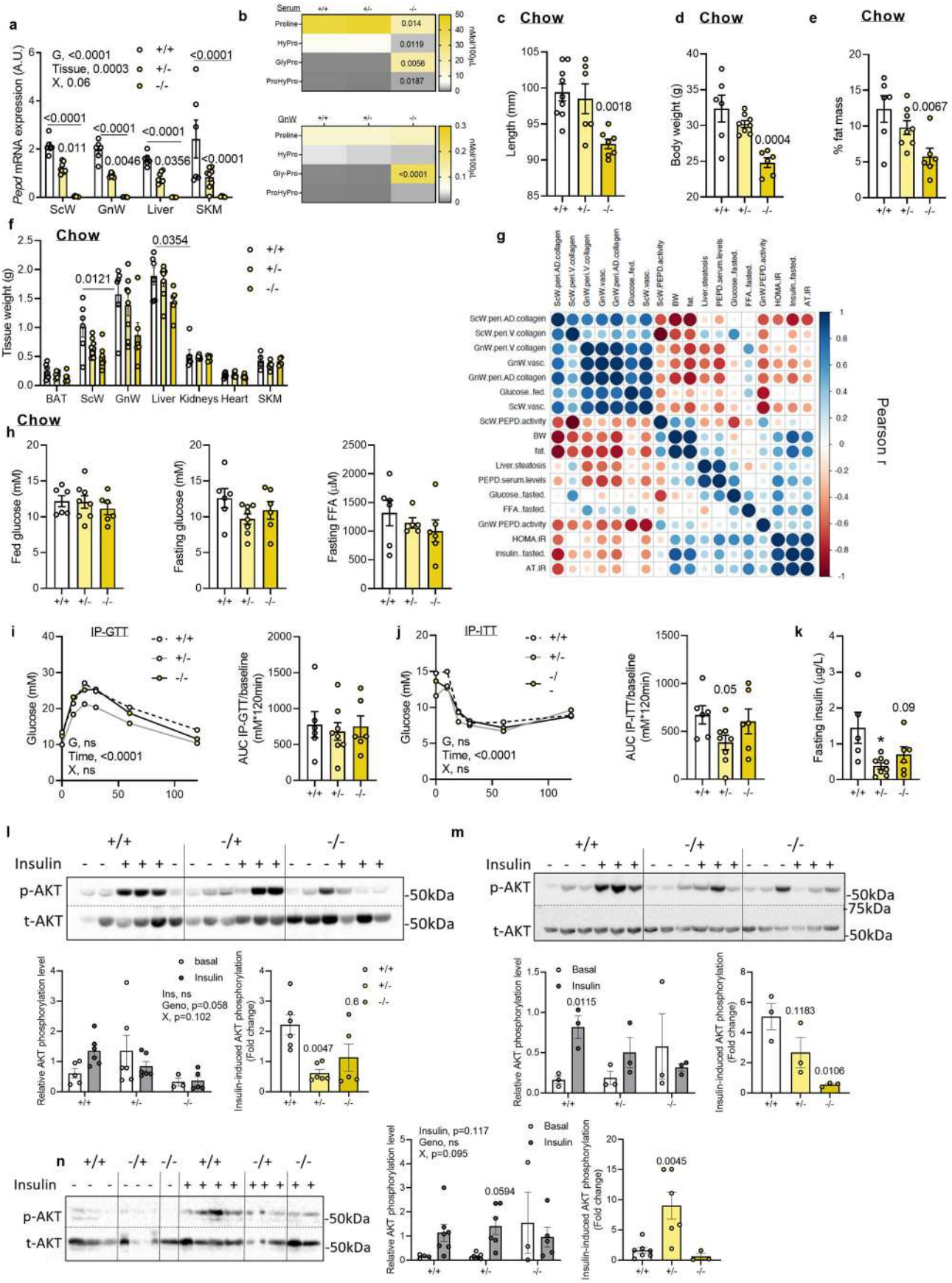

Extended Data Fig. 3 | See next page for caption.

Extended Data Fig. 3 | Pepd silencing promotes AT fibrosis but does not affect metabolic parameters in chow fed mice. a. *Pepd* RNA relative expression in ScW, GnW, liver and gastrocnemius (SKM) from *pepd* WT (n = 6), HET (n = 8) and KO mice (n = 5). **b**. Level of amino acids related to proline metabolism in the serum or GnW explant medium from *pepd* WT (n = 6), HET (n = 8) and KO mice (n = 5). **c-f, h, k**. Body length (c), body weight (d), fat mass % (e), tissue weight (f), fed glucose, fasting glucose and FFA (blood levels h), and fasting insulin blood level (k) in *pepd* WT (n = 6), HET (n = 8) and KO (n = 5) mice fed chow diet. **g**. Pearson correlations matrix between ScW and GnW ECM remodelling markers, PEPD serum levels and metabolic parameters in *pepd* mice fed chow (n = 19 biologically independent samples). **i, j**. Blood glucose levels up to 120 minutes after an intraperitoneal injection of glucose (2 g/kg) in a glucose tolerance test (i, IP-GTT) or insulin (0.75 IU/kg) in an insulin tolerance test (j, IP-ITT), and respective AUC adjusted to basal, in *pepd* WT (n = 6), HET (n = 8) and KO (n = 5)mice fed chow diet. **l-n**. Representative images of blots and quantification of total and phosphorylated (Ser473) AKT in GnW (l), liver (m) and gastrocnemius (n) of pepd WT (n = 6-11), HET (n = 6-12) and KO n = 6-8) mice fed chow diet after i.p injection of saline or insulin. 2way ANOVA with Dunnett's (a) or Sidak's (l, k, l-n) post-hoc multiple comparisons test; G, genotype; X, interaction. Data is presented as mean values +/− SEM. Data was analysed using a One way ANOVA followed by a Dunnett (b-f, h, k) or Sidak (i, j, l-n) post-hoc multiple comparisons test.

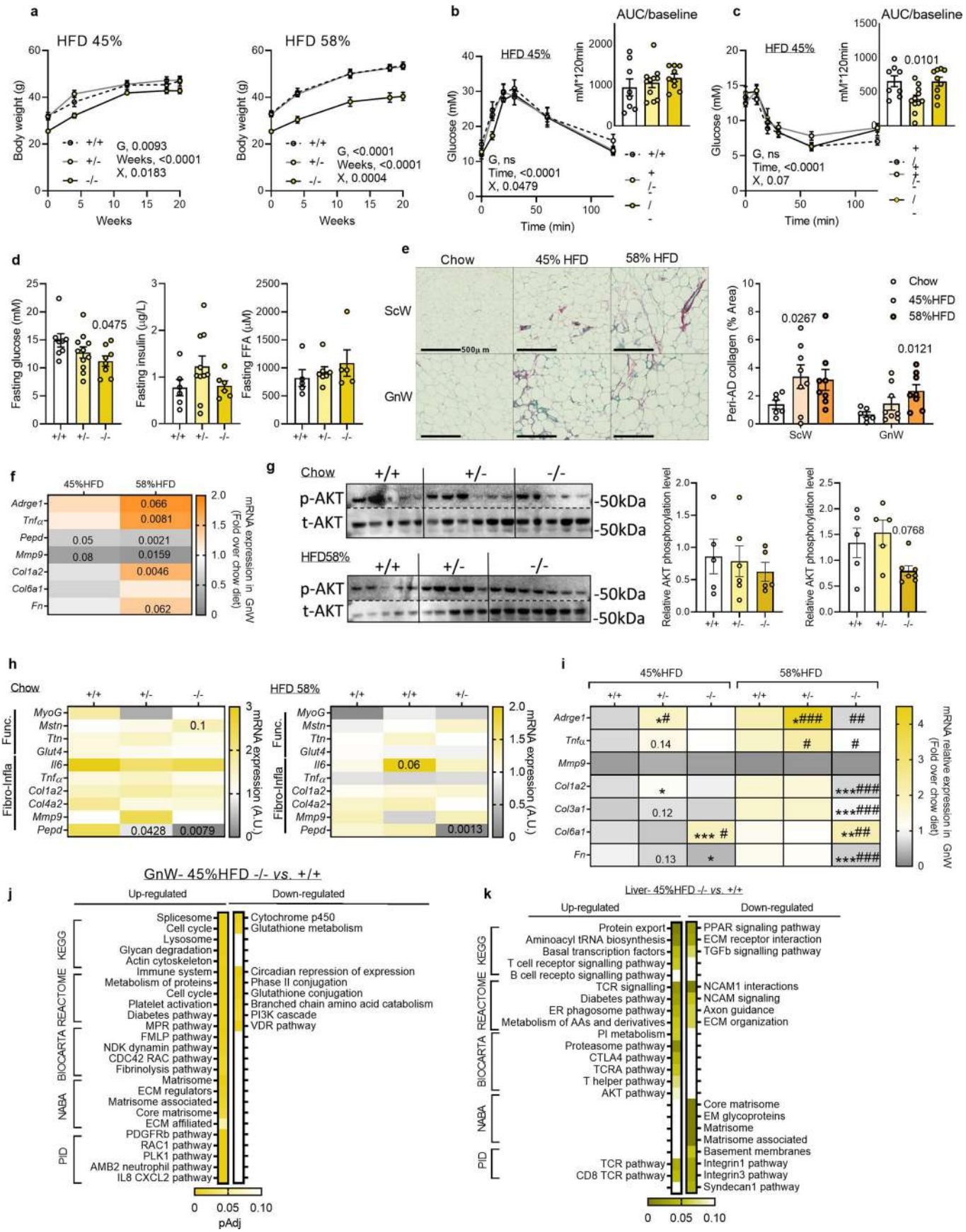

Extended Data Fig. 4 | See next page for caption.

Extended Data Fig. 4 | Pepd silencing exacerbates metabolic disturbances in HFD 58%-fed mice. Body weight curves and fat mass % curves of *pepd* WT, HET and KO mice after 20 weeks HFD 45% (n = 8, 11, 9 biologically independent animals per group, respectively) and HFD 58% (n = 8, 11, 8 biologically independent animals per group, respectively). **b, c**. Blood glucose levels up to 120 min. after an intraperitoneal injection of glucose in a glucose tolerance test (b) or insulin (0.75 IU/kg) in an insulin tolerance test (c) with the representative AUC in *pepd* WT (n = 9), HET (n-11) and KO (n = 9) mice fed HFD 45%. **d**. Fasting glucose, insulin and FFA blood levels in *pepd* WT (n = 8), HET (n = 11) and KO (n = 8) mice fed HFD 45%. **e**. Representative images of red Sirius staining in ScW and GnW from C57Bl/6 mice fed chow (n = 6), 45%HFD (n = 8) and HFD 58% (n = 8, 20 weeks) conditions and quantification of peri-adipocyte collagen content (peri-AD) represented in % Area (excluding perivascular staining).**f**. Heat map of gene expression in GnW from C57Bl/6 mice fed 20 weeks with chow (n = 6), 45%HFD (n = 8) and HFD 58% (n = 8). Results are expressed as fold change over chow diet. **g**. Representative images of blots and quantification of total and basal phosphorylated (Ser473) AKT in gastrocnemius muscle of pepd WT, HET and KO mice fed chow (n = 5, 6, 5 biologically independent animals per group, respectively), and HFD 58% conditions (n = 5, 5, 7 biologically independent animals per group, respectively). **h**. Heat map of gene expression of fibro-inflammatory and functional markers in gastrocnemius of *pepd* WT, HET and KO mice fed chow (n = 6, 7, 6 biologically independent animals per group, respectively), and HFD 58% conditions (n = 8, 7, 8 biologically independent animals per group, respectively). **i**. Heat map of gene expression in GnW from *pepd* WT, HET and KO fed HFD 45% (n = 6, 10, 9 biologically independent animals per group, respectively) and HFD 58% (n = 8, 9, 9 biologically independent animals per group, respectively) expressed as fold change variation over chow diet; *$p < 0.05$ compared to chow, #$p < 0.05$ compared to WT. **j, k**. Pathway enrichment analysis of the DEGs in GnW (i) and liver (j) from *pepd* KO mice (n = 9) compared to WT mice (n = 8) fed HFD 45%, using different data bases (KEGG, Reactome, Biocarta, NABA and PID). The heat maps indicate the level of significant changes (false discovery rate-adjusted p-value). Data is presented as mean values +/− SEM. Data was analysed using a 2-way ANOVA followed by a Turkey post-hoc multiple comparisons test; G, genotype; X, interaction (a-c, **i**), or a one way ANOVA followed by a Sidak (b, c, e) or Dunnett (d, g, h) post-hoc multiple comparisons test. A two-tailed Student's *t*-test was also used to analyse the data (f).

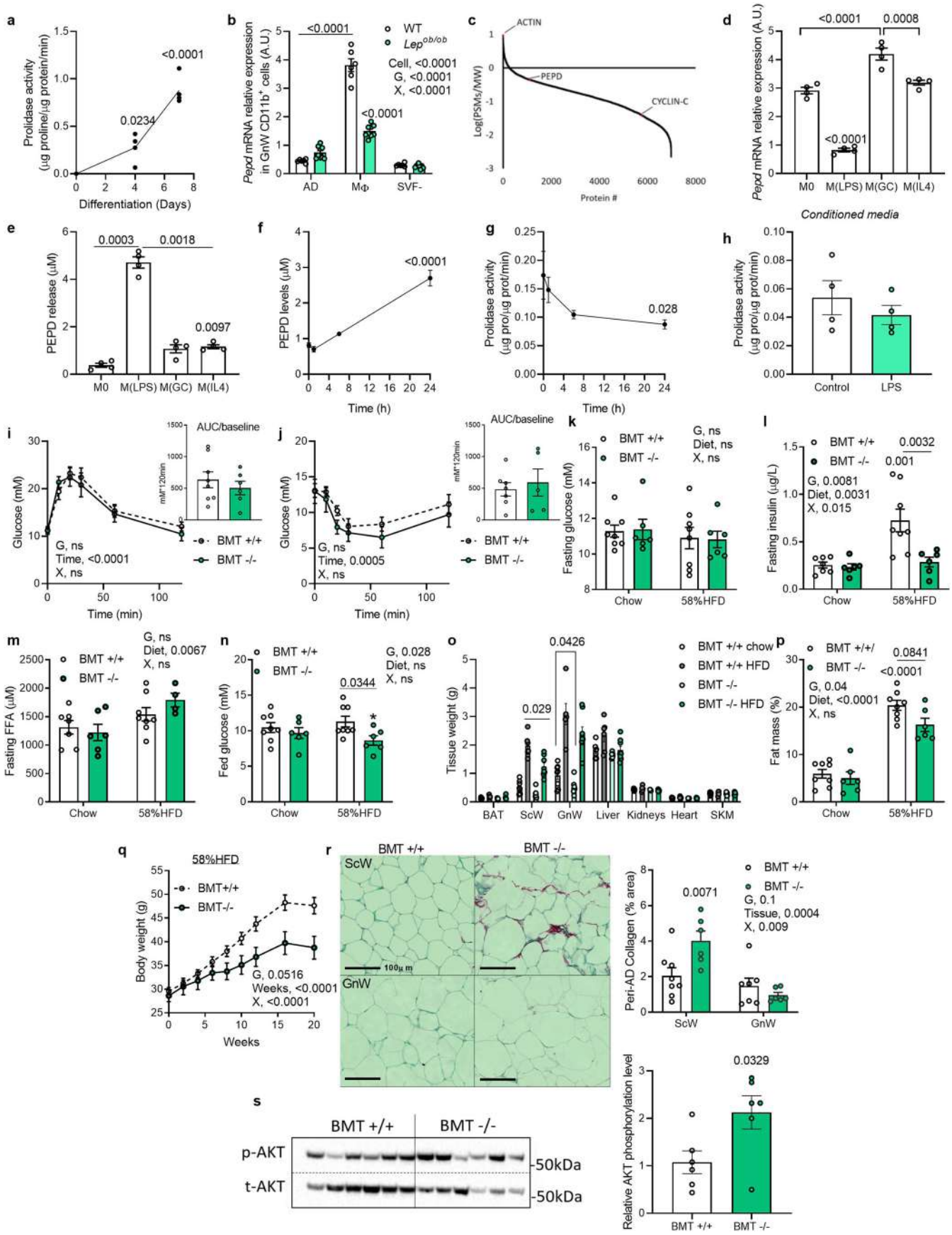

Extended Data Fig. 5 | See next page for caption.

Extended Data Fig. 5 | Pepd silencing in hematopoietic cells prevent obesity and associated metabolic disturbances. a. Prolidase activity in BMDMs during differentiation (n = 4 biologically independent samples). **b**. *Pepd* mRNA relative expression in adipocytes (AD), Mϕ (CD11b positive cells) and negative stroma-vascular fraction (SVF^{-}) isolated from GnW of WT (n = 6) and $Lep^{Ob/Ob}$ mice (n = 9). *compared to AD WT, # compared to Mφ WT. **c**. Abundance of PEPD measured by mass spectrometry in unstimulated human iPS-derived Mϕ differentiated from FPS10C iPS line. Relative abundance of PEPD in comparison of other detected protein in the same sample is plotted in the graph- where actin and cyclin are representing examples of high and low abundant proteins respectively. **d, e**. *Pepd* mRNA expression (d) or PEPD ELISA in culture media from BMDMs treated or not (M0) 6 h (d) or 24 (e) with LPS, dexamethasone (GC) or IL4 (n = 4 biologically independent samples). BMDMs were treated with LPS for 1,6 or 24 h: **f, g**. PEPD level in culture media (f) and prolidase activity in BMDMs (g). **h**. Prolidase activity in culture media from BMDMs treated without (control) or with LPS (100 ng/ml, 24 h) (n = 4 biologically independent samples). **I, j**. Blood glucose levels up to 120 min. after an intraperitoneal injection of glucose (2 g/kg) in a glucose tolerance test (i) or insulin (0.75 IU/kg) in an insulin tolerance test (j) in BMT WT (n = 8) and KO mice (n = 6) fed chow. Respective AUC are represented. **k-n**. Fasting glucose (k), fasting insulin (l), fasting FFA (m) and fed glucose (n) blood levels in BMT-WT (n = 8) mice compared to BMTKO mice (n = 6) fed chow and HFD 58% (20 weeks).**. o, p**. Tissue weight (o) and Fat mass % (p) in BMT +/+ (n = 8) and −/− (n = 6) mice fed chow and HFD 58% for 20 weeks. **q**. Body weight curve in BMT-WT (n = 8) mice compared to BMTKO mice (n = 6) mice between 0 and 20 weeks HFD 58%. **r**. Representative images of red Sirius staining ScW and GnW from BMT-WT (n = 8) mice compared to BMTKO mice (n = 6) fed HFD 58% and quantification of peri-AD collagen represented as %. **s**. Representative images of blots and quantification of total and basal phosphorylated (Ser473) AKT in GnW of of BMT WT and KO mice fed HFD 58% (n = 6/group). Data is presented as mean values +/− SEM. Data was analysed using a One way ANOVA followed by a Dunnett (a, f, g) or Tuckey (d, e) post-hoc multiple comparisons test, or using a 2-way ANOVA followed by a Tukey (b, k—p, r) or Sidak (I, j, q) post-hoc multiple comparisons test; G, genotype; X, interaction. A two-tailed Student's *t*-test was also used to analyse the data (h-j, s).

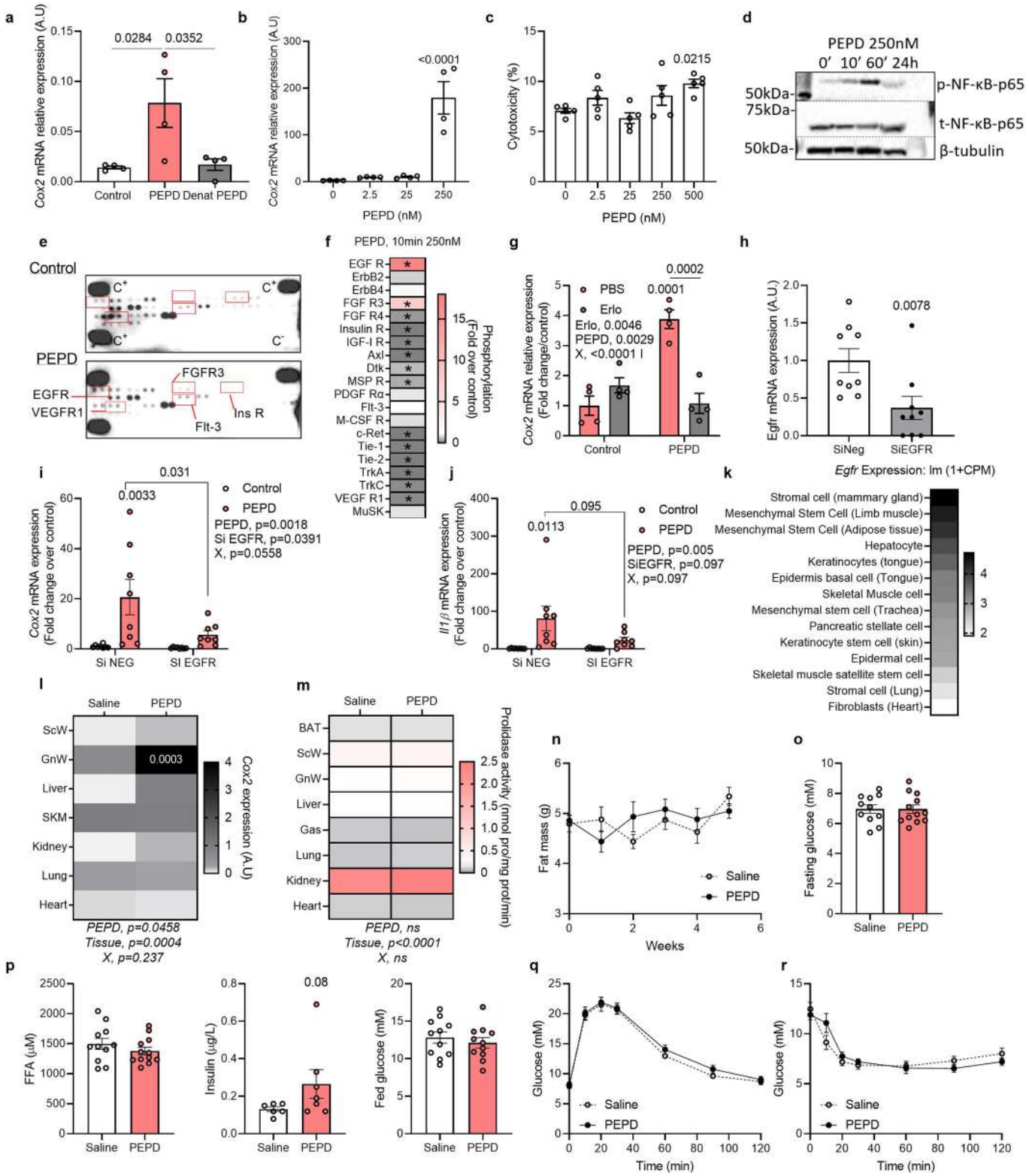

Extended Data Fig. 6 | See next page for caption.

Extended Data Fig. 6 | Purified PEPD protein promotes fibro-inflammation in macrophages through EGFR signaling. a. Cox2 mRNA relative expression in BMDMs treated or not (control) 4 h with purified PEPD protein active or denaturated (denat PEPD) (n = 3 biologically independent samples).**b**. Dose response effect of 4 h treatment with purified PEPD protein on cox2 mRNA relative expression in BMDMs (n = 4 biologically independent samples). **c**. % of cytotoxicity in BMDMs after 4 h treatment with purified PEPD protein (n = 4 biologically independent samples). **d**. Representative images of blots of total and phosphorylated (Ser 536) NF-kB protein and beta-tubulin in BMDMs (n = 4 biologically independent samples) treated with purified PEPD protein (0, 10, 60 min or 24 h, 250 nM). **e, f**. Tyrosine-kinase receptor phospho-Array of multiple analytes (e) and quantification (f) of phosphorylation levels in cell extract from BMDMs treated without (control) or with purified PEPD protein (10 min, 250 nM). Data from one experiment of a pool of 4 independent macrophage preparations. **g**. Cox2 mRNA relative expression in BMDMs (n = 4 biologically independent samples) pre-treated (Erlo) or not (PBS) with Erlotinib 5 μM, prior 24 h treatment with (PEPD) or without (control) purified PEPD protein. * compared to control PBS, # compared to PEPD PBS. **h-j**. mRNA expression of Egfr (h), Cox2 (i) and Il1β (j) in RAW macrophages transfected with Si-EGFR or its negative control (Si-NEG) prior treatment with (PEPD) or without (control) purified PEPD protein (250 nM,24 h). **k**. Tissue and cell distribution of egfr expression from Tabula muris DataBase; **l, m**. Heat map of Cox2 mRNA expression (l) and prolidase activity (m) in different tissues from C57Bl/6 mice injected with saline or purified PEPD (n = 11 biologically independent animals per group). **n-p**. Fat mass (n), fasting glucose (o), free fatty acids (FFA, p) and insulin levels (p), and fed glucose level (p) in PEPD-injected mice compared to controls (n = 11 biologically independent animals per group). **q, r**. Blood glucose levels up to 120 minutes after an intraperitoneal injection of glucose (2 g/kg) in a glucose tolerance test (q, IP-GTT) or insulin (0.75 IU/kg) in an insulin tolerance test (r, IP-ITT) in PEPD-injected mice compared to controls (n = 11 biologically independent animals per group). Data is presented as mean values +/− SEM. Data was analysed using a One-way ANOVA followed by a Dunnett (b, c) or Tuckey (a) post-hoc multiple comparisons test, or using a 2-way ANOVA followed by a Tukey (g, l, j) or Sidak (l-n, q, r) post-hoc multiple comparisons test. A two-tailed Student's *t*-test was also used to analyse the data (h, o, p).

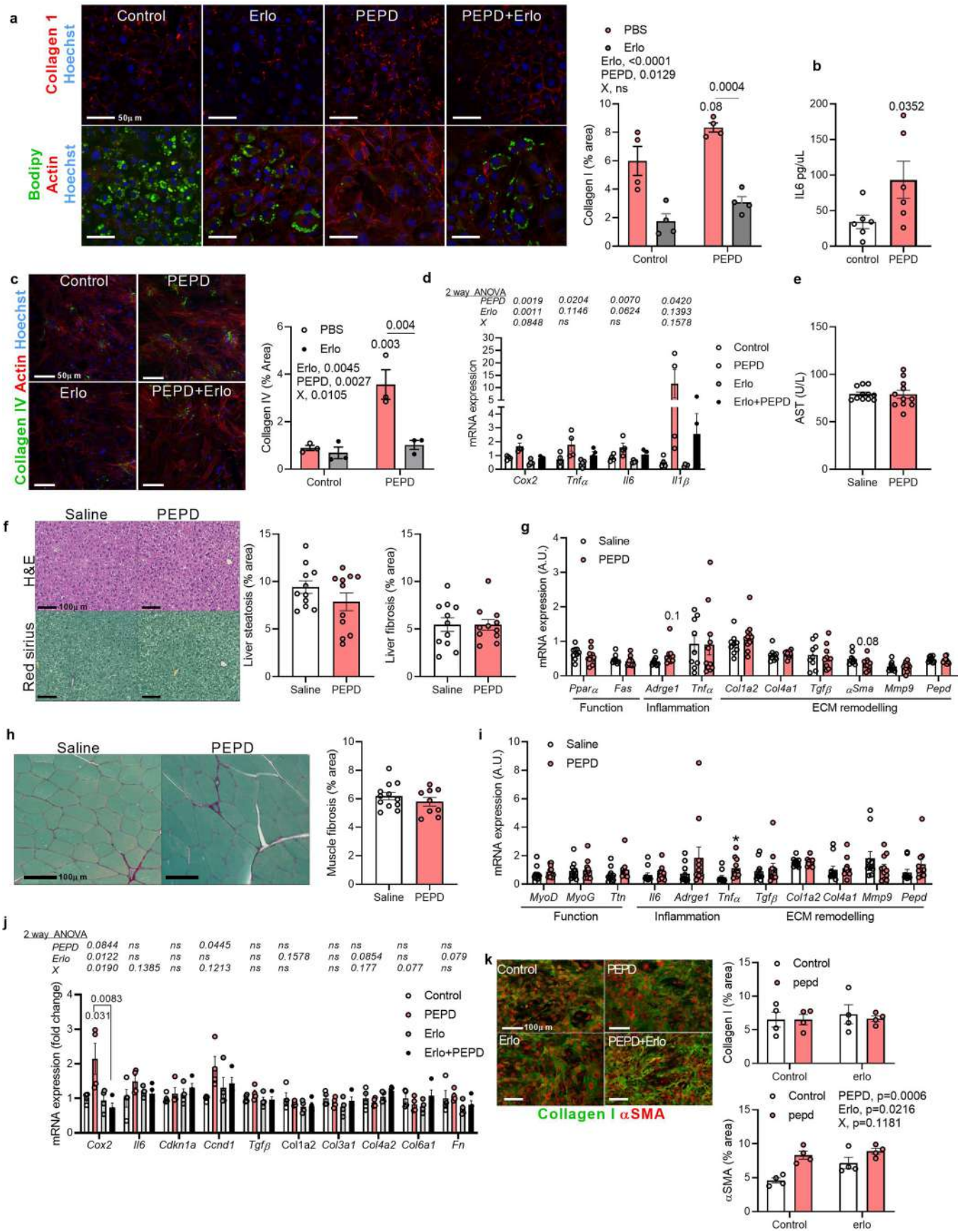

Extended Data Fig. 7 | See next page for caption.

Extended Data Fig. 7 | Purified PEPD protein promotes fibro-inflammation in pre-adipocytes and stellate cells through EGFR signaling. a. Representative images of confocal analysis of anti-Collagen type I (in red,) and Bodipy staining (lipid accumulation in green) (i) and corresponding quantifications of collagen I staining (j) in 3T3-L1 adipocytes (n = 4 biologically independent samples) pre-treated (Erlo) or not (PBS) with Erlotinib (5 μM) prior treatment with (PEPD) or without (control) purified PEPD protein (250 nM) during the first 5 days of adipogenic differentiation. * compared to control PBS, # compared to PEPD PBS. X, interaction. **b**. Il-6 level in culture media of mature adipocytes isolated from ScW of C57Bl/6 mice treated or not (control) with purified PEPD protein (250 nM, 24 h, n = 6 biologically independent animals per group). **c**. Representative images of confocal analysis of anti-Collagen type IV (in green,) and Actin staining (in red) and corresponding quantifications of collagen IV staining in stellate cells (n = 3 biologically independent samples) pre-treated (Erlo) or not (PBS) with Erlotinib (5 μM) prior treatment with (PEPD) or without (control) purified PEPD protein (250 nM). **d**. Gene expression profile in stellate cells (n = 4) pre-treated (Erlo) or not (PBS) with Erlotinib (5 μM) prior treatment with (PEPD) or without (control) purified PEPD protein (250 nM). **e**. AST serum level in PEPD-injected mice compared to controls (n = 11/group). **f**. Representative images of H&E and Sirius staining in the liver from PEPD-injected mice compaired to control (n = 11 biologically independent animals per group, a), and quantification of lipid droplet (steatosis) and collagen contents (fibrosis). g. Liver gene expression profile in PEPD-injected mice compared to controls (n = 11 biologically independent animals per group). **h**. Representative images of red Sirius staining in gastrocnemius from PEPD-injected mice compaired to control (n = 11 biologically independent animals per group), and quantification of collagen content (fibrosis). **i**. Gastrocnemius gene expression profile in PEPD-injected mice compared to controls (n = 11 biologically independent animals per group). **j**. Gene expression profile in muscle fibroblasts pre-treated (Erlo) or not (PBS) with Erlotinib (5 μM) prior treatment with (PEPD) or without (control) purified PEPD protein (250 nM, 5 days). **k**. Representative images of confocal analysis of anti-Collagen type I (in green,) and αSMA staining (in red), and corresponding quantifications of collagen I and αSMA stainings in muscle fibroblasts (n = 4 biologically independent samples) pre-treated (Erlo) or not (PBS) with Erlotinib (5 μM) prior treatment with (PEPD) or without (control) purified PEPD protein (250 nM, 5 days). Data is presented as mean values +/− SEM. Data was analysed using a 2-way ANOVA followed by aTukey post-hoc multiple comparisons test (a, c, d, j, k), or using a two-tailed Student's *t*-test (b, e-i).

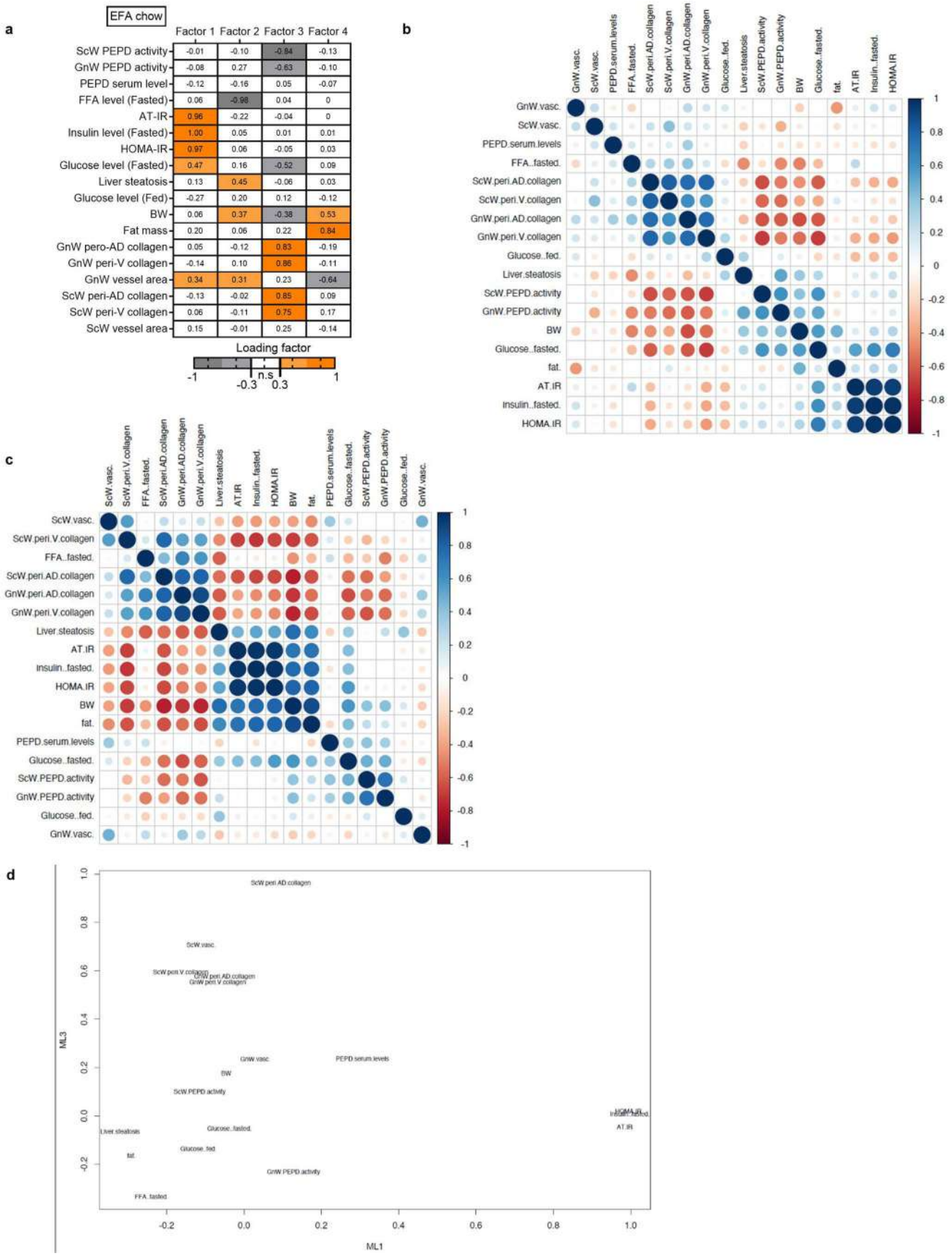

Extended Data Fig. 8 | See next page for caption.

Extended Data Fig. 8 | High PEPD serum levels is associated with AT insulin resistance and drives the differences between the pharmacologic and genetic animal models of PEPD down-regulation. a. Heat map representing the four factors extracted through EFA performed among mice fed chow. The columns report the factors loadings of the observed variables. **b, c**. Pearson correlation matrix between ScW and GnW ECM remodelling markers, PEPD serum levels and metabolic parameters in the mice from the four models (PEPD, CBZ-Pro, BMT and PEPD-injection) fed chow (b) or chow+HFD (c). Metabolic/fibro-inflammatory parameters from the four animal models (that is CBZ-Pro, PEPD, BMT and PEPD-injection) were plotted according to factor 1 and 3.

nature portfolio

Corresponding author(s): Dr. Vanessa Pellegrinelli and Prof. Antonio Vidal-Puig

Last updated by author(s): Mar 4, 2022

Reporting Summary

Nature Portfolio wishes to improve the reproducibility of the work that we publish. This form provides structure for consistency and transparency in reporting. For further information on Nature Portfolio policies, see our Editorial Policies and the Editorial Policy Checklist.

Statistics

For all statistical analyses, confirm that the following items are present in the figure legend, table legend, main text, or Methods section.

n/a	Confirmed	
☐	☒	The exact sample size (*n*) for each experimental group/condition, given as a discrete number and unit of measurement
☐	☒	A statement on whether measurements were taken from distinct samples or whether the same sample was measured repeatedly
☐	☒	The statistical test(s) used AND whether they are one- or two-sided *Only common tests should be described solely by name; describe more complex techniques in the Methods section.*
☐	☒	A description of all covariates tested
☐	☒	A description of any assumptions or corrections, such as tests of normality and adjustment for multiple comparisons
☐	☒	A full description of the statistical parameters including central tendency (e.g. means) or other basic estimates (e.g. regression coefficient) AND variation (e.g. standard deviation) or associated estimates of uncertainty (e.g. confidence intervals)
☐	☒	For null hypothesis testing, the test statistic (e.g. *F*, *t*, *r*) with confidence intervals, effect sizes, degrees of freedom and *P* value noted *Give P values as exact values whenever suitable.*
☒	☐	For Bayesian analysis, information on the choice of priors and Markov chain Monte Carlo settings
☒	☐	For hierarchical and complex designs, identification of the appropriate level for tests and full reporting of outcomes
☐	☒	Estimates of effect sizes (e.g. Cohen's *d*, Pearson's *r*), indicating how they were calculated

Our web collection on statistics for biologists contains articles on many of the points above.

Software and code

Policy information about availability of computer code

Data collection

RNA-Seq: reads (Supplementary Information, supplementary Table 1) were mapped to the most recent ENSEMBLE version GRCm38.p5 of the mouse reference genome sequence (GRCm38.p5) using STAR v2.5.1b (Dobin, A. et al. Bioinformatics 29, 15–21 (2013)) including the annotations as hints for exon-intron borders. FeatureCounts v1.5 (Liao, Y., Smyth, G. K. & Shi, W. Nucleic Acids Res. 41, e108 (2013)) was applied for the generation of count tables based on the mapping files. Customised python scripts (Haak, M. et al. Front Mol Biosci 5, 62 (2018)) were deployed for downstream processing, including the raw counts' normalisation to the total number of assigned reads per gene (TPMs) and the combined exon length (FPKMs), respectively. Codes and Scripts are available On Github: https://github.com/bpucker/RNA-Seq_analysis. An Archive version of the code is also available in Zenodeo. The DOI (10.5281/zenodo.6192463) is displayed in the README on github.

GC-MS: Data was acquired using MassHunter Workstation Software.

Confocal data: Images were obtained using a confocal microscope (Leica TCS SP8; Leica Microsystems CMS GmbH)

EFA: Factors extraction was computed using the Maximum Likelihood Estimate (MLE) method, implemented in the function fa of the psych R package (Revelle W (2021). psych). Plots were produced either using in house scripts or using built-in functions of the FactoMineR R package (Lê, S., Josse, J. & Husson, F. FactoMineR J. Stat. Soft. 25, (2008)).

PCA: Principal components analysis of the Lukk and the own dataset were calculated in R version 3.1.2 using the prcomp function of the stats package (R Core Team (2020). https://www.R-project.org/).

Data analysis

RNAseq analysis: raw counts were subjected to differential gene expression analysis via DESeq2 (Love, M. I., Huber, W. & Anders, S. Genome Biol. 15, 550 (2014)) and different R packages (available on Github, https://github.com/bpucker/RNA-Seq_analysis). Obtained DEGs were annotated via customised python scripts (available on Github, https://github.com/bpucker/RNA-Seq_analysis). Pathway enrichment analyses

were performed with PIANO (Väremo, L., Nielsen, J. & Nookaew, I. Nucleic Acids Res. 41, 4378–4391 (2013)), using the gene set collection C2 retrieved from the Molecular Signatures Database (MSigDB) (Liberzon, A. et al. Bioinformatics 27, 1739–1740 (2011) ; Subramanian, A. et al. Proc. Natl. Acad. Sci. U.S.A. 102, 15545–15550 (2005)).

GC-MS analysis: Peak integration and quantification was performed using MassHunter Workstation Quantitative Analysis software (version B.07.00, Agilent).

Histology analysis: Fibrosis and steatosis analysis were performed semi-automatically using HALO software (HALO; Indica Labs).

Confocal analysis: Staining quantification was performed using Fiji software (https://imagej.net/software/fiji/)

Immunoblot analysis: bands were quantified using Fiji software (https://imagej.net/software/fiji/)

Statistical analysis: Data were analysed using GraphPad Prism (version 8.0.2)

For manuscripts utilizing custom algorithms or software that are central to the research but not yet described in published literature, software must be made available to editors and reviewers. We strongly encourage code deposition in a community repository (e.g. GitHub). See the Nature Portfolio guidelines for submitting code & software for further information.

Data

Policy information about availability of data

All manuscripts must include a data availability statement. This statement should provide the following information, where applicable:

- Accession codes, unique identifiers, or web links for publicly available datasets
- A description of any restrictions on data availability
- For clinical datasets or third party data, please ensure that the statement adheres to our policy

All the raw data and uncropped immunoblots are available in Source Data files (Figures and immunoblots) and upon request (Extended Data Figures). DEGs and pathways from RNA-seq analysis can be found in Supplemental Tables. The RNA sequencing dataset is deposited in GEO under accession number GSE198358.

Field-specific reporting

Please select the one below that is the best fit for your research. If you are not sure, read the appropriate sections before making your selection.

☒ Life sciences ☐ Behavioural & social sciences ☐ Ecological, evolutionary & environmental sciences

For a reference copy of the document with all sections, see nature.com/documents/nr-reporting-summary-flat.pdf

Life sciences study design

All studies must disclose on these points even when the disclosure is negative.

Sample size	No statistical methods were used to predetermine the total number of animals needed for this study. he number of animals or independent experiments were determined based on pilot data and are all indicated in the figure legends.
Data exclusions	Data were excluded when identified as outliers. Grubbs' test, also called the ESD method (extreme studentized deviate) was used to determine whether one of the values is a signficant outlier from the rest. Grubbs's test was performed on GraphPad website: https://www.graphpad.com/quickcalcs/Grubbs1.cfm. Excluded data are shown in the raw data files (Source Data File).
Replication	In vivo studies: For the CBZ-Pro experiment, a pilot experiment was performed and successfully replicated during the "real "experiment, performed once, shown in the manuscript. For the time course HFD of the Pepd mice, the experiment has been performed and successfully replicated 3 times (3 batches of mice). For the BMT experiment, the experiment has been performed once. In vitro studies: Each in vitro experiment was performed at least 3 times and all attempts were successful. A representative experiment is presented in the manuscript.
Randomization	Regarding the pepd mice. Animal allocation to cages (4 mice/cage) was not randomised as we ensured each cage had mice from the three genotypes. Allocation to diet were not randomised as we ensured each group (chow and HFD, control and CBZ-Pro) had the same average of initial body weight.
Blinding	The investigators were blinded during the experiments and assessment of the outcome. Blinding was not performed during animal allocation to diet and/or treatment groups as we ensured each group (chow and HFD, control and CBZ-Pro) had the same average of initial body weight.

Reporting for specific materials, systems and methods

We require information from authors about some types of materials, experimental systems and methods used in many studies. Here, indicate whether each material, system or method listed is relevant to your study. If you are not sure if a list item applies to your research, read the appropriate section before selecting a response.

Materials & experimental systems

n/a	Involved in the study
☐	☒ Antibodies
☐	☒ Eukaryotic cell lines
☒	☐ Palaeontology and archaeology
☐	☒ Animals and other organisms
☐	☒ Human research participants
☒	☐ Clinical data
☒	☐ Dual use research of concern

Methods

n/a	Involved in the study
☒	☐ ChIP-seq
☒	☐ Flow cytometry
☒	☐ MRI-based neuroimaging

Antibodies

Antibodies used

The antibodies used in the study are: anti-collagen I (Abcam, ab21286, RRID:AB_446161), anti-αSMA 1A4 (Sigma, A2547, RRID:AB_476701), anti- PEPD (Abcam , ab86507, RRID:AB_1952335), anti-phospho-NF-κB p65 (Ser536) (93H1, Cell signalling, #3033, RRID:AB_331284), anti-NF-κB p65 (Cell signalling, #3034, RRID:AB_330561), anti-β-Actin (Abcam, ab8227, RRID:AB_2305186), anti-GADPH (Cell signalling, #97166S, RRID:AB_2756824), anti-β-Tubulin (Cell signalling, #2146S, RRID:AB_2210545), anti-phospho-AKT (Ser473) (D9E) (Cell Signalling, #4060, RRID:AB_2315049), anti-AKT (#9272, RRID:AB_329827), MACS mouse CD11b microbeads (Miltnyibiotec, 130-049-601), Anti-rabbit IgG, HRP-linked (Cell signalling, #7074, RRID:AB_2099233), Anti-mouse IgG, HRP-linked (Cell signalling, #7076, RRID:AB_330924), Alexa555-conjugated anti-rabbit (Life technologies, A21428, RRID:AB_141784), Alexa488-conjugated anti-mouse (Life technologies, A21202, RRID:AB_141607).

Validation

Anti-collagen I (ab21286) was validated fo ICC/IF in previous publications as indicated by the manufacturer (PMID: 33534863 (fibroblasts); PMID:33284954 (muscle)). Anti- PEPD (ab86507) was validated in previous publications (PMID: 29233996; PMID: 23212918) as well as in the lab using a PEPD KO animal as a control. Anti-αSMA 1A4 (A2547) was validated by the manufacturer ("Immunocytochemistry was performed on smooth muscle cells from bovine aortas using the monoclonal anti-ACTA2 antibody. Cells were first grown on glass cover slips and fixed in 50% acetone/EtOH for 10 minutes at 4 degrees") and in the lab (PMID: 32694734). Anti-phospho (#3033) and total NFkB (#3034) were validated by the manufacturer ("Western blot analysis of extracts from HeLa and NIH/3T3 cells, untreated or TNF-α treated (#2169, 20 ng/ml for 5 minutes), using Phospho-NF-κB p65 (Ser536) (93H1) Rabbit mAb (upper) or NF-κB p65 Antibody #3034 (lower).") and in the lab (PMID: 34531575; 26201685). Anti-GADPH (#97166S) was validated by the manufacturer ("Western blot analysis of extracts from various cell lines using GAPDH (D4C6R) Mouse mAb.") and in the lab (PMID: 26628376; PMID: 30478315). Anti-β-actin (was validated by the manufacturer ("Suitable for: WB, IHC-P, ICC/IF [...]Success from the first experiment – confirmed specificity through extensive validation") and in the lab (PMID: 30478315; PMID: 34531575; PMID: 26628376). Anti-tubulin (#2146) was validated by the manufacturer ("Western blot analysis of extracts from various cell lines using β-tubulin Antibody") and in the lab (PMID: 23919961).

Eukaryotic cell lines

Policy information about cell lines

Cell line source(s)

The cell lines used in the study were: 3T3L1 Cells (Zen-Bio, SPL1F) and RAW264.7 cells (TIB-71, ATCC).

Authentication

3T3L1 Cells (Zen-Bio, SPL1F) and RAW264.7 cells (TIB-71, ATCC) were not authenticated. However, RAW264.7 cell line has been previously used in the lab and its macrophage identity has been validated by PCR (this study and PMID:34531575). Similarly, 3T3L1 cell line has been previously used in the lab and its adipogenic identify has been validated by PCR (this study and PMID:3047831).

Mycoplasma contamination

The cell line have not been tested for mycoplasma contamination

Commonly misidentified lines
(See ICLAC register)

No

Animals and other organisms

Policy information about studies involving animals; ARRIVE guidelines recommended for reporting animal research

Laboratory animals

8-10 weeks old male C57Bl6/J mice were purchased from Charles River (JAXTM Strain, RRID:IMSR_JAX:000664) . Pepd KO mice (Pepdtm1a(KOMP)Wtsi) were generated by the Wellcome Trust Sanger Institute Mouse Genetics Project on a C57Bl6/J background by mating heterozygous mice (MFPW; EPD0224_1_C04). Pepd homozygous (null and WT) and heterozygous pups were observed in normal Mendelian ratios. In respect to the 3R, only a subpopulation of the pups born was selected for each study. 8-10 weeks old male Pepd WT, HET and KO were used for each experiment. 8-10 weeks old male wild type and leptin-deficient mice, LepOb/Ob(C57BL/6J-Lepob) were on a C57BL/6 J background (JAXTM Strain, RRID:IMSR_JAX: 000632). This research has been regulated under the Animals (Scientific Procedures) Act 1986 Amendment Regulations 2012 following ethical review by the University of Cambridge Animal Welfare and Ethical Review Body (AWERB) under pathogen-free conditions and housed according to UK Home Office guidelines. All animal work was carried out in the Disease Model Core unit. Animals were housed 3–4 per cage in a temperature-controlled room (22°C) with a 12-h light/dark cycle (with 'lights on' corresponding to six am), with 55% relative humidity. Animals had ad-libitum access to food and water. A standard chow diet (DS-105, Safe Diets) was administered to all animals from weaning, consisting of 64.3% carbohydrate, 22.4% protein and 13.3% lipid of total calories. Only male mice were used for in vivo experiments and preparation of BMDMs.

Wild animals	No wild animals were used in the study.
Field-collected samples	No field collected samples were used in the study.
Ethics oversight	This research has been regulated under the Animals (Scientific Procedures) Act 1986 Amendment Regulations 2012 following ethical review by the University of Cambridge Animal Welfare and Ethical Review Body (AWERB). Mice were housed 3–4 per cage in a temperature-controlled room (21°C) with a 12 hr light/dark cycle, with 'lights on' corresponding to six am. Animals had ad-libitum access to food and water. A standard chow diet (DS-105, Safe Diets) was administered to all animals from weaning, consisting of 64.3% carbohydrate, 22.4% protein and 13.3% lipid of total calories."

Note that full information on the approval of the study protocol must also be provided in the manuscript.

Human research participants

Policy information about studies involving human research participants

Population characteristics	Three human cohorts were used in the study: In cohort 1, we analysed a group of 154 samples [84 visceral (VsW) and 70 subcutaneous (ScW) adipose tissues] from non-obese (age 53.6±12.2 years-old, BMI 25.9±2.9 kg/m2) and obese (age 44.3 ±8.9 years-old, BMI 44.8±7.3 kg/m2) participants. Cohort 2 was divided in sub cohorts: 2a, including 8 lean (age 46.3±4 years-old, BMI 23.9±0.6 kg/m2) and 8 obese non-diabetic subjects (age 40.5±2.5 years-old, BMI 51.1±2.8 kg/m2); 2b, including 6 obese non-diabetic (age 35.3±5.3 years old, BMI 44.7±1.8 kg/m2) and 8 obese diabetic subjects (age 36.5±5.89 years-old, BMI 46.78±2.07 kg/m2); 2c, including 6 obese non-diabetic (age >18 years old, BMI >35 kg/m2) and 6 obese diabetic subjects age >18 years old, BMI >35 kg/m2); 2d, including 10 lean (age 43.9±4.3 years-old, BMI 27.4±1 kg/m2) and 9 obese subjects (age 44.4±2.3years-old, BMI 42.8±0.5 kg/m2); and 2f including 6 obese non-diabetic (age 36.5±5 years-old, BMI 46±3.1 kg/m2) and 7 obese diabetic subjects (age 46.9±5.5 years-old, BMI 43.7±2.6 kg/m2). In cohort 3, 46 VAT and 36 SAT samples from morbidly obese subjects (age >18 years old, BMI > 35 kg/m2) were analysed.
Recruitment	Human subjects from cohort 1 and 3 were recruited at the Endocrinology Service of Girona "Dr Josep Trueta" Hospital. These subjects were of Caucasian origin and reported that their body weight had been stable for at least three months before the study. Subjects were studied in the post-absorptive state. They had no systemic disease other than obesity, and all were free of any infections in the previous month before the study. Liver diseases (specifically tumoral disease and HCV infection) and thyroid dysfunction were excluded by specific biochemical tests. Human subjects from cohort 2 were candidates for elective (lean subjects) and bariatric surgery (obese subjects) in "Pitié-Salpêtrière Hospital", Paris. Subjects were excluded if they suffered from anaemia, abnormal thyroid-stimulating hormone (TSH) level, human immunodeficiency virus (HIV) and/or hepatitis C virus (HCV) infection, severe hepatic and/or renal failure, known inflammatory disorder. In addition, subjects receiving or having received for more than 1 week in the last 3 months drug(s) that impact adipose tissue mass were also excluded (i.e. systemic steroids, neuroleptics and anti-HIV therapy).
Ethics oversight	Subjects from cohort 1 and 3 s= gave written informed consent, validated and approved by the ethical committee of the Hospital of Girona "Dr Josep Trueta", after the purpose of the study was explained to them. Some additional samples were provided by the FATBANK platform promoted by the CIBEROBN and coordinated by the IDIBGI Biobank (Biobanc IDIBGI, B.0000872), integrated with the Spanish National Biobanks Network, and they were processed following standard operating procedures with the appropriate approval of the Ethics, External Scientific and FATBANK Internal Scientific Committees. Regarding cohort2, studies were conducted in Paris (France) following the Helsinki Declaration and approved by the Ethics Committee of Clinical Research (CPP Ile-de-France 1, Fibrota study N° clinical trial NCT01655017). Signed informed consents were obtained in all lean and obese individuals in agreement with ethic regulation.

Note that full information on the approval of the study protocol must also be provided in the manuscript.